INTERACTION OF FUNCTIONAL GROUPS IN TISSUE ADHESIVE: EXPERIMENTAL ANALYSIS AND COMPUTATIONAL MODELING

LIM KEE PAH

School of Materials Science and Engineering

A thesis submitted to the Nanyang Technological University
in fulfillment of the requirement for the degree of
Doctor of Philosophy

2009

Acknowledgements

I would like to show my respect and gratitude to my project supervisor, Asst. Prof. Tan Lay Poh. She is inspiring, meticulous and critical in doing research; and is tolerant, generous, and helpful in personality. Together, we contemplated ideas and shaped the project's edifice, a process through which I have gained a lot on research philosophy.

I would like to thank Prof. Stachurski, Prof. Subbu and Dr. Suresh who provided ideas in the early stage of the project. I also thank Assoc. Prof. Chen Zhong and Assoc. Prof. Lu Xuehong, my Thesis Advisory Committee members, who have guided the path of my work.

I want to extend the list to include the students who had been working with me at different stages. They are Juliana Wong Wei Shan, Wong Hui Kian, Ezran and Lia Pratomo. I am also grateful to the lab technical staffs in MSE who had provided helps in my experiments. They are Nelson Ng, Serene Kok, Wu Shucheng, See-Toh Swee Sing, Yuan Quan and Tan Kek Koon.

My family has been giving me endless support and patience. My colleagues and friends in MSE have been giving me accompaniment and encouragement in the otherwise lonesome journey. I have them to thank. Last but not least, I thank NTU for funding this research project.

Contents

List of Figures

List of Tables

Summary

The development of new tissue adhesives (TAs) has been very slow, to say the least, for the past decade. Synthesis of new TAs is by and large through trial and error and therefore very costly and time consuming. This thesis introduces some new aspects of study into the field of TA with the intent of assisting and even guiding the choice of functional groups that may promote adhesiveness in TAs.

Atomistic modeling and simulation is an increasingly potential tool in studying the origins of observable phenomena. Here, it is introduced to study TAs for the first time. Of all theories available, classical molecular mechanics and dynamics (MM/MD) were implemented as it is most suitable to handle the size of the system of interest and the time of simulations. As an introductory work, the thesis studied the (i) physical interactions of small functional molecules with collagen triple-helix; and (ii) the physical interactions of oligomer molecules with collagen surface in both dry and wet conditions. From there, a hypothesis of tissue adhesion was formulated.

The simulation works, based on classical theory, were then examined by two experimental adhesion measurements. They were atomic force measurements in AFM (atomic force microscope) and lap shear tests. The former was also unprecedented in the field and it measured the interaction forces at molecular level. A few types of functional groups were tested on collagenous tendon substrates in dry and wet environments. The latter is a typical test used by many to assess adhesive joint strengths. Different adhesives

were used to bond dry and wet collagenous substrates together and the joint strength was assessed by stressing in shear direction.

Results showed that small molecules, in general, have strong physical adsorption on collagen but this interaction weakens as the molecules polymerize or cross-linked. Presence of water is indeed very unfavorable to adhesiveness in TAs and interactions are seriously perturbed, as observed in simulations and experiments. Also, peptide/amide group shows strong adhesiveness, and therefore protein glues have great potential. Finally, while adsorption is crucial, diffusion mechanism, which could be equally important, is proposed for future study.

Chapter 1
Introduction to Tissue Adhesives

1.1 Background of Tissue Adhesives

In definition, tissue adhesives (TAs) are surgical tools supplied in liquid form that are hardened upon application and, at the same time, adhere firmly onto target biological tissue surfaces through physical and/or chemical interactions, after which continuous solids that are able to sustain common physiological loadings are formed. The design objective of TAs is primarily to hold the approximated traumatized tissue together with sufficient strength, up to the point in time when the tissue heals up sufficiently to support itself. In this perspective, TA is similar to biodegradable sutures that are now commonly used to close internal lacerations. The former, however, could provide a quick, easy-to-use and convenient way for surgeons and less traumatic for patients.

Polymeric system as TAs

Polymers, or massive biological molecules (such as proteins, polysaccharides, etc., which can be perceived as 'polymers' in biological forms), be it thermoplastic or thermoset, appear to be good candidates for such applications due to the fact that, generally, solid polymers are formed from liquid monomer precursors; and the reaction occurs spontaneously in adequate conditions. These conditional factors include temperature, pH, water content, salt level, the use of catalysts, the use of photon radiation, positioning of

the broken tissue, etc. For most TAs, two or more reactive liquid monomer components are mixed *in situ* and a solid cross-linked network is formed upon chemical reaction (termed as "cross-linking system". For some TAs like cyanoacrylate systems, monomer liquid goes through addition polymerization to form a solid piece of entangled linear chains (termed as "polymerization system"). Other than these options, oligomers or polymers can be dissolved into volatile solvents with low boiling points, and then the evaporation of solvent leaves the solid polymer matrix behind during application (termed as "solvent evaporation system").

Current Wound Closure Techniques

The current wound closure technique that is utilized the most is suturing. Suturing technique has become the most important and promising techniques after many generations of medical teachings; and every surgeon in any operating room is required to master the technique dexterously. Traditional non-degradable sutures always require removal – perceived as "a second surgery" for patients – that causes inconvenience and anxiety. The introduction of synthetic biodegradable sutures, based on poly(lactic acid), poly(glycolic acid) and poly(ε-caprolactone), had then broadened the versatility of the technique for it to be used in virtually any locations without the need of removal. However, suturing is in fact a traumatic technique and is not suitable in certain locations. In suturing, holes are unavoidably created around the wound. These holes act as leaking channels for blood, air and other body fluids, especially when suturing is performed to vascularized tissues and organs, such as lungs and eyes. Furthermore, the loading patterns by which the suture lines exert onto the wound tissue are always not uniform. In other

words, parts of the tissues (i.e. those that are in contact with suture) experience a stronger stress than the others. Extensive scar formation has also observed with suturing technique [1-3] and this attribute makes it unpopular in cosmetic surgeries.

The other wound closure techniques that are currently in use include stapling, laser irradiation, and laser soldering. Each of them has their unique and advantageous traits, for instance, stapling is stronger in strength; and laser soldering is rapid and gives complete wound sealing. They are however only sparingly used in some special cases because these techniques are destructive in nature, as in the case of suturing. To mend the tissues together, they have to be punctured or destroyed in the first place. Staple holes also share the common problem with suture holes – they act as leaking channels. Laser irradiation and soldering may cause unnecessary necrosis in the tissues due to the overheating and denaturization of the local proteins [4-6]. Furthermore, these techniques require more sophisticated skills from surgeons, as compared to suturing technique. Removal operation is needed for stapling, too. Therefore, these techniques are implemented only when there is a real need, for example, when the wound is too big, or when suturing is impractical.

Advantages of TAs over other Wound Closure Techniques

The concept of TAs then fills perfectly into the gap. To close a wound, surgeons should just carefully approximate the lacerated tissues and then apply the TA topologically and hold for one minute or so for the adhesive to adhere and harden. No further unnecessary damage is done to the tissue and the mastery of the technique truly requires just some

practices. Since TAs are designed to be biodegradable/bioerodible, the need of removal operation is eliminated. These advantages, which outperform (or, at least, compensate) the other wound closure techniques, come into mind immediately when one conceives the idea of TAs. TAs also serve as sealants and hemostats. The continuous TA films, conforming to the wound tissue surface, can stop bleeding or air leakage from the wound. (Polymeric sealants are often used as adjunct tools with suture to prevent leakage from suture holes [7-10].) The films perform as barriers to external infection sources, too. Drugs like growth factor and antibiotic can be incorporated into the TA polymeric matrix. Controlled release of these drugs to the underlying tissue can promote better wound healing process and better outlook of healed tissues. (Incidentally, biodegradable sutures are designed to deliver drugs too.) Moreover, since TA is applied topologically, its minimal contact with tissue subsurface should elicit a lower degree of foreign body reaction, which would otherwise unavoidably lead to fibrosis and scar formation.

Requirements for TAs

The most basic requirement of TAs is that they should exhibit sufficient and appropriate adhesiveness in wet/moist environments, which are notorious that it prevents or mitigates adhesion, at internal tissues. Not many materials actually possess adhesiveness readily in wet. The biological environments, in which TAs are used, have imposed many stringent requirements on the materials. The critical traits needed for TAs to function in biological environments include biocompatibility, biodegradability/bio-erodibility, non-immunogenicity, non-cytotoxicity and non-carcinogenicity. In contrast, they should be thrombogenic to a certain extent so that they can stop excessive bleeding from the

traumatized tissues. These requirements are not only applicable to the hardened polymer, but also its liquid pre-polymers and its degradation products. This usually requires more sophisticated considerations as monomers/small molecules are more reactive and toxic as compared to the hardened polymer.

The hardening process should be rapid enough, so that the total operation time can be reduced and hemorrhage can be stopped as soon as possible. To be competitive, TAs' hardening time must be comparable to that of suturing, the currently dominant wound closure technique. However, the hardening time should not be too short as surgeons need some buffer time in handling the wounds and glues. The heat released by the exothermic hardening process should be minimal so as not to cause damage to the tissue.

The requirements on the material's mechanical properties are equally important. The fluidity and the viscosity of the adhesive pre-polymers must be in the appropriate range so that they can spread across and wet the substrate surfaces completely. Good elasticity and plasticity is required especially for the uses at locations like joints and lungs. The yield strength, ultimate strength, burst strength, breaking strength and toughness as well are all of concern since TAs should carry the loads exerted onto the broken tissue by the patient's daily motions. Last but not least, the cost of TA must be taken into consideration. Most currently available TAs are significantly costlier than sutures.

1.2 Problem Statement of the Thesis

The first application of TAs in modern medical records was the application of the well-known "quick glue" by paramedics in Vietnam War to aid the soaring demands of wound closures for traumatized soldiers. The main component of the glue is the cyanoacrylate, which hardens within 30 seconds. Later, the discovery and uses of the human blood pool-derived fibrin adhesives was another inspiring case to encourage surgeons and chemists to put their effort in designing new adhesive materials for biomedical uses. Concentrated fibrin, when mixed with thrombin under the presence of Ca^{2+}, hardens in less than 1 min. Cyanoacrylate adhesives are acclaimed for its fast-setting and strong adhesion properties but they can only be used on external skin surface due to the non-biodegradability (the glue degrades at a very slow rate) and toxic degradation product [11, 12]. Fibrin glues can be used on both external and internal tissues but the adhesion strength is weak in many situations and therefore its functions reduce to be merely an adjunct as sealant and hemostat in most cases [7, 10]. Undoubtedly, new TA systems are needed.

For more than two decades, chemists and material scientists were striving to modify the chemistry and structure of the existing polymers or to develop novel systems from scratch to meet the requirements. Plenty of TA developments and syntheses were based on one common strategy made up of two steps: (1) choosing the readily available and FDA-approved polymers, such as poly(lactic acid), poly(glycolic acid), poly(ε-caprolactone), poly(ethylene glycol) and copolymers of the above, and (2) attaching them with the allegedly adhesive functional groups, such as alcohols, urethanes, acrylates, and

more recently, DOPA groups, etc [13-18]. Through these syntheses, functionalized polymeric systems, light curing systems, biomimetic systems have especially been made popular. (A complete review on the development of various TA systems is presented in *Chapter 2*.)

In theory, incorporating adhesive functional groups onto the non-adhesive polymer backbone should increase the adhesiveness of the material. If the polymer is biocompatible and biodegradable, it would then be a perfect marriage that leads to a material that fulfills the basic requirements of TAs – adhesiveness and biocompatibility. This strategy and its underlying hypothesis are straightforward and reasonable, as supported by the previous studies on the improvement of adhesion on engineering materials such as glasses [19].

However, most of the outcomes of these syntheses have fallen short of expectation. Although increments in the adhesion forces relative to the unmodified polymers has been observed in all published works, the magnitudes are still not sufficient to be used as TAs [15, 17, 20-23]. Surprisingly, the most fundamental requirement of TA – adhesiveness – were lacking in many of the cases. We believe that this is because ***the fundamental understanding of the adhesion of materials at molecular level on biological tissue surfaces is inadequate***.

Scientists understand that functional groups give polarity and reactivity to organic molecules and probably could promote adhesiveness. However, adhesion, as a

complicated phenomenon ranging from atomistic and molecular level to macroscopic level, is not easy to explain. The three elements – adhesive, substrate (or adherent), and environment – are all important determining factors in the question of whether good adhesion joint can be formed. Both chemistry and physical aspects of all these elements are significant. One very important aspect where TA is concerned is the presence of water/moisture on the substrate. How will this affect the adhesion of the polar functional groups to the substrate? What are the functional groups that should be present, in the first place? Jumping into experimental work or adhesive synthesis with these lingering questions is like looking for a needle in a stack of hay.

Hence, functional groups that are effective in tissue adhesion need to be first identified before synthesis. The key of this thesis is to sort out the adhesiveness of the functional groups, under both dry and wet environments, that can guide to map the future directions in TA syntheses.

1.3 Objectives and Scope of the Thesis

While the main direction of TA research is to develop new systems for use in internal organs, the objectives of this thesis, as a part of contribution to that main direction will be more fundamental. The objectives are:

(1) To study the physical adsorption mechanism in tissue adhesion;

(2) To identify the common functional groups that is adhesive to biological tissues;

(3) To devise a hypothesis of tissue adhesion based on theoretical and empirical studies.

The thesis aims to achieve the goals with some novel strategies. There are three sections in study, which are, (1) theoretical modeling of the tissue adhesion; (2) microscopic measurements of adhesion forces; and (3) macroscopic measurements of adhesion forces. The first two study methods are totally unprecedented and new in the field of TA development and are first introduced to have a better understanding of tissue adhesion; and the third part is to test out and refine the hypothesis from the modeling work. From the integrations of these sections, the thesis shall provide some insights into the correlation of molecular interactions and performances of adhesive joints.

This thesis dedicates a large portion to the theoretical study of adhesion, in which well-established molecular mechanics and dynamics (MM/MD, based on classical mechanics and dynamics), with the aid of computer, are applied to study specifically the

adsorption behaviors of various *functionalized small molecules* and *polymers* on a *model biological substrate*. There are a few other proposed mechanisms (see *Section 2.1*), adsorption is one of them. It is the most fundamental prerequisite for any other forms of interactions to occur and so it is pinpointed in this thesis.

The computer modeling study is made up of two parts. In Part I, adsorption interactions between small functionalized molecules and a segment of collagen triple-helix (CTH), which is chosen as the model biological tissue, are simulated. In Part II, adsorption interactions between short polymeric chains and collagen surface are simulated. The effect of water on the adsorption events is also directly or indirectly examined. The discussion is limited to only physical interactions because chemical interaction, which involves formation of covalent bonds with substrate, is not easy to form on biological surfaces. Only molecular mechanics and dynamics are considered and quantum mechanical effects are neglected.

Later, the thesis concentrates on empirical measurements where the results serve as supporting and complementary data to the hypothesis put forward in theoretical study. Adhesion forces are measured both microscopically and macroscopically in experiments. Atomic force microscope is used to measure the microscopic adsorption force between functionalized probe tips and collagenous substrate at molecular level. Four types of common functional groups, i.e. amine, carboxylic acid, hydroxyl and alkyl, are attached onto the probe and they are pressed against a collagenous substrate to yield the non-specific interaction force of interest. Joint test in lap shear configuration is done to

measure the macroscopic joint strengths. The joints are formed by two commercial tissue adhesives and two common adhesives on collagenous substrate.

1.4 Structure and Organization of the Thesis

The thesis is presented in three main sections: (1) MM/MD simulations, (2) AFM measurements of physical interaction, and (3) Lap-shear mechanical tests. Section 1 makes up more than half of the thesis and is the backbone that underlines the theme of the study. Results obtained from simulations are compared to that of section 2, both of which are the study of physical interaction at molecular level. In section 3, strengths of real joints with TAs of different functional groups are assessed and subsequently correlated to the simulation and AFM studies. Due to the difference of the background for each part, the literature review, the methods, and the discussions are presented in individual relevant chapters. All findings are then linked up in the final concluding chapter.

In *Chapter 2* of the thesis, the background of general theory of adhesion mechanisms is discussed and the various types of TAs, which are either commercialized or still under research, are reviewed. This chapter is important as it showed that the lack of basic understanding of functional groups in TA development.

In *Chapter 3*, the theory of the molecular mechanics and dynamics is presented along with a review on the use of molecular modeling and simulation on material interactions. This chapter forms the grounded basis for the following MM/MD works. *Chapters 4* and *5* then present the two parts of the modeling study: the former is the affinity of small functional molecules to a segment of collagen triple-helix; the latter is

the interactions between short oligomer chains and a collagen surface, under dry and wet conditions.

Experimental studies by atomic force measurement and lap shear test are shown in *Chapter 6* and *Chapter 7*, respectively. In the closing section in these chapters, their relevance to the modeling study is discussed.

Chapter 8 propounds some guidelines for the design of an effective TA based on all results and discussions and draws a conclusion to reemphasizes the hypothesis of tissue adhesion that has been made. Limitations of the study are mentioned. Recommendations for future studies in the field of TAs are also proposed in that chapter.

Chapter 2

Literature Review on the Current State of Tissue Adhesives

2.1 The Theories of Adhesion in General

So far, there has no one complete and self-sufficient theory that can fully explain the adhesion phenomena. Different schools of thoughts about the adhesion have been proposed but none of those works for all. Currently, the popular understandings on possible adhesion mechanisms accepted by many are: (1) **adsorption mechanism**; (2) **diffusion mechanism**; (3) **mechanical interlocking**; (4) **electrostatic attraction**. In fact, the contemporary belief is that each one of them plays a role, in different proportions, in an adhesion event. The proportion of each contribution is depending on the properties of the adhesive, adherent and conditions.

Adsorption mechanism is the hypothesis in which the adhesive molecules are attracted to adsorb onto the surface of adherent, either by means of chemical bonding (primary bonding, e.g. covalent bonds) or by means of physical bonding (secondary bonding, e.g. hydrogen bonds, van der Waals interactions, metal ion complexes, etc). This mechanism is always ubiquitous in any case since van der Waals interactions are present between any two substances. For instance, pressure-sensitive adhesives, which is often seen on the back of the post-it notes on our desktop, adhere to adherent based

purely on the reversible van der Waals interaction [24]. In some special cases, adhesives that are designed to carry certain functional groups adhere onto well-studied adherent surfaces by forming chemical bonds. The primary bonds are generally stronger and hence more desirable. However, chemical bonds generally require demanding conditions and specific chemistry requirements, e.g. catalysts, to form. Sometimes, the needs of excitation energy or of catalysts impose more difficulties on TAs to function at biological substrates.

Diffusion mechanism is not less important than adsorption. In this hypothesis, the adhesive and adherent molecules inter-diffuse into each other at some depth to form an inter-phase layer, which results in entangled network that binds the two moieties together. One example is the ironed-on adhesives on badges that bind tightly onto fabrics upon applying heat through ironing. The low-melting point adhesives melt and diffuse into the fibrous network of fabrics to form a strong joint. Diffusion is a time- and temperature-dependent process, although it is usually a spontaneous process, which is entropy-driven, when the right condition is met. It follows that if a strong joint were to be resulted from diffusion mechanism, sufficient elapsed time should be given before the inter-phase layer has formed. One of the pre-requisites is that, of course, the two materials are not "phobic" of each other, i.e. there is a certain degree of affinity between them so that adsorption, in the first place, could happen. Since the temperature under which TAs is always fixed, i.e. the adherent at ~ 37 °C and the surrounding environment at ~ 20 – 25 °C, there is no much room for us to increase the diffusion rate by altering temperature. And, since TAs requires a short setting time (see *Section 1.1*), we need to have adhesive molecules with

high coefficient of diffusion. From practical point of view, polymerization adhesive systems would outdo the others because small monomer molecules are fast diffusers.

Mechanical interlocking was proposed after the repetitive observations of the general fact that adhesion joints on unpolished surfaces are usually stronger than those on polished ones. Furthermore, increasing the microscopic surface irregularities by means of, for example, sand-blasting usually helps to improve the performance of the adhesion joint formed thereon, as compared with those without processing. In the hypothesis, the surface irregularities provide micro-environments, i.e. micron-sized spaces or pores, into which the adhesive molecules fill, reside and cure. The hardened adhesive, usually accompanied by crystallization or swelling in size, is then locked in these irregularities. Again, for this event to occur, affinity between the adhesive and the adherent (i.e. adsorption) is the pre-requisite otherwise the adhesive would not even wet the surface and fill into the pores. For adsorptive moieties, the surface irregularities serve an additional function, that is, to increase the contact area between the adhesive and adherent and therefore maximize the adsorption energy. Furthermore, in the use of TAs, it is not possible to alter the surface roughness of the soft tissues and hence this mechanism is regarded as a consistent parameter.

Electrostatic attraction hypothesis says that when adhesives and surfaces are oppositely charged, and one of them is electrical insulator, the moieties would attract and adhere due to coulombic interaction between them. In one way, this can be

subcategorized under the adsorption mechanism hypothesis. Also, this hypothesis is framed mainly for the more practical point of view, for instance, how to prepare a good polymer coating on metal surface, and the similar practice is generally not feasible for biological tissues. By no means could the biological tissues be moderately or strongly charged and even if they could, the charge is expected to slowly dwindle away in the electrolytic environment. Throughout the report, electrostatic attraction mechanism is combined in the adsorption mechanism and is not discussed separately.

This scope of this thesis, as a head start, focuses only on adsorption mechanism. This mechanism is deemed to be the most important one because it is universal to all interacting moieties and it is a prerequisite for the other mechanisms to function. Other mechanisms, especially diffusion, are also relevant to tissue adhesion but in order for diffusion to occur the affinity between the adhesive and substrate has to be first established. Hence, the scope here will only cover adsorption mechanism, which is already a very big topic.

2.2 Tissues Adhesives in Market and under Researches

2.2.1 Cyanoacrylate Adhesives

Cyanoacrylates are renowned fast-setting strong instant glues which is widespread in household applications. It is a hard, clear and glass-like resin which will rapidly polymerize at room temperature in few seconds without any supply of catalyst, on virtually any substrate. Its usage in clinical applications was first reported in the early 1960's by Coover et al. [25] and it received the most attention among all tissue adhesives since then due to its fascinating properties. Cyanoacrylate monomer is a molecule that is highly polar and has a chemical structure as shown in *Figure 2.1*.

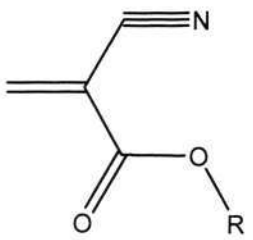

R = alkyl (eg. ethyl, butyl, octyl)

Figure 2.1 The chemical structure of a n-alkyl cyanoacrylate molecule.

Due to the great electron-drawing ability of the cyano group, the monomers can polymerize in a very rapid manner through anionic polymerization that is catalyzed by weak nucleophiles, such as water. This polymerization is an exothermic process, which cause temperature increase in local site where the adhesive is applied. The amount of the

heat and the increase in temperature depends on the amount of applied cyanoacrylates [11]. *Histoacryl*^{TM}, a commercialized cyanoacrylate adhesive product, was compared with silk sutures and results show that it was less prone to inflammatory and giant cell reaction compared to silk sutures [26]. The bond strength of butyl-ester cyanoacrylate was compared with another two tissue adhesives, namely fibrin adhesive and mussel protein adhesive and it shows a superior strong bonds with cartilage, bone and skin tissue [27]. It has been used in facial plastic surgery, scalp wounds, otorhinolaryngology and childhood lacerations and is considered as an alternative to suturing [28].

However, many regulatory institutions have held back the usage of cyanoacrylate adhesives for internal organs. In practice, surgeons use cyanoacrylate adhesives for external wounds only and in unusual circumstances or emergency cases. It was found that during the degradation process toxic and carcinogenic material, e.g. formaldehyde and alkyl cyanoacetate, are liberated. Formaldehyde is toxic and is also claimed as a human carcinogen when it is present in high amount [12]. When it is used in external tissues, the adhesive usually remains in place for a period of time and then it can either slough away or be washed away as the skin cells regenerate themselves and the natural healing process takes over.

In summary, cyanoacrylates are still not the most ideal tissue adhesive in their current form. It will be considered as a perfect tissue adhesive only when the toxicity issues and improvement in their degradation rate are addressed.

2.2.2 Fibrin Adhesives

Fibrin adhesive was first implemented by Grey in cerebral surgery [11]. After the protein separation technology was developed in 1938, purification of thrombin and fibrinogen became possible and their combination was first used in 1944 in World War II to enhance the adhesion of skin grafts in soldiers with severe burn injuries [10]. The year 1972 was marked by a renaissance of fibrin sealing developed in Vienna for reuniting nerves in humans [29]. In the late 1970's, the utility of fibrin adhesives in cardiovascular surgery was recognized. Since then, fibrin adhesives have been used in conjunction with sutures in a wide range of surgical procedures, including cardiothoracic, head and neck surgery, thyroid surgery, neurosurgery and vascular surgery [30].

Fibrin adhesives are surgical haemostatic agents derived from human plasma that are designed to reproduce the final steps of the physiological coagulation cascade to produce a stable fibrin clot. The formulation of a typical fibrin adhesive comprises of fibrinogen (human plasma), thrombin (human or bovine plasma), calcium chloride, Factor XIII (human plasma or placenta), and fibrinolytic inhibitors. The clotting process is basically a polymerization process of fibrin monomers, which are products of fibrinogen cleavage upon reaction with thrombin. The mechanism is illustrated in Figure 2.2.

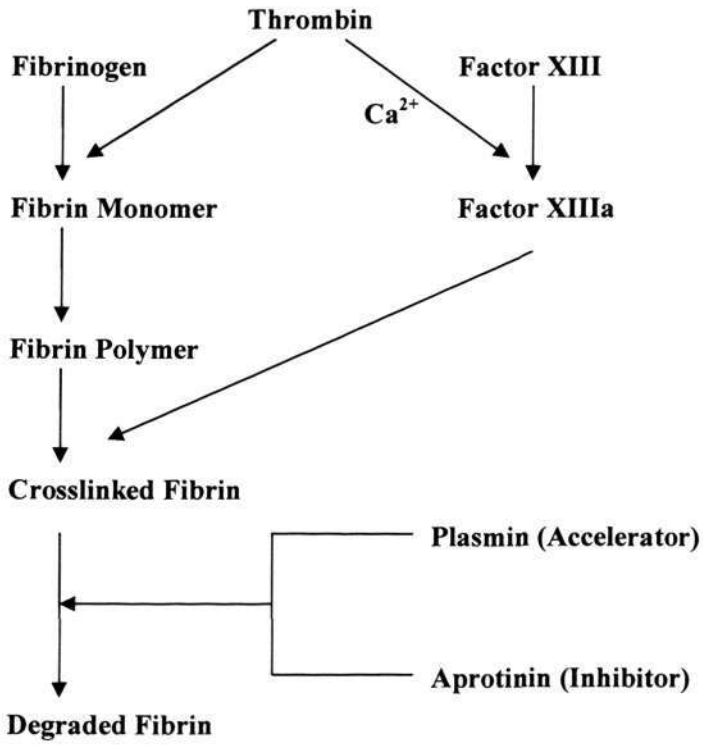

Figure 2.2 The hardening mechanism of fibrin adhesives.

Thrombin plays a pivotal role in the coagulation mechanism. In the first place, it cleaves the peptide bonds in the fibrinogens and converts them into fibrin monomers, which will form a soluble soft fibrin polymer clots. At the same time, in the presence of Ca^{2+}, it converts Factor XIII into Factor XIIIa, which promotes the cross-linking process of the fibrin polymers. In order for the clots to anchor to the injury site, cross-linking between fibrin and adhesive glycoproteins as well as cellular glycoproteins must be promoted [31, 32]. The concentrations of fibrinogen and thrombin are very important in terms of the strength of the resulting clots and the set time. It is reported that higher fibrinogen and thrombin concentration results in higher strength and that higher thrombin concentration results in rapid polymerization. After the clot has been formed, it tends to be lysed by plasmin and lose its strength. Since tissue will take some time to regain its full strength, the support cannot be removed within this period. Fibrinolytic inhibitors, such as aprotinin, is also one of the ingredients in the adhesives to help delay the rapid plasmin-mediated lyses of stable fibrin clots[33].

Those fibrinogen adhesives available commercially are usually supplied in two separate syringes: one with mixture of fibrinogen/aprotinin and another with thrombin/calcium chloride. The adhesives achieve 75% of its strength in the first ten minutes after mixing and the full strength is claimed to be reached in 2 hours [34]. Preparation steps for fibrin sealant could be quite a tedious task because the products need to be stored in fridge and require thawing right before application [7].

Moreover, fibrin adhesives show a poor mechanical strength and sometimes it may not meet the requirements [27]. The possibility of viral transmission is also a main issue of concern because it is derived from individuals' plasma which may carry viruses. This is the main reason why U.S. Food and Drugs Administration (FDA) was barring fibrin adhesives before 1978. Therefore, the donors to the government-licensed blood transfusion/plasmapheresis centers complying with national standards must be carefully selected and screened according to legal requirements and international scientific criteria. In the manufacturing process, a number of steps such as precipitation, chromatography, pH treatment, filtration, pasteurization, vapor heating, solvent-detergent treatment, can be done to reduce viral load to a high extent [7]. This long and tedious process renders the glue extremely pricey.

Nevertheless, it can be a very good adjunct to sutures. On one hand, sutures provide the required mechanical strength and on the other, fibrin adhesives reinforce the strength and at the same time stop hemorrhage, i.e. blood leakage from suture hole [30].

2.2.3 Gelatin-Based Adhesives

Resorcinol-Formaldehyde-Glutaraldehyde (GRFG) Adhesives

Gelatin, with a cross-linking agent such as formaldehyde or glutaraldehyde, is capable of setting through gel formation in a few minutes. Resorcinol is added into the formulation to improve the bond strength by producing a more complex cross-linked network [35]. BioGlue is a currently approved gelatin adhesives in United States for the limited use as an adjunct to sutures/staples to achieve haemostasis.

GRFG glue was used to treat aortic dissections for the first time in the late 1970s [36] and today its main usage is in the thoracic and general vascular operations because it can fill in the dissection and close the cavity to provide a stronger arterial wall [37, 38]. Its ability to adhere to wet surface, moderate degradation rate, and adjustable curing profile has also improved its competency over other type of tissue adhesives. In addition, the bonding strength of GRFG adhesives were reported to be comparable to the cyanoacrylates in both wet and dry conditions (simulating internal surface and external surface conditions) and to be 4 times stronger than that of fibrin adhesives. Its bond strength on other soft tissues such as hepatic and renal tissues has also gained satisfactory results and increases its potential to be used in other parts of body.

However, the worries about the toxicity and carcinogenicity of the formaldehyde have limited the expansion of its application. Therefore, in most formulation the formaldehyde is replaced by glutaraldehyde and glyoxal, which are less toxic

[39].Furthermore, the inflammatory effects and the long-term stability of these adhesives are still questionable [40].

Gelatin-Poly(L-Glutamic Acid) Adhesives

A group of researchers from Japan, led by Y. Otani, had developed another type of gelatin-based biological glue, which is a hydrogel containing aqueous mixture of gelatin and poly(L-glutamic acid) which can be cross-linked by water-soluble carbodiimides (WSC). While gelatin forms the matrix of the adhesive, poly(L-glutamic acid) reduces the gelation time up to a level which is comparable to that of fibrin glues. Yet, this adhesive exhibited firm adhesion to the mouse skin and other soft tissues with a higher bonding strength than fibrin glue [14]. A series of tests on haemostatic capability in dog spleen [41] and air-leak sealing effect in rat lung [42] were also conducted by the same group after 1996. The success rate of complete haemostasis was reported to be significantly greater than that of fibrin glue and no air leakage was observed at the lung pressure as high as 50cm H_2O. To prevent the premature setting of the components during storage, urea was added and exhibited good prevention of spontaneous physical cross-linking process and no significant side effect [22]. However the adhesive is still in the clinical trial stage and hence has not been approved for commercial use yet.

2.2.4 Protein adhesives

Most marine creatures possess some very unique characteristics to overcome the harsh environment in the sea. For instance, mussels and barnacles can produce very strong moisture-resistant adhesives to stick themselves onto rocks, the ship hulls, woods and plants even in wet environment with fluctuating salinities, under a wide range of temperatures and vigorous bombardment of waves and tides. When mussels get close to a substrate, they place their foot very close to the surface and expel all the water to create a partial vacuum. Then it pumps liquid protein produced by special glands in its foot into the area at where the protein immediately forms sticky foam that contains numerous tiny threads. These threads are insoluble polymer fibers that adhere to the surface stiffly [43].

Therefore, much attention in research of TA in the recent year has been directed to bio-mimic this natural glue. The early investigation of the adhesive polyphenolic proteins extracted from *Mytilus Edulis*, a common mussel, revealed that this protein consists of a specific decapeptide sequence which is believed to play the key role in adhesion. These peptide includes proline/hydroxyproline, serine, threonine, lysine, tyrosine/3,4-dihydroxyphenylalanine (DOPA), and alanine [44] which form either hydrogen bonds, ionic bonds, or metal complex bonding with substrates. The presence of lysine, tyrosine and DOPA residues on the polymer also provide the essential crosslink sites that strengthen the proteins' polymeric network. Atlantic mussel, *Geukensia demissa*, another type of mussel, is also capable to excrete adhesive protein. However, instead of the decapeptide sequence, an abundant tripeptide sequence is observed. This sequence is glycine-dihydroxyphenylalaine-lysince sequence [45]. As a result, Deming and Yu had

proposed that it was not the residue sequence that actually gives the stickiness but the presence of specific functionality groups [46]. DOPA residue is regarded as the primary adhesion and crosslink sites on mussel adhesives protein. Their research work in 1999 concluded that the catechol functionality on DOPA residues is the primary factor responsible for moisture-resistant adhesion and the oxidized o-quinone functionality is mainly responsible for cross-linking [47].

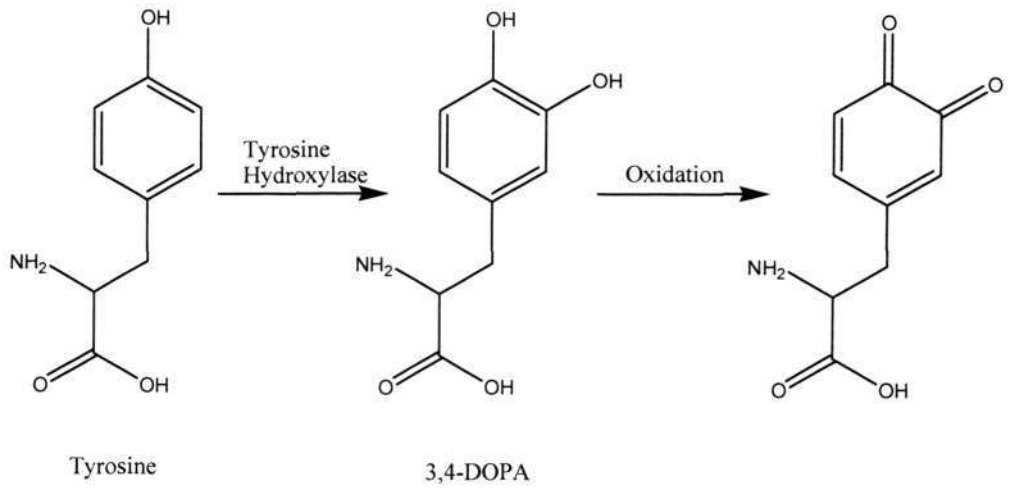

Figure 2.3 The hydrolysis and subsequent oxidation process of Tyrosine to yield adhesive groups.

Several ways had been implemented to produce these protein adhesives. In the early stage, researchers harvested the polyphenolic proteins from Mytilus Edulis. However, this output of the method is very low because extraction of only 1kg of adhesive protein would need 100,000 common mussels.

Then, scientists from Gentex [48] employed genetic engineering path. They coded for the protein and inserted this gene into yeast cells, which would in turn produce a larger batch of protein resins. Simon et al. working along similar path tried to extract the

adhesive protein from tobacco plants, which is relatively easy to genetically modify [30]. However, it has not been too successful and therefore, some chemists started to explore incorporating the DOPA residue into their polymers.

Protein adhesive may have great potential in the future but it is still at infantile stage at this point of time. A number of aspects, including biocompatibility, biodegradation or bio-absorbability, haemostatic effect, bonding strength, toxicity, and inflammatory issues, still have to be carefully investigated.

2.2.5 Chitosan-based Adhesives

Chitosan is the partially N-deacetylated product of chitin, which is poly-β-(1→4) linked N-acetyl-D-glucosamine abundantly present in the exoskeleton of arthropods and crustaceans. Chitosan has a hydrogel-forming property. It is nontoxic, biocompatible and biodegradable under the presence of lysozyme [49] and some other enzymes. Its potential in wound-healing acceleration [50] and haemostatis [51, 52] has also been observed. It showed a very good haemostasis performance in which it brought down the whole-blood clotting time by about 40% of normal.

K. Ono et al. [16] has reported a photo-cross-linkable tissue adhesive using chitosan as the backbone of the polymer. In this system, azide and lactose were introduced into the chitosan molecules to provide it with the ability for being photo-crosslinked and the enhanced solubility in water at neutral pH. Azide groups receive the energy from UV irradiation and convert into highly reactive nitrene groups, which

interact quickly with each other or with amino groups of the chitosan to generate azo groups and thus causing gelation. Hydrogel was obtained within 60s under UV irradiation and bonding strength of higher concentration sample was comparable with fibrin glue. Cell culture did not show any cytotoxicity in various cells. Further study of bursting strength was assessed with removed thoracic aorta, trachea, and lung of farm pigs and rabbits [21]. In these tests, the sealing effect was proved to be better than that of fibrin glue. In vivo tests have also been done in rabbits and all the animals survived after one month after implantation. Histological examinations showed that a fraction of the chitosan hydrogel was phagocytosed by macrophages, had partially degraded, and had induced the formation of fibrous tissues around the hydrogel. Polyampholytic hydrogels were also created by mixing deacetylated and *O*-carboxymethylated chitins in aqueous solution at various compositions [17]. The adhesion strength was enhanced by the cross-links formed though ionic interactions between cationic and anionic groups.

2.2.6 Polyester-based Adhesives

Polyesters such as polylactide, polyglycolide and polycaprolactone have been used extensively in biomedical products. Firstly, they are biocompatible and biodegradable. The degradation products are also biocompatible and bio-absorbable. They can be synthesized with a wide range of molecular weight. Their degradation profile in aqueous environment is tailorable by altering the compositions or preparation steps. Absorbable suture threads are also made of these materials. It may have potentials in synthetic biodegradable tissue adhesives and the following paragraphs review some of the development.

Polyester in Urethane Adhesives

Polyesters were end-capped with urethane functionality to make the urethane adhesive biodegradable. The urethane pre-polymer were prepared by reacting the biodegradable polyesters with an excess of diisocyanate such as hexamethylene diisoyanate (HMDI), toluene diisocyanate (TDI), or diphenylmethane diisocyanate (MDI) in order to produce polyesters with terminal isocyanate functionalities [13]. Isocyanates can form urethane bonds that connect the polymer chains to form a network when they are in contact with water. This polymer was first applied to tissue bonding in the late 1950s [53], and to repair bone fractures [54]. In vivo performance of polyurethane adhesives showed some adverse tissue response. Therefore further improvements are still necessary before it can be widely used.

Polyesters in Hydrogels

Other than that, polyesters were made into bio-absorbable synthetic hydrogels, a more recently emerging tissue adhesive. One of these hydrogels has been commercialized under the trade name, *FocalSeal*^{TM}, which is used as sealant in surgery of lungs. Hydrogel is formed by the photo-polymerization process of water-soluble block oligomers. An oligomer comprising a central block of poly(ethylene glycol) (PEG), followed by the hydrolyzable block such as lactate oligomeric segments at both ends, is end-capped with photo-polymerizable acrylate acid groups. During in-situ application, three layers of these pre-polymers, with slight compositional change, are brushed onto the tissue. Photo-polymerization process is then accomplished by irradiating visible light of specific wavelengths for around one minute [55, 56]. The concern of heat related tissue necrosis

due to the photo irradiation is minimized because the formulation contains more than 80% of water. The hydrogel then gradually breaks down by hydrolysis at the ester linkage and liberates biocompatible products which can be excreted. The strength of this adhesive was shown to be must superior than that of fibrin adhesives.

Temperature-responsive Branched Polyesters

Recently, a new generation of polyester tissue adhesives was being developed and the hardening mechanism is based on the temperature-dependent rheological behavior of these polymers. As known in polymer science, polymers with low molecular weight have a sensitive temperature-dependent viscosity. This means that as there is a small temperature drop in the environment, the flowability of low molecular weight polymer can increase by a great amount. Cohn and Lando [15] have produced oligomeric branched polyester that were synthesized using trimethylolpropane (TMP) as the trifunctional central molecule, with lactoyl and caprolactone segments added on the three arms on this central molecule. While the lactoyl segments provide the mechanical and adhesive strength of the materials, incorporation of a small amount of caprolactone into the oligomers can alter the flexibility of the polymer chains, resulting in a great shift in glass transition temperature. By choosing the oligomer with the most appropriate glass transition temperature and adhesive strength, this material can then be used as tissue adhesive. The authors concluded that the TMP(LA_{16}-CL_2-LA_{16}-CL_2-LA_{16})$_3$ possessed the best combinations of temperature and mechanical properties. It exhibits an outstanding adhesive behavior under in vitro conditions with a remarkably higher adhesive strength that those attained by *Dermabond*^{TM} and *Histocryl*^{TM}. Furthermore, this low molecular

weight block copolymer display low viscosity at a clinically acceptable temperature and become much more viscous at 37°C. However, the adhesion mechanism of the polyesters remains obscure.

Chapter 3
Theory and Literature Review on Molecular Modeling and Simulation

3.1 Overview of Modeling and Simulation Theories

As laid down in the objectives (see *Section 1.4*), the identification of adhesive functional groups is the primary concern in this thesis. It is aimed to provide an alternative and less costly way – computational modeling and simulation method – to predict the adhesiveness of certain functional groups. Computational modeling and simulation has recently become a very essential and value-adding tool in many aspects of scientific research, thanks to the advancement in the hardware, e.g. high computational speed, memory and storage – which were not achieved until recent decades. This thesis explores the potentials of using the computational modeling and simulation methods to study the interaction between molecules/polymers and biological tissues. As a whole, there are different modeling and simulation tools on various levels based on their theories, scales of study, fundamental assumptions, complexity in mathematical formulations, durations of runs, and areas of applications, as stated below:

(1) *Ab initio* methods;

(2) Density functional theory (DFT) methods;

(3) Molecular mechanics and dynamics (MM/MD) methods;

(4) Meso-scale modeling methods; and

(5) Finite element analysis (FEA) methods.

Ab initio (literally means "from the beginning" in Latin) method is the most fundamental atomistic simulation done by solving Schrödinger equations to obtain the wave-functions. It represents the most accurate method but the time and storage space needed are also tremendous; and so it can usually handle only small systems. The next closest approximation is the DFT in which spatially dependent electron density functions are used to approximate the wave functions. This method still needs a rather long duration though quicker than *ab initio* method. To have a balance of both short processing time and to include more molecules in atomistic simulation, MM/MD will be a good choice. The bonding and non-bonding interactions are all described in mathematical forms – based on classical mechanical and dynamics – whose parameters are validated through empirical and/or *ab initio* studies. At larger length scales, *meso*-scale simulations ('*meso*' means 'intermediate' in Greek) and FEA suffice the requirements, at the expense of the loss in accuracy of atomistic information (which may be unnecessary at that length scale). *Figure 3.1* is a summary of simulation methods at all time-scale and/or length-scale and their accuracies.

MM/MD method is implemented for the study in this thesis because of a few considerations. First, the adsorption behavior is a molecular phenomenon that happens at nano-scale; hence quantum mechanical and all-atom empirical methods fit this purpose. Second, biological tissue surface and macromolecules are made up of the number of atoms that is best described by all-empirical methods at acceptable simulation time and degree of accuracy (*Figure 3.2*).

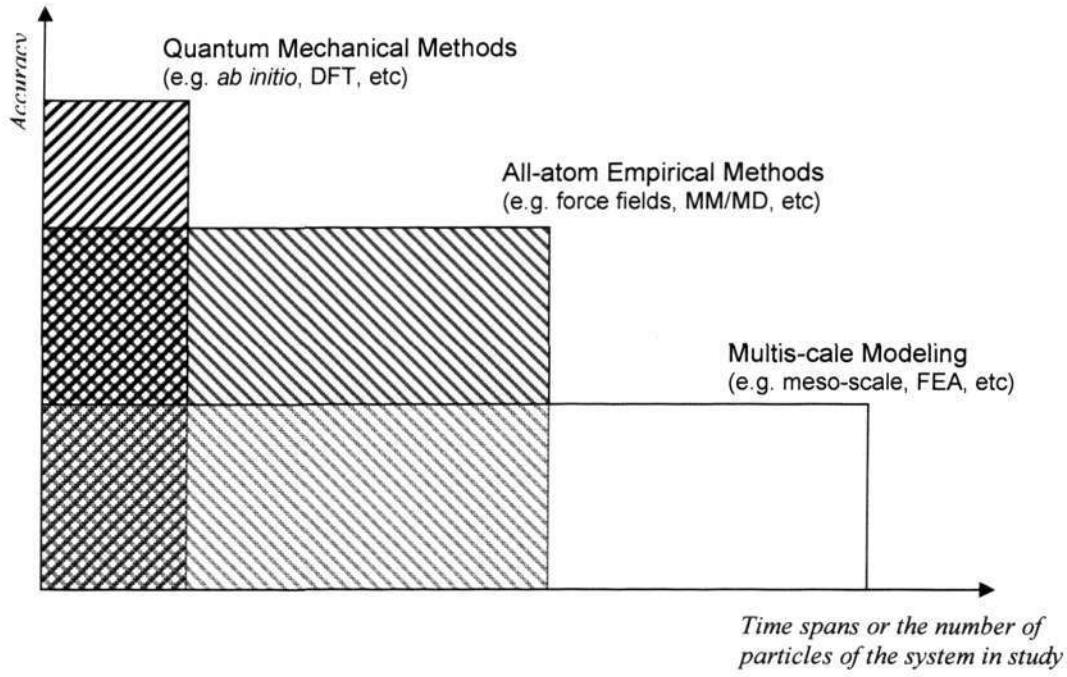

Figure 3.1 the time-span or the number of particles that each simulation methods can effectively handle, and the degree of accuracy of these methods.

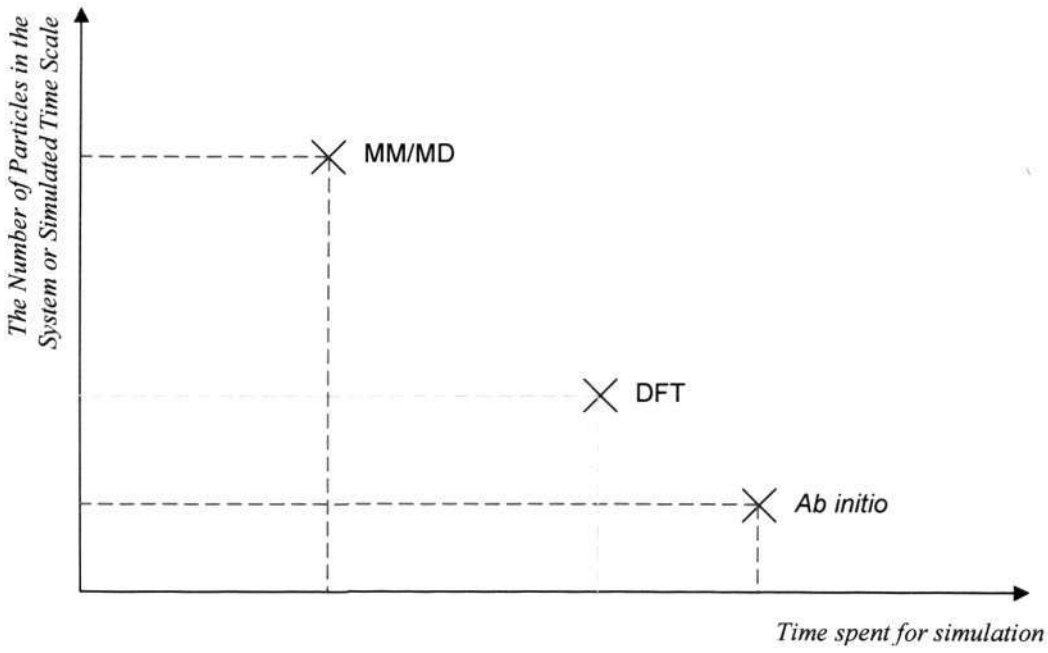

Figure 3.2 Comparison of the atomistic simulation methods in terms of the dimensional scale of the system studied and the time required in running the simulations.

3.2 Theory of Classical Atomistic and Molecular Simulation

3.2.1 The Material Studio Software

Material Studio is a modeling software providing different simulation environments for modeling at various scales. It is developed by *Accelrys* and has gained growing popularity in research and engineering fields. The particular program used for the atomistic MM/MD simulations in this thesis is called *Discover*, which executes all the jobs including atom typing (i.e. assignment of force fields to the atoms constructing the molecules), charge assignment, structural optimization and dynamics run.

3.2.2 The Force Fields, the COMPASS and its Parameterizations and Validation

Force field, in the context of MM/MD, is an approximated mathematical function describing the potential energy surface on which the atomic nuclei move in a structure. Its development is based on Born-Oppenheimer approximation, which assumes that the motions of electrons and nuclei in a structure can be decoupled due to their huge difference in mass. Two separate equations are yielded: the first describes the electronic motion that given rise to the potential energy surface; and the second describes the motion of the nuclei on this potential energy surface. At the extreme of accuracy, the first equation should be solved by *ab initio* quantum mechanical/chemical codes, which would cost a huge amount of efforts. Therefore, empirical fits to the potential energy surface are available to improve simulation efficiency. Using force field to describe the potential energy surface, the second Born-Oppenheimer equations can be solved.

COMPASS (Condensed-phase Optimized Molecular Potentials for Atomistic Simulation Study) is one of these force fields. It is however distinct from the other force fields because it is the first force field in which most of the parameters derived from *ab initio* calculations. After that, these parameters (especially van der Waals parameters) were adjusted based on the gas phase experimental data to yield good agreement with experiments. For covalent molecular systems, the adjustment was done based on molecular dynamics simulations of liquids. Finally, these parameters are extensively validated using various calculation methods, including extensive molecular dynamics simulation of liquids and polymers [57-59]. The mathematical expression of the COMPASS force field is shown as followed:

$$E_{pot} = \sum_{b}[K_2(b-b_o)^2 + K_3(b-b_o)^3 + K_4(b-b_o)^4]$$

$$+ \sum_{\theta}[H_2(\theta-\theta_o)^2 + H_3(\theta-\theta_o)^2 + H_4(\theta-\theta_o)^2]$$

$$+ \sum_{\phi}\{V_1[1-cos\phi] + V_2[1-cos2\phi] + V_3[1-cos3\phi]\}$$

$$+ \sum_{\chi} K_\chi(\chi-\chi_o)^2 + \sum_{b}\sum_{b'} F_{bb'}(b-b_o)(b'-b_o')$$

$$+ \sum_{\theta}\sum_{\theta'} F_{\theta\theta'}(\theta-\theta_o)(\theta'-\theta_o') + \sum_{b}\sum_{\theta} F_{b\theta}(b-b_o)(\theta-\theta_o)$$

$$+ \sum_{b}\sum_{\phi}(b-b_o)(V_1 cos\phi + V_2 cos2\phi + V_3 cos3\phi)$$

$$+ \sum_{b'}\sum_{\phi}(b'-b_o')(V_1 cos\phi + V_2 cos2\phi + V_3 cos3\phi)$$

$$+ \sum_{\theta}\sum_{\phi}(\theta-\theta_o)(V_1 cos\phi + V_2 cos2\phi + V_3 cos3\phi)$$

$$+ \sum_{\phi}\sum_{\theta}\sum_{\theta'} K_{\phi\theta\theta'} cos(\theta-\theta_o)(\theta'-\theta_o') + \sum_{i>j}\frac{q_i q_j}{\varepsilon r_{ij}}$$

$$+ \sum_{i>j}\left[2\left(\frac{r_{ij}^o}{r_{ij}}\right)^9 - 3\left(\frac{r_{ij}^o}{r_{ij}}\right)^6\right]$$

(Equation 3.1)

In total there are thirteen terms in the COMPASS. The first three terms describe the most basic distortions in molecules – bond stretching, angle bending and torsions – respectively. The fourth is the out-of plane distortion. The fifth to eleventh terms describe all the cross-term coupling interactions. In sequence, they are bond-bond, angle-angle,

bond-angle, bond-torsion, bond-torsion (1-3), angle-torsion and angle-angle-torsion, respectively. Then, the twelfth and the thirteenth terms (the non-bond terms) describe the secondary interactions – coulombic and van der Waals (vdW) interactions – respectively. VdW is described by the Lennard-Jones 9-6 equation, which give "softer" repulsion at close proximity compared to the conventional 12-6 equation. All these terms are importantly involved in the structural optimization and dynamics run, and the last two non-bond terms play pivotal roles in the final analyses of physical adsorptions. (The parameters of certain atoms are attached in *Appendix 1*.)

3.2.3 Simulation Factors

Non-bond Cutoffs

The computation of both the two non-bond terms in *Equation 3.1* involves *r*, the distance between particles. The asymptotic mathematical forms imply that they eventually approaches zero at far enough distances. Therefore, to save time and storage space, it is common to impose cutoff distances to the non-bond terms, i.e. distances beyond which the interaction energies of widely separated pairs are completely neglected. This however generates a square step on the energy function at the cutoff. A small extension of distance past cutoff, which is termed as spline width, can be set to smooth the edge by some polynomial functions. Beyond the spline width, an even smaller buffer width is set. This interval includes atoms in a buffer region that might move close enough together to contribute to the energy calculation.

Dielectric Constant

Dielectric constant in the coulombic term is set as unity for vacuum environment. Although this value coincides with the dielectric constant of vacuum in physical world, it has a different physical meaning – for instance, the dielectric constant of pure water at 20°C is 80.1 (at 20°C) in physical world but 4 (as suggested in Material Studio manuals), regardless of the temperature, in the simulation space.

Periodic Boundary Condition

Periodic boundary condition is a commonly used strategy in atomistic simulation to represent a structure of atom array at larger scale by an atom array in smaller scale that can be handled by the operating system. After constructing a small-scale structure (a "cell"), applying periodic boundary condition commands the system to treat the structure as if it is repeating itself, adjacent to the cell, in all three x,y,z-directions. This strategy treats the cell as one center piece of the bulk structure, and includes the interactions between atom at the edge of the cell and atom on the adjacent mirror cell within the preset cutoff distance.

Fixed Atom Constraints

Constraints are imposed onto selected atoms so that they are pinned at given locations in space (i.e. coordinates) throughout the simulation. Carefully applying constraints to certain atoms can reduce the expense of a calculation and improve efficiency because some terms in the energy expression involving only fixed atoms can be eliminated. More importantly, constraints are used to maintain more realistic molecular structures and

configurations, especially when an agitation dynamics process is included in the simulation workflow. If the constraints are absent, some defined molecular structures may be seriously perturbed in these agitations. In the thesis, constraints are used to ensure that the triple-helical structure of collagen can be preserved.

3.2.4 Optimization of Molecular Structure

The as-sketched molecular structures, especially for big molecules, are neither perfect nor stable, as they might contains a lot of strains ("hot spots") in their bond lengths, bond angles, torsion angles, etc. These imperfections have to be perfected by optimizing the structure via established mathematical algorithms.

Currently, three optimization algorithms are often used. Structural optimization is also frequently referred to as structural minimization since this is in fact minimization of the given potential energy expression in a multi-dimensional space. These minimization algorithms are (1) steepest descent; (2) conjugate gradient; and (3) Newton-Raphson method. Generally speaking, structural optimization is a two-step process. First, the energy of a conformation of a structure is evaluated; second, the conformation is adjusted to reduce the energy to a lower value based on the force fields. This process is done by *line search* – where lines are drawn over the potential energy surface to generate a point of lower values until minimum (within a given convergence limit) is reached. The three algorithms basically are different from each other in terms of their line search methods.

In steepest descent algorithm, the line search direction is simply defined along the direction of the local downhill gradient, $-\nabla E(x_i + y_i + z_i)$. One characteristic of this algorithm is that the new line is always perpendicular to the previous one, and therefore, the required number of iterations to reach minimum is great since the directions of the lines are reversed from the previous in every step. Nonetheless, it is a very robust method and is applicable to most structures, including the ones with complicated potential energy surfaces. This is frequently used as the first stage of an optimization process.

In conjugate gradient algorithm, the line search direction is determined by both the previous direction, scaled by a constant factor, and the current gradient. Mathematically, it is expressed as:

$$\boldsymbol{h}_{i+1} = \boldsymbol{g}_{i+1} + \gamma_i \boldsymbol{h}_i$$

(Equation 3.2)

Where $\boldsymbol{h}_{i+1}$ is the new direction vector leading from point i+1

$\boldsymbol{g}_{i+1}$ is the gradient at point i+1;

$\boldsymbol{h}_i$ is the previous direction; and

γ_i is scaling factor determined by either $\gamma_{i+1} = \frac{(\boldsymbol{g}_{i+1} - \boldsymbol{g}_i)\cdot \boldsymbol{g}_{i+1}}{\boldsymbol{g}_i \cdot \boldsymbol{g}_i}$ (*Polak-Ribiere* method) or $\gamma_i = \frac{\boldsymbol{g}_{i+1}\cdot \boldsymbol{g}_{i+1}}{\boldsymbol{g}_i \cdot \boldsymbol{g}_i}$ (*Fletcher-Reeves* method).

Since more parameters and equations are involved, the time used in each iteration step is considerably longer than that of steepest descent. Nonetheless, the efficiency is better

when closer to minimum. So, it is usually used in fine-tuning steps after first 10-100 iterations of steepest descent algorithm.

Newton-Raphson method is a more sophisticated method that uses the second derivative (the curvature) of the force field, in addition to the gradient of a search direction, to identify the minimum of the function along that direction. The predicted minimum along the direction can be obtained by the following equation:

$$r_i = r_{i-1} - \boldsymbol{A}^{-1}(r_{i-1}) \cdot \nabla E(r_{i-1})$$

(Equation 3.3)

Where r_{i-1} is a starting point determined from the previous iteration;

$\boldsymbol{A}^{-1}(r_o)$ is the inverse matrix of second partial derivatives of the energy with respect to the coordinates at r_o (A is referred to as Hessian matrix too); and

$\nabla E(r_{i-1})$ is the gradient of the potential energy at r_{i-1}.

This is usually used after conjugated gradient as value closer to the true minimum can be generated rather effectively and efficiently. However, it handles systems with a size smaller than 100 atoms because of the tremendous memory space needed to store the second derivative matrices.

For the studies in the thesis, these three algorithms are implemented back to back, as recommended, with the transitions set at certain convergence levels. These criteria are mentioned in the method sections in the following chapters.

3.2.5 Dynamics Run

Dynamics run is a simulation process in which the locations and motions of atoms in a system is calculated at a preset temperature and/or pressure. The return of the simulation is a trajectory file that consists of all atomic configurations, atomic velocities and other information recorded at certain intervals throughout the run. The trajectory file can then be analyzed to yield equilibrium thermodynamics properties of interest.

Newtonian's Equations of Motions

Dynamics, in its simplest form, is nothing but the integration of the most familiar Newton's second law, as seen in most elementary physics textbooks:

$$\boldsymbol{F}_i(t) = m_i \boldsymbol{a}_i(t)$$

(Equation 3.4)

where $\boldsymbol{F}_i(t)$ is the external force;

m_i is the mass of the object; and

$\boldsymbol{a}_i(t)$ is the resulted acceleration.

Relating the force with the potential energy, *Equation 3.4* can be expressed in a more relevant form in modeling and simulation:

$$-\frac{dV_i(r_i)}{dr_i} = m_i \frac{d^2 r_i}{dt^2}$$

(Equation 3.5)

where r_i is the coordinates of the i-th atom;

$V_i(r_i)$ is the potential energy surface; and

t is time elapsed.

Having the initial atomic coordinates and velocities set and the force fields assigned, iterating integrations of *Equation 3.5* can yield subsequent coordinates and velocities at predetermined intervals at a defined temperature. In this sense, the classical MM/MD simulations are deterministic, i.e. the coordinates and velocities at any later time are determined by the initial coordinates and velocities. Nevertheless, a random number seed can be set to randomly generate the initial velocities (initial coordinates is set from the previous sketching or optimization operation) and so the outcome of dynamics runs cannot be repeated exactly.

Temperature Control

Temperature is a state variable specifying the thermodynamic state of a system. It is meaningful only at equilibrium. This macroscopic quantity is related to the kinetic energy of the system through equipartition principle. The kinetic energy of the system can be calculated from the individual atomic velocities and hence temperature can be calculated by the equation:

$$\langle \sum_{i=1}^{N} \frac{p_i^2}{2m_i} \rangle = \langle K \rangle = \frac{N_f k_B T}{2}$$

(Equation 3.6)

where p_i and m_i is the momentum and mass of the i-th atom, respectively;

N is the total number of atoms in the system;

K is the kinetic energy of the system;

N_f is the degree of freedom;

k_B is Boltzmann constant; and

T is temperature.

On the left side, the term describes the average kinetic energy of the atoms whose atomic velocity distribution is described by the Maxwell-Boltmann equation. Since the degree of freedom for a non-periodic system is *(3N-6)*, *Equation 3.6* can be restated as:

$$\sum_{i=1}^{N} \frac{m_i v_i^2}{2} = \frac{(3N-6)k_B T}{2}$$

(Equation 3.7)

where v_i is the velocity of the i-th atom.

Equation 3.7 determines the initial temperature set forth by the initial atomic velocities. The kinetic and potential energy, however, are exchanging during dynamics run and therefore temperature varies. Anderson thermostat (i.e. temperature control method) is used in the thesis to ensure that the computed velocities are adjusted appropriately according to statistical mechanics principles. Anderson method randomizes the velocities of all atoms at a predefined collision frequency.

NVT Ensemble Control

One intrinsic presumption behind Newton's equations of motion is that the energy of the system is conserved, i.e. constant energy. This is however not accurate for most natural phenomena when heat exchange and external pressure are present. Some extended forms of molecular dynamics are required. NVT is a statistical ensemble that controls a simulated system with constant-number (of atoms), constant-volume, and constant-temperature. It is also referred to as the canonical ensemble. This is suitable for systems

where periodic boundary condition is not applicable or where pressure is not a significant factor, as in the cases of studies in this thesis.

3.3 Review on Molecular Modeling Works in Biomaterials

Computer modeling and simulation have been applied to biomolecular science and have gained increasing attention in the field because it provides a simple and relatively inexpensive way to predict the behaviors of biomolecules. Also, for some concept that is difficult to prove by current state-of-art experimental techniques, computational study sheds some light to improve understanding and prediction based on the theoretical proposition and/or experimental parameterization of developed mathematical model. Recently, the marriage between careful *ab initio* models and mature parameterization through real experimental data has created a more powerful tool in predicting the atomistic and molecular interactions of molecules at nano-scale. The study of inter-molecular interactions of biomolecules or polymers using computer simulation had also been explored. Molecular mechanics (MM) and dynamics (MD) is the most widely used method because it is less time-consuming and less memory-consuming (relative to *ab initio* method) and it produces reasonable results at atomistic and molecular level. William G. Pitt et al studied the interfacial interaction between a protein molecule and a synthetic polymer surface surrounded by explicit water molecules based on molecular dynamics methods that were established by a school of theoretical scientists [60]. The results showed the viability of MD to be applied to study interaction force between molecules/surfaces. Aaron M. Bujnowski and Pitt then further study the orientational distribution of the water molecules surrounding the structure and concluded that the water molecules adjacent to the hydrophobic PE surface exhibit a stronger structuring [61], which should give rise to hydrophobic interaction [62]. At the same time, Natarajan et al

were studying the interface between polypropylene and poly(1,4-cis-butadiene) using molecular dynamics method to calculate the theoretical work of adhesion between the surfaces [63]. One of the most prominent studies of interfacial interactions using MD are the works produced by Latour et al, in which the adsorption behaviors of polymer molecules on functionalized SAM surface are studied using MD [64, 65]. Similar and increasingly sophisticated studies had recently been done, too [66, 67]. From these studies, it is clear that MM/MD is a potential tool in the study of tissue adhesion.

Chapter 4
Computational Modeling and Simulation Part I: Study on Molecule Adsorption on Collagen Triple-Helix

4.1 Introduction

The molecular simulation works consists of two parts. In Part I, interactions between small functionalized molecules and collagen triple-helix are simulated; and in Part II, interactions between oligomers and collagen surface are simulated. Part II is addressed in the next chapter.

This chapter presents the findings on Part I computational simulation studies on the affinities of small molecules, which are characterized by the functional group they carry, to a collagen triple-helix (CTH). 18 small organic molecules are selected based on their functional groups; for each of them, 30 molecules were placed around a CTH, which is chosen as a biological tissue representative. The structure of the assembly was then structurally optimized and equilibrated at physiological temperature, following which the interaction energies between the molecules and CTH can be calculated and analyzed.

4.2 Collagen: Selection of the Model Tissue

The structures and compositions of biological tissues are very complicated. They are, in fact, far more complicated than that of which any computational model can handle. Macroscopically, internal body environments are made up of muscles, fats, soft tissues and hard tissues. Each of them, microscopically, is made up of a network of extracellular matrices, cells, structural components, body fluids, free biological molecules, etc., whose basic structures are proteins, polysaccharides, lipids, nucleic acids, and water. Furthermore the relative proportions of the constituents vary from locations to locations. It is still not feasible to build up such environment because: (1) the atomistic and molecular modeling and simulation system at current state can model only up to about a few thousands of particles at maximum, giving the constraints from computer memory, processing speed and processing time; (2) at the length scale of molecular level, the number of the molecules involved (esp. macromolecules) are limited and does not represent biological tissue as a whole, which is of larger scale. Therefore, in this thesis, a representative and reasonable substrate was needed for modeling. After careful considerations, collagen was chosen as the target substrate due to the following four main reasons:

(1) Ubiquity – Collagen is the single most abundant protein in human body and it can be found in many locations, for examples, tendon, cartilage, ligaments, skin, and most types of connective tissues. TA design that targets at collagen has the potential benefit to be effective at different organs and tissues. Even if the target

tissue is lacking of collagen, the study still provides a fundamental platform onto which further investigation and development can be added on.

(2) Structural property – Collagen fibers are known for its toughness and tensile strength (in longitudinal direction). As how it is grouped as structural protein, the chief function of collagen in physiology is to provide mechanical support to the body's tissues. Anchorage of TAs onto collagen results in a stronger joint at biological and hence a firm adhesion could be ensured.

(3) Structure regularity – Collagen has very regular molecular structure at every level (*Fig 4.1*). The primary structure is a sequence of certain amino acids, i.e. glycine, proline, hydroxyproline (which is a unique post-translational amino acid to collagen), glutamic acid, arginine, etc. The appearance of the glycine-proline-hydroxyproline (Gly-Pro-Hyp) tends to be more frequent. This level of regularity is termed as the secondary structure, which is a determining factor of the helical structure of collagen, i.e. tertiary structure. Three strands of collagen helices are attracted to each other by inter-molecular hydrogen bonds to form a triple-helix at a dimension of ~ 15 nm in diameter – which can be viewed as a stiff nanoscopic rod. These rods pack in parallel with a hexagonal packing array that forms a collagen fiber (quaternary structure). Simulations of such regular and relatively simple structure are easier to run.

(4) Sample availability – Theoretical (or semi-empirical with force field-based methods) simulation results requires some solid experimental results for

verification and comparison. In the thesis, microscopic (AFM) and macroscopic (lap-shear tests) measurements would be carried out and correlated to the simulation results. Bovine tendon is a readily available collagenous substrate that could be used in the experimental studies.

A general chemical structure of collagen is shown in *Figure 4.1*, which essentially is the repeating Gly-Hyp-Pro. The chemical structure of the real collagen is more complicated as more different amino acid residues are involved (e.g. glutamic acid, asparagines, etc).

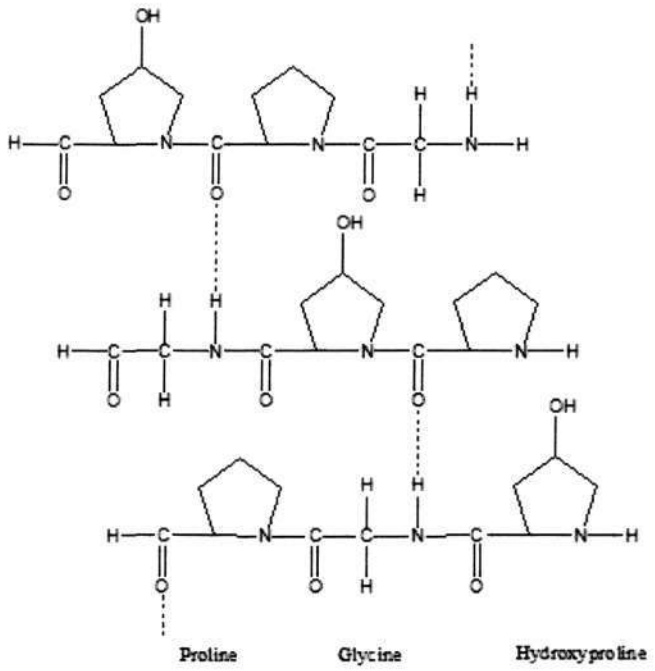

Figure 4.1 Chemical structure of collagen triple helix 1V6Q [68, 69].

4.3 Simulation Methods

4.3.1 Acquisition and Equilibration of Collagen Structure

A segmental structure of collagen triple helix, named 1V6Q, was imported from online protein databank. The structure and parameters of 1V6Q was obtained by X-ray diffraction data of the collagen crystal at room temperature at a resolution of 1.25 Å [69]. The segment of the collagen triple helix possesses three strands of peptides chains, each with 7 repeating units, forming a left-handed triple helix. The chemical composition of each of the chain consists of rigid sequence of glycine-proline-hydroxyproline, which is a very typical and prominent sequence in collagen. At the interior of the helix, the hydrogen atom on the secondary amine in peptide linkage on one strand forms hydrogen bond with the oxygen atom on the carbonyl group in peptide linkage on another strand. With these hydrogen bonds, the triple-helix structure is held unchanged under the constant thermal vibration.

Throughout our course of simulation, the coordinates of the α-carbons of each peptide residue were constrained in space, i.e. they were not allowed to move or translate in space during the dynamics run under elevated temperature environment. This was done to ensure that the overall collagen structure is not destructed during the subsequent energizing process; otherwise it would be "denatured" into gelatin, protein structure that has lost its crystallinity. On the contrary, the simulation would not be as-realistic if too many atoms are constrained. Constraints imposed only on the α-carbons were tested to be the most appropriate condition.

After imposing constraints, the triple-helix was minimized, i.e. structural-optimized, to a convergence level of 0.001 kcal/mol/Å. Then a 10 ps dynamics run, i.e. equilibration at 310 K or 37 °C, at a time step of 1 fs, for the structure were conducted with NVT ensemble. In other words, there are 10,000 steps in each dynamics run.

4.3.2 Selection and Construction of Small Functional Molecules

The objectives were to identify the functional groups that are effective in physical adsorption onto collagen and to compare their competitiveness with water molecules, which are ubiquitous in internal organs. To achieve these objectives, functional groups that are frequently encountered in most organic molecules and/or polymer were listed down. They were end-capped with hydrogen atom or methyl group, without altering the necessary compositional requirement of the functional groups, so as to complete the structure and maintain the bonding stability yet the unique characteristics of the functional groups of question were maintained. Adding hydrogen atom or methyl group, the resultant molecule is also the simplest form that contains the particular functional group. For example, to study ketone group, on either side of the carbonyl group, which is the necessary composition requirement for ketone to form, a methyl group is added. The resultant molecule is dimethyl ketone, which is the simplest molecular form in which ketone functional group could be identified. The molecules that were studied are shown in *Figure 4.2*. Upon construction, they were then minimized to refine the structure so as to acquire the least distorted conformations.

One interesting feature of this study was that the molecules are varied from one another by replacing one functional group with another. This made up the whole spectrum of molecules that are related to one another in terms of their structural and chemical similarity. For example, this progressive change should reveal the difference among the affinities of functional groups to collagen in a clearer way. Besides these basic molecules, some other molecules with greater complexity were also constructed for the sake of the understanding of the effect of certain changes in the molecular structure and chemistry. They are discussed in the later sections.

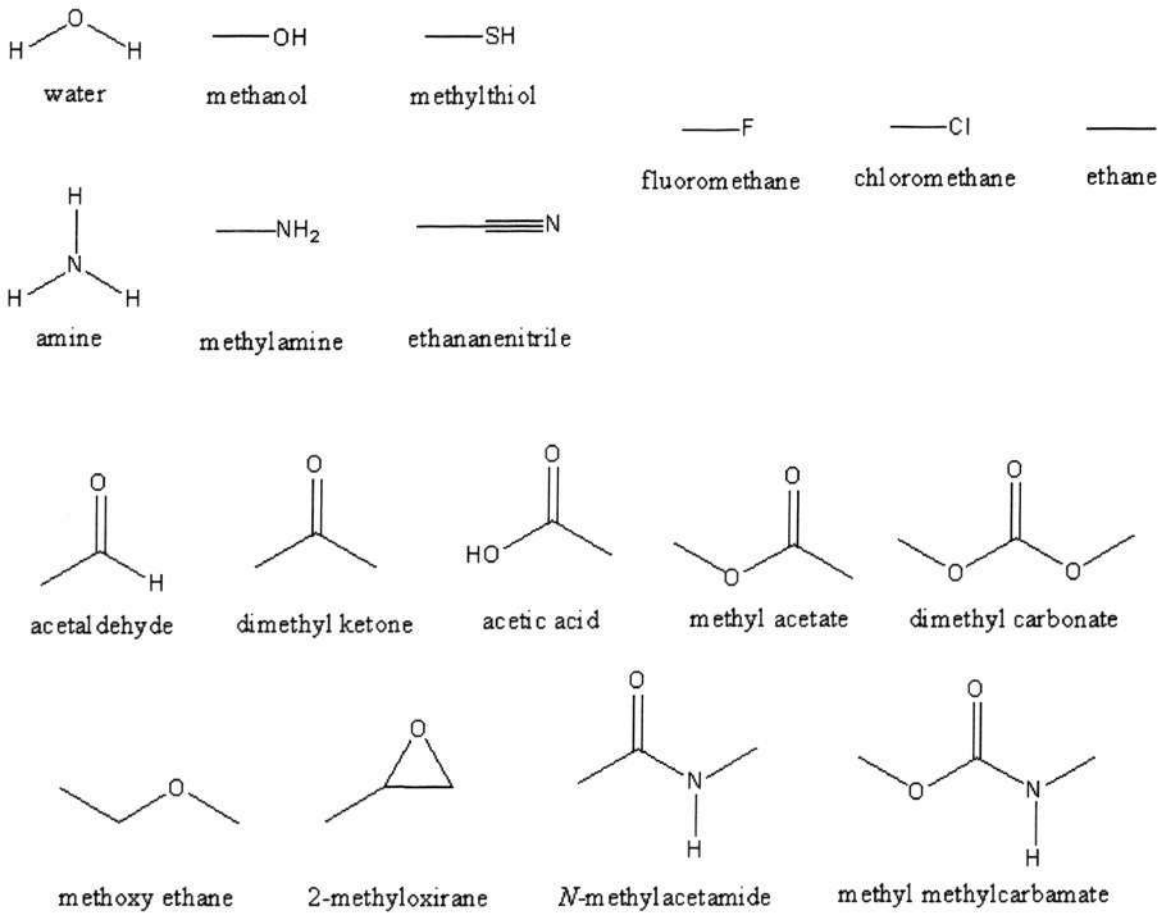

Figure 4.2 The chemical structures of the small molecules studied. They were the simplest structure into which their characteristic functional groups can be built.

Table 4.1 The molecules in study, their corresponding functional groups and chemical structure.

Functional Group	Molecule	Simplified Representation
Water	Water	H_2O
Free amine	Amine	NH_3
Secondary amine	N-Methylacetamide	$CH_3(CONH)CH_3$
Carbonate	Dimethyl carbonate	$CH_3(OCOO)CH_3$
Ester/Acetate	Methyl acetate	$CH_3(COO)CH_3$
Ketone	Dimethyl ketone	$CH_3(CO)CH_3$
Urethane	Methyl methylcarbamate	$CH_3(COONH)CH_3$
Nitrile	Ethananenitrile	$CH_3(C\equiv N)$
Epoxy	2-Methyloxirane	$CH_3(CHOCH_3)$
Fluoride	Fluoromethane	CH_3F
Aldehyde	Acetaldehyde	CH_3CHO
Acid	Acetic acid	CH_3COOH
Alcohol	Methanol	CH_3OH
Primary amine	Methylamine	CH_3NH_2
Ether	Methoxyethane	$CH_3OCH_2CH_3$
Thiol	Methylthiol	CH_3SH
–	Ethane	CH_3CH_3

4.3.3 Dynamics Set-Up

Up to this step, a segment of a strand of collagen triple helix had been equilibrated; and 18 selected molecules with different functional groups had been constructed and minimized. The next step was to put them together, simulating their trajectories in space over time at physiological temperature and then computing the interaction energies, or affinity, between the collagen and small molecules. First, 30 of each kind of molecule were evenly placed around the equilibrated CTH at randomly chosen locations. This was followed by minimization of the system to avoid the overlapping of the molecules, if any, at a convergence level of 0.001 kcal/mol/Å.

For all minimization, dynamics run, and single-point energy calculation in this study, the summation method of vdW and coulombic interaction is atom-based. Dielectric constant is set to be 1.00, which represents the vacuum environment. It is a dimensionless quantity because it is not the real physical dielectric constant but a constant that is used in atomistic computational context. Cut-off distance, spline width and buffer width, i.e. parameters that limit the extent to which atoms are "sensing" the presence of each other, were set at 9.5 Å, 1.00 Å, and 0.50 Å, respectively.

Following the minimization, the equilibration of system at 37 °C were then conducted in molecular dynamics simulation, in which Newtonian's equations of motions were solved for each time interval. As for statistical ensemble, canonical (NVT) ensemble is chosen. In other words, the number of atoms and the volume of the system were constant; and the temperature was well defined throughout the 10 ps simulated time. The pressure, as the first assumption, was set constant at the atmospheric level. Time step was taken to be 1 fs. The final trajectory (the final picture frame that contains the data of the positions, velocities and accelerations of the atoms in the system after 10 ps of simulated equilibration process) was extracted and the structure underwent the last minimization step.

Finally, to obtain the interaction energy between small molecules and CTH, three energies were first calculated: (i) total energy (including internal energy and non-bonding energy) of collagen alone; (ii) total energy of molecules alone; and (iii) total energy of both interacting collagen and molecules. The interaction energy was then obtained by

subtracting the first two energy components from the last one. The interaction energy is comprised of only two terms: van der Waals interaction and electrostatic interaction because the internal energies were all cancelled out in the subtraction operation. Van der Waals interaction can be further split into two terms: repulsive term and attractive term, as implied in the Lennard-Jones 9-6 equation.

4.4 Results

As mentioned, eighteen types of functional groups (or molecules) were selected. Most of them are frequently encountered in organic molecules and polymers. Some of them, in addition, are known to be the adhesive groups in commercial adhesives or sealants, e.g. epoxy, urethane, cyano and acrylate groups.

The bar chart shown in *Figure 4.3* ranks the total non-bond interaction energies of various molecules with CTH from the strongest to the weakest. Note that negative energy means attraction between the molecules and collagen (i.e. affinity) and positive; repulsion. In this thesis, when the molecule shows great negative non-bond interaction energy, it is said to be interacting strongly with collagen. The term "non-bond interaction energy" here refers to physical interaction, or secondary interaction, as no chemical bond is formed between the collagen and the molecules. The greater the absolute value of the energy, the stronger the physical interaction. As discussed in theory, this interaction energy is the sum of two components, which are, van der Waals (vdW) interaction and electrostatic interaction, corresponding to *Equation 3.1* and *Equation 3.2*, respectively. They are shown in Figure 3, too

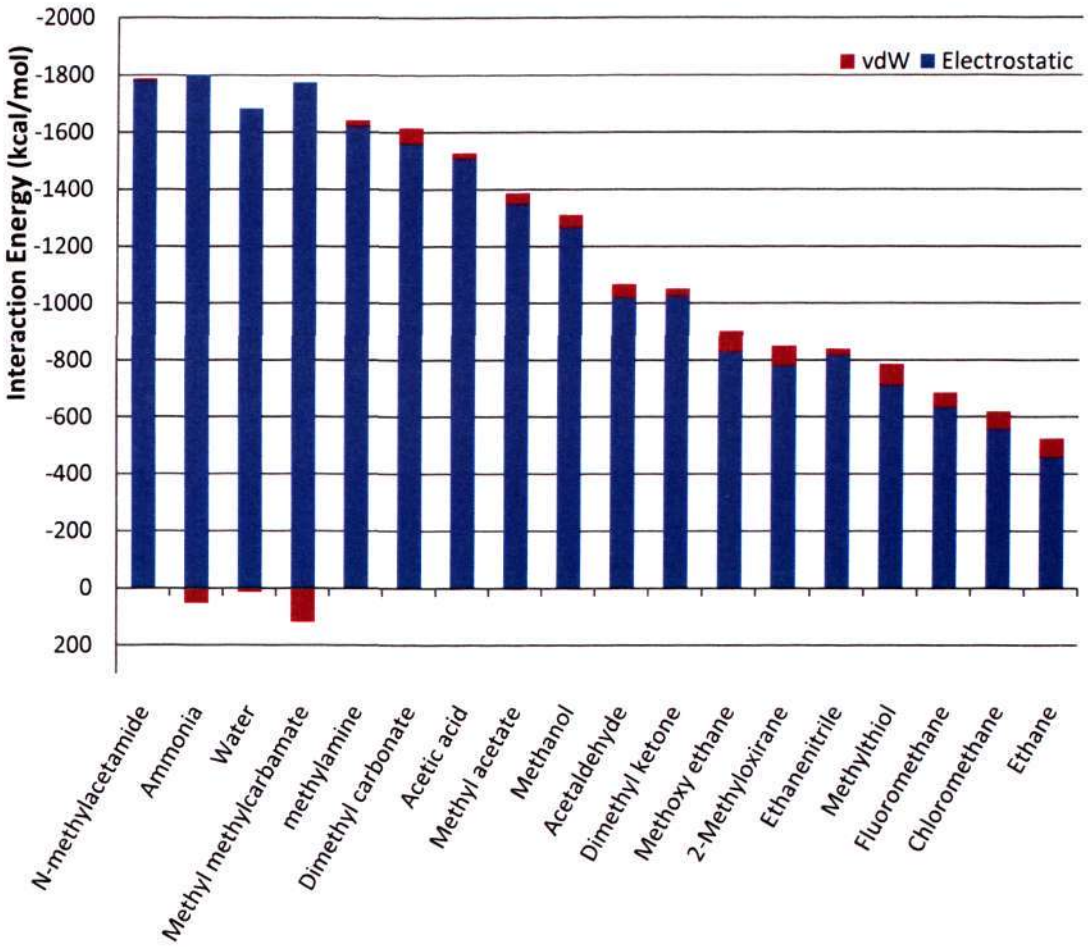

Figure 4.3 Molecules with various functional groups are arranged in descending order in term of interaction energies with collagen triple-helix from left to right.(Note: Interaction energy shown here is contributed collectively from all 30 molecules.)

4.5 Discussions

The Magnitude of Physical Adsorption Energy

It has been reported that the bond energy of C-C covalent bond is ~ 87 kcal/mol; that of hydrogen bonding is ~ 35 kcal/mol; and that of vdW is > 2 kcal/mol [70]. In Figure 4.3, the energies are calculated for physical interaction between 30 molecules and collagen. Even for the molecule with greatest interaction, *N*-methylacetamide, where the interaction energy is reported collectively as -1788 kcal/mol for 30 molecules, the interaction energy per molecule is -59.6 kcal/mol. This value takes into account all vdW and electrostatic interactions between each atom on the molecules and each atom on the collagen (within a cut-off distance of 9.5 Å and spline width of 1.0 Å; as a comparison, C-C bond distance is 1.54 Å). Moreover, the number of atoms in N-methylacetamide is 12 and so the average interaction energy per atom in a molecule is 4.97 kcal/mol, which is reasonably accurate.

VdW and Electrostatic Components

It is clear that, for all molecules, the contribution of the electrostatic component to total non-bond energy overwhelms that of vdW component. VdW component is much smaller. In a few cases, vdW component is near to zero or even positive in value. This implies that the adsorption of small molecules onto the CTH is more electrostatic-driven than vdW-driven. The implication is reasonable because of the complex distributions of partial charge, which collectively set up a complicated surrounding electrostatic field, on the atoms in the molecules and collagen. The small molecular size renders the molecule free

and mobile to "surf" on the electrostatic field until it adapts and conforms to a position and configuration of minimum energy. In other words, the molecules search for the locations on CTH where the local partial charges are of opposite kind. In this way, the electrostatic attraction between these unlike charges results in a decrease in electrostatic energy.

Imagine that if vdW interaction alone is considered without the intervention of electrostatic interaction, the particles would achieve an equilibrium distance where vdW total energy will be at its minimum, at which the dispersive and repulsion terms in LJ equation (Eq 3.2) are balanced. In the instance of electrostatic interaction intervention the potential surface topography and consequently the equilibrium distance is also altered. Attractive electrostatic force pulls the particles closer and the equilibrium distance is hence shorter and vice versa. In conclusion, instead of balancing the two terms in LJ equation, the system now needs to balance three terms, two LJ terms and an additional coulombic term.

This can explain the near-zero or positive vdW energy, mostly observed in highly polar molecules. For highly polar molecules, e.g. water, ammonia, dimethyl urethane, the electrostatic attraction is strong and therefore they tend to be drawn closer to the collagen (which is also partially polar) at a distance at which the vdW repulsion (a short range interaction) begins to dominantly offset the vdW attraction. Yet, the total non-bond energy is still negative in value due to the stronger electrostatic attraction.

Water, an important molecule

Referring back to Figure 4, water occupies a place at the higher end of the rank. Water strongly adsorbs onto collagen surfaces because of its strong polarity and small size. The strong water adsorption is definitely not favorable for the development of tissue adhesives targeted for internal use as it competes with the adhesive for adhesion sites. For an adhesive to be in contact with the tissue surface, a critical requirement for good adhesion, this water layer has to be depleted so that the true surface is exposed. This would not only promote adsorption of adhesive onto relevant surface functional group, but also promote adhesive diffusion into the sub-surface. Although the real mechanism could be quite complicated, good adhesive should at least possess stronger attraction force to the surface than that of water and, at the same time, repel water molecules if possible. However, as shown, water is too competitive among all. Only two kinds of molecules (or functional groups), i.e. dimethyl amide and ammonia, have greater absorption than water.

Ammonia molecule, similar to water molecule, has strong polarity and small size. Its electrostatic component is greater than that of water molecule; however, this attraction also draws the molecule closer to the collagen, which results in net vdW repulsion. Nonetheless, it still has slightly stronger adsorption to collagen than water molecule. Despite its stronger adsorption, ammonia is a free molecule and it is impossible to incorporate "ammonia group" into adhesive molecule because the N atom must be completely bonded to three hydrogen atoms. H atoms maintains the strong polarity of the

molecule; by changing just one H atom into a methyl group, the adsorption drops to a level well below that of water, as illustrated by the methylamine molecule.

On the other hand, dimethyl amide, which contains amide group, or equivalently, peptide linkage in protein, shows the strongest affinity to collagen by occupying the highest position in the rank. The electrostatic component for dimethyl amide is weaker than that of ammonia (greater than that of water) but the vdW component is attractive. The resultant total non-bond energy is therefore greater. This result may provide a good guide to the development of tissue adhesives. The density of this amide group in protein molecule/complex is very high and this could probably explain the observed adhesion of fibrin glues, which is essentially a kind of protein. (Incidentally, the strength of the glue however relies on the cross-linked structure.)

On the other end of the spectrum, ethylene shows the lowest interaction energy with collagen. This weak adsorption of ethylene was quite predictable because it was viewed as a molecule without any functional group. Or, alternatively, it can be viewed as comprising of merely alkyl groups, which is the most fundamental unit for all polymeric materials. The electrostatic energy of ethylene is still the dominant component despite its overall non-polarity. It is reasonable to conclude that the local partial formal charges on small molecule, even for the non-polar ones, are sufficient to cause electrostatic attraction. VdW energy, again, plays merely a trivial role in determining the adsorption of small molecules onto CTH.

Progressive Dissimilarity among Molecules

It would be more comprehensive if we arrange the functional groups into a chart as shown in Figure 4.4. On the left hand side, it starts with methane, the molecule with the least affinity to collagen. As progressing to the right, the chart continues with four branches, into which related functional groups are categorized. They are arranged in a way that the collagen affinity is increasing, with the arrows pointing to the molecule with stronger affinity.

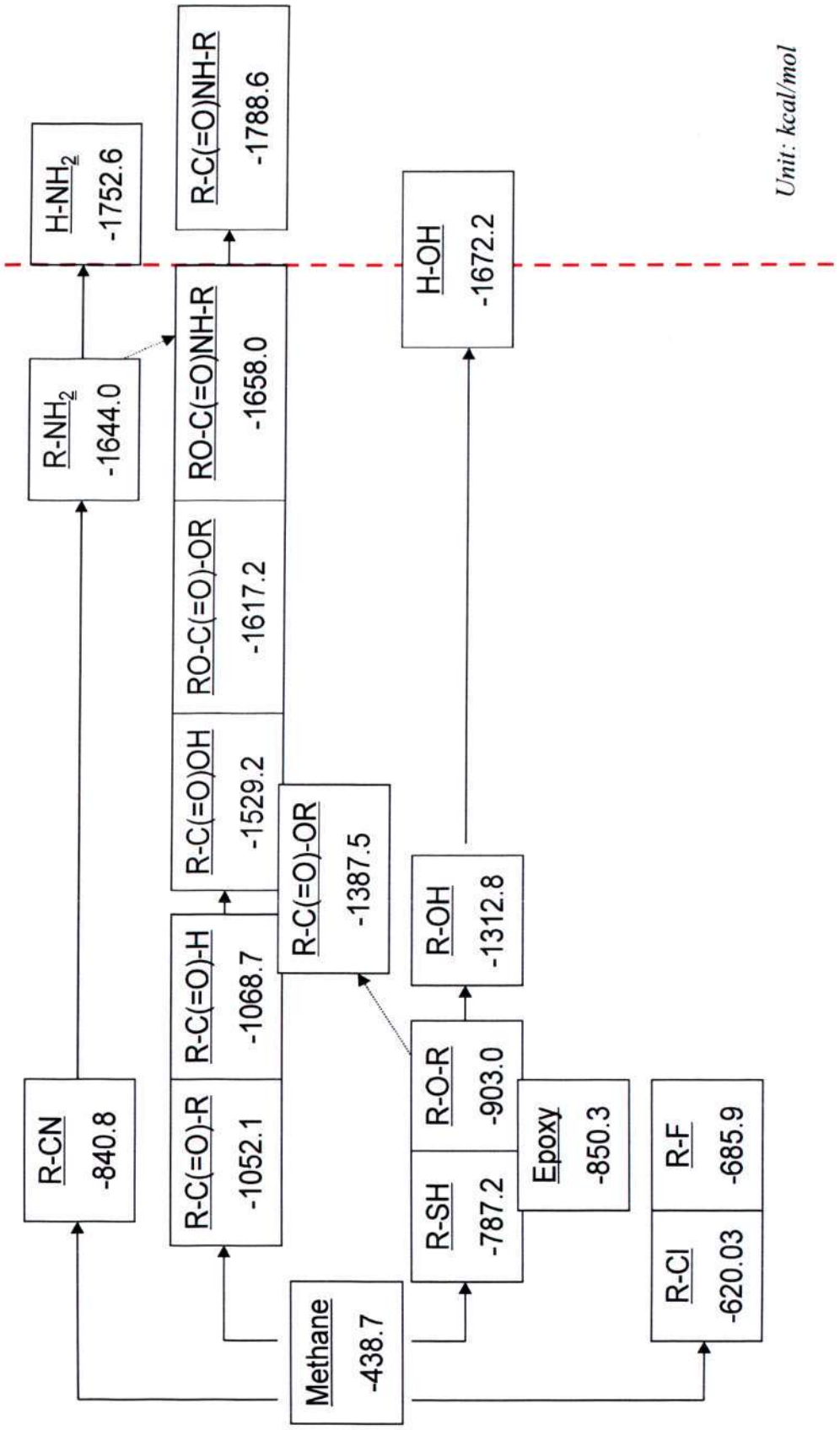

Figure 4.4 Progressive arrangement of molecules based on their interaction energies. The chart groups the molecules into four main branches, i.e. N-containing; carbonyl-containing; hydroxyl-containing; and halide-containing molecules, with some crossover. .(Note: Interaction energy shown here is contributed collectively from all 30 molecules.)

The first branch, located at the top, includes the molecules/functional groups that contain N atom; the second branch includes the molecules with carbonyl (C=O) group; the third branch contains molecules with thiol, methoxy and alcohol; and the last branch contains the halide molecule. Besides, the branches could be merged at some point along the line where the functional groups begin to show common structural or compositional similarities, as represented by the sloped arrows. The R in the chemical representations is either hydrogen (–H) or methyl group ($–CH_3$). With the chart, it is more convenient to visualize the effectiveness of each functional group in adsorption onto collagen.

The location of water is marked by the red dotted line since it is the archenemy to be expelled from the wet collagen surface if other molecules were to adsorb onto collagen. As discussed earlier, water has a very strong adsorption while there are only two kinds of molecules that we studied can outdo water –dimethyl amide and ammonia in this aspect. A red dotted line is marked at the position of water to highlight the challenge that has to be overcome for adsorption of tissue adhesive to occur.

In the first branch, the N-containing series starts with ethanenitrile (-840.8 kcal/mol), with also a substantial increase as compared to fluoromethane. Ethanenitrile is a molecule with a methyl group and a cyano functional group (–C≡N), which is an electron-withdrawing group that render the cyanoacrylate adhesives (together with the acrylate group that is bonded to the same C) to be highly polar. However, the performance of cyano group is not as satisfying as the rest of the N-containing functional group. When the cyano group is replaced by an amine group, as in the methylamine

molecule (the simplest primary amine), the adsorption is greatly improved (-1644.0 kcal/mol), that is, the interaction energy is increased by nearly two-fold. It is clear that primary amine group is a good functional group to be considered to improve a molecule's affinity to collagen. Furthermore, it says that the adhesion mechanism of the quick-glue – cyanoacrylates – on collagen is not based on the cyano group. Ammonia, the last member in the branch, can be viewed as replacing the methyl group in methylamine with a hydrogen atom. This modification, evidently, further improved the affinity to collagen.

Next, the third branch is focused. It started off with a thiol group (–SH, -787.2 kcal/mol), which is a relatively weak adhesive group. Replacing thiol group with alcohol group (–OH, -1312.8 kcal/mol), the adsorption energy increases greatly. (Oxygen and sulfur are both VIA elements in periodic table. They have similar hybridization.) It can be derived from the above example in the first branch that when R is –H, the molecule have a stronger attraction to collagen as compared to the cases when R is $–CH_3$. This is again seen in the third branch: R–OH is effectively stronger than R–O–R (R is methyl for both molecules here). This is due to the greater polarity of the former molecule that forms better electrostatic attraction. Conversely, when the methyl group in methyl amine is replaced with a hydrogen atom, water molecule is formed. By the same principle, water is therefore more polar than methylamine and it has strong interaction with collagen. Interestingly, epoxy, which is commonly used as commercial adhesive, shows rather low interaction with collagen. This hints that epoxy is not an effective group when adhesion to tissue surfaces is concerned.

The second branch, which contains the most number of molecules, also includes the molecules with oxygen atom(s) in the functional groups. One oxygen is present in the carbonyl (C=O) group and another; on the backbone next to the carbonyl. Ketone group (-1052.1 kcal/mol) is the first member in the series. It is followed by aldehyde group (-1068.7 kcal/mol) which has a very close interaction energy to that of ketone. The branch then continues with ester group (-1387.5 kcal/mol) and acid group (-1529.2 kcal/mol), both of which has one more oxygen atom in the functional group – but ester is terminated with a methyl group and acid is terminated with a hydrogen atom. When one more oxygen is added into the molecule to form a carbonate group (-1617.2 kcal/mol), the interaction again gets stronger. From here, it can be seen that if the number of oxygen atoms in a group is increased, it will generally be more attracted to collagen. Urethane group, which is also frequently employed in commercial adhesives, occupies the next place. Its application in tissue adhesive has also been explored [13, 71]. Urethane group is formed by reacting an isocyanate group (–N=C=O) and a hydroxyl (–OH) group in the presence of catalyst. This serves as a mean to cure urethane adhesive when diisocyanate pre-polymer and polyol pre-polymer are mixed. This simulation study shows that, other than executing curing process, urethane groups render the polymer to adsorb onto collagen as well. Finally, the branch ends with amide group (peptide group), which has been discussed in previous section.

The last branch is formed by functional groups carrying halogen atoms. The effect of incorporating halogen-containing functional group is however not remarkable, despite halogen's strong electronegativity. Chloromethane (-620.03 kcal/mol) is obviously stronger in interaction with collagen than methane but it is in fact the weakest molecule among the other functionalized molecules. Fluoromethane (-685.9 kcal/mol), with the most electronegative atom in its functional group, did not show strong interaction with collagen as well.

In this section, the importance of the presence of functional group in a molecule to improve adsorption (and hence adhesion) to collagen is justified. The relative strengths of the functional groups were compared. In general, functional groups with N and O atoms are attracted to collagen while N seems to be slightly more effective than O. The more N or O atoms the functional group has, the stronger the affinity. On the other hand, halogen atoms are not so effective.

Effect of the Covalent Bond Types

The three types of covalent bonds, i.e. single bond, double bond and triple bond, are also investigated by comparing ethane, ethene and ethyne. These bonds are very common in synthetic polymers. The detailed breakdowns of the interaction energies of these molecules are listed in *Table 4.2*. Two extra parameters were added at the bottom row of the energy table. R/D is the ratio of repulsive vdW and dispersive vdW component; it implies the position of the molecules relative to collagen. V/E is the ratio of vdW and electrostatic; it shows their relative contributions to the total non-bond energy.

Table 4.2 Non-bond energy breakdown for small molecules with similar structure but different covalent bond types. (Ethane contains single bond; ethene double and ethyne triple.)

	Ethane	**Ethene**	**Ethyne**
Total Non-bond	-526.71	-957.00	-919.71
vdW	-67.45	-53.22	-61.34
Repulsive	199.90	225.37	156.04
Dispersive	-267.35	-278.59	-217.38
Electrostatic	-459.25	-903.78	-858.37
-R/D	0.7477	0.8090	0.7178
V/E	0.1469	0.0589	0.0715

As a "non-functionalized" molecule, ethane, as known, has the weakest adsorption on collagen among all other molecules. Here, it ranks the lowest among the molecules of different bonding conditions, despite its greater number of atoms per molecule. Ethene, with a similarly plain chemical composition but different in the number of atom and the type of bonding, has a distinctively stronger adsorption due to a vast improvement in the electrostatic component. Ethyne, however, still adsorbs better than ethane but slightly weaker than ethene.

It is seen that the vdW interaction does not necessarily increase with the number of atoms per molecule, although the mass of the molecule is one of the major determinants of vdW energy. The partial charges of the atoms are getting stronger from ethane to ethyne and therefore the electrostatic components of ethene and ethyne are greater. The large electrostatic force draws the molecule closer to the collagen and hence increases the repulsive vdW component. Since ethene is a bulkier molecule than ethyne, it causes a greater repulsion when approaching collagen.

The stronger affinity of the molecules with double bonds to collagen is an advantage to addition polymerization system, in which the monomer possesses double bonds.

Effect of the Length of the Alkyl Group

In the previous sections, all functional groups were compared based on the simplest molecule that they could construct. Next, we are going to compare the molecules that have same functional group but differ in the length of the attached alkyl chain. On one hand, it is known from *Equation 3.2* that the vdW energy increases with increasing number of atoms in one molecule. On the other, the results above showed that alkyl group (represented by the "non-functionalized" ethane) is ineffective in interacting with collagen. Furthermore, in polymer physics, the polymer molecule loses its mobility and agility as the chain gets longer. It is also bulkier than small molecule and therefore that it is not possible for them to stay in less accessible locations. So the net results of these counter-effects will be analyzed.

Three types of functional groups were compared: pure alkyl chain; alcohol; and amine. Each type of functional group was attached with methyl, ethyl, propyl and decyl to produce four molecules. The results are tabulated in *Table 4.3*. V/E is the ratio of vdW and electrostatic; it shows their relative contributions to the total non-bond energy. Since the small molecules exhibits certain levels of polarity that results in electrostatic interaction, V/E ratio is small for most of the molecules studied. Within the vdW component, -R/D is the ratio of repulsive vdW and dispersive vdW component; it implies

the position of the molecules relative to collagen – greater -R/D means that the molecules are residing at a distance closer to the distance at which only vdW component prevails. Since electrostatic interaction, which is attractive, is acting on top of vdW, the molecules are drawn closer to the surface and increase the relative weight of repulsive to dispersive components in vdW.

Table 4.3. Non-bond energy breakdown for molecules having same functional group but different alkyl length. (a) Alkane; (b) alcohol; and (c) amine.

(a)

	Methane	**Ethane**	**Propane**	**Decane**
Total Non-bond	-438.71	-526.71	-627.51	-347.61
vdW	-48.42	-67.45	-81.82	-51.39
Repulsive	171.37	199.90	190.77	108.66
Dispersive	-219.78	-267.35	-272.59	-160.05
Electrostatic	-390.29	-459.25	-545.69	-296.22
-R/D	0.7797	0.7477	0.6998	0.6789
V/E	0.1240	0.1469	0.1499	0.1735

(b)

	Methanol	**Ethanol**	**1-Propanol**	**1-Decanol**
Total Non-bond	-1312.78	-1285.93	-1385.17	-603.18
vdW	-45.03	-23.77	-52.87	-43.54
Repulsive	230.47	333.72	306.14	148.46
Dispersive	-275.50	-357.49	-359.01	-192.00
Electrostatic	-1267.76	-1262.16	-1332.30	-559.65
-R/D	0.8366	0.9335	0.8527	0.7732
V/E	0.0355	0.0188	0.0397	0.0778

(c)

	Amine	**Methylamine**	**Ethylamine**	**1-Propylamine**	**1-Decylamine**
Total Non-bond	-1752.16	-1644.04	-1672.30	-1675.07	-767.52
vdW	50.49	-21.70	-41.47	-52.26	-20.68
Repulsive	252.06	345.03	326.61	338.56	214.73
Dispersive	-201.57	-366.73	-368.07	-390.83	-235.41
Electrostatic	-1802.65	-1622.35	-1630.83	-1622.80	-746.83
-R/D	1.2505	0.9408	0.8873	0.8663	0.9121
V/E	-0.0280	0.0134	0.0254	0.0322	0.0277

For alkane molecules, the interaction energy increases from methane to ethane, and then to propane (*Table 4.3a*). Both vdW and electrostatic components increase. Comparing propane with ethane (as well as ethane with methane), the molecule size is not much bigger and therefore it should retain sufficient mobility, which are needed to mingle around the CTH surface and look for docking positions. The increase in the number of atoms boosts the energy components; while the size of the molecule do not restrains the search for energy-minima. As a result, the affinity of small linear alkane molecule to collagen gets stronger with larger molecular weight. However, when the molecule gets bigger, as for decane (10 carbons in the backbone), both vdW and electrostatic components diminishes. That results in an extensive reduction in total interaction energy. Of the two components, electrostatic energy drops is much greater.

Similar trends are also observed for alcohol and primary amine molecules (See *Table 4.3b* and 4.3*c*). When the molecules are small, they have strong affinity to collagen. When the molecules are increased by substituting long alkyl chain, their affinities vanish. However, for these functional molecules (as opposed to the "non-functionalized" alkane), affinities of small molecules, e.g. methanol, ethanol and propanol, are very close to one another. No trend is observed between affinity and size for small functional molecules. With the polar and "active" functional groups, the trade-off between vdW and electrostatic components in small molecules are less predictable. For tissue adhesive, this decrease in interaction energy in molecule with long alkyl chain is not a good sign because polymeric adhesives are usually characterized by long hydrocarbon backbone/network.

Effect of the Number of Functional Groups per Molecule

In this section, two or more functional groups were bonded to the molecule and the effect on the molecule's affinity to collagen was analyzed. Two kinds of functional groups were analyzed here: the "active" alcohol group, which had shown strong adsorption to collagen; and the "inactive" tertiary butyl functional group, which is a bulky alkyl group that has weak adsorption. The non-bond interaction energy breakdowns are shown in *Table 4.4*.

Table 4.4 Non-bond energy breakdown for multifunctional molecules. Active functional group: (a) alcohol; Inactive functional group: (b) tertiary-methyl.

(a)

	Ethanol	**1,2-Ethan-2-ol**	**1,1-Ethan-2-ol**	**1,1,1-Ethan-3-ol**
Total Non-bond	-1285.93	-1730.72	-1835.11	-2264.35
vdW	-23.77	42.61	3.42	127.73
Repulsive	333.72	499.88	422.75	727.21
Dispersive	-357.49	-457.27	-419.33	-599.49
Electrostatic	-1262.16	-1773.33	-1838.53	-2392.07
-R/D	0.9335	1.0932	1.0082	1.2131
V/E	0.0188	-0.0240	-0.0019	-0.0534

(b)

	Tert-buthylamine	**Di(tert-butyl) amine**	**Tri(tert-butyl) amine**
Total Non-bond	-1631.63	-1207.20	1586.977
vdW	-28.34	-84.67	2652.162
Repulsive	444.66	277.14	3535.826
Dispersive	-473.00	-361.81	-883.663
Electrostatic	-1603.29	-1122.54	-1065.19
-R/D	0.9401	0.7660	4.0013
V/E	0.0177	0.0754	-2.4899

In *Table 4.4a*, the numbers of hydroxyl functional groups are one, two and three in ethanol, ethan-2-ol and 1,1,1-ethan-3-ol, respectively. For ethan-2-ol, the two groups were placed on different carbon atom in the two-carbon molecule, thus resulted in two molecules, i.e. 1,1-ethan-2-ol (on the same carbon) and 1,2-ethan-2-ol (on different carbon). The results show that as the number of the functional groups increases, the interaction of the molecule with collagen is greater. Although ethanol is not a molecule with a very strong affinity to collagen, as discussed in the previous section, the interaction energy however changes tremendously upon the addition of a second functional group. Moreover, when the two hydroxyl groups are placed on the same carbon (1,1-ethan-2-ol), the affinity is stronger than when the groups are placed on separate carbons (1,2-ethan-2-ol). The interaction energy further increases when three hydroxyl groups are added to the molecule. The core reason for this increase lies in the increase of electrostatic energy. Adding more polar groups to a molecule makes its electrostatic interaction with collagen very active. This strong interaction attracts the molecule close to the collagen even if the vdW repulsion starts to increase to a great extent – the fact that is reflected in the R/D and V/E ratios.

On the other hand, when more tert-butyl groups (an "inactive" functional group) is added to a molecule, the electrostatic interaction gets weaker and the vdW repulsion gets stronger (*Table 4.4b*). Therefore, as far as adhesion onto collagen is concerned, the presence and numbers of "active" functional groups are crucial while "inactive" functional groups (e.g. alkyl) should be reduced if possible. Putting together the conclusions from preceding sections, while the backbone of the polymer is mainly made

up of carbon (especially true for addition polymerization system), active groups should be incorporated as side groups as much as possible for better interactions.

There is good correlation between this observation and the good performance of cyanoacrylate glues. In *Figure 2*, both cyano (-840.8 kcal/mol) and acrylate groups (-1387.5 kcal/mol) are not strong adhesion groups to collagen. The two groups are bonded to the same carbon atom in cyanoacrylate monomer. Since both of them are "active" functional groups, i.e. they render the molecule to be adsorptive to different extents, they improve the affinity of cyanoacrylate molecule to collagen. To show this, cyanoacrylate molecule was constructed and the adsorption to collagen was simulated. The non-bond energy breakdowns are shown in *Table 4.5*. The adsorption energy of cyanoacrylate is -1404.18 kcal/mol, a value that is greater than that of the two individual functional groups. It can be conjectured that cyanoacrylate monomers are drawn close to collagen and then diffuse into collagen subsurface quickly. Then, upon contact with water, their polar double bonds break to form radicals and a quick polymerization occurs. Adsorption is therefore essential for the early stage in which monomers are attracted to diffuse into the surface, while the strength of the joint is decided by the diffusion depth of the adhesive.

Table 4.5 Interaction energy breakdown for cyanoacrylate monomer.

	cyanoacrylate
Total Non-bond	-1404.18
vdW	-69.93
Repulsive	284.70
Dispersive	-354.63
Electrostatic	-1334.24
-R/D	0.8028
V/E	0.0524

Comparison among Isomers

Next, we examined if the different arrangements of carbon atoms in isomers affects the adsorption of the molecules. Three pairs of molecules were compared here: Ethylamine and dimethylamine (C_2H_7N); propylamine and trimethylamine (C_3H_9N); and 1-butylamine and tert-butylamine (C_4H_9N). The non-bond interaction energy breakdowns are presented in *Table 4.6*.

Table 4.6 Non-bond energy breakdown for multifunctional molecules. Active functional group: (a) alcohol; Inactive functional group: (b) tertiary-methyl.

	Ethylamine	**Dimethyl-amine**	**Propylamine**	**Trimethyl-amine**	**1-Butylamine**	**Tert-butylamine**
Total Non-bond	-1672.30	-1424.64	-1675.07	-952.54	-1801.74	-1631.63
vdW	-41.47	-18.87	-52.26	-30.69	-49.93	-28.34
Repulsive	326.61	433.92	338.56	465.20	382.02	444.66
Dispersive	-368.07	-452.79	-390.83	-495.88	-431.95	-473.00
Electrostatic	-1630.83	-1405.77	-1622.80	-921.86	-1751.81	-1603.29
R/D	0.8873	0.9583	0.8663	0.9381	0.8844	0.9401
V/E	0.0254	0.0134	0.0322	0.0333	0.0285	0.0177

It should be noted that, among the molecules, ethylamine, propylamine, 1-butylamine and tert-butylamine are primary amine, in which the nitrogen atom is bonded to two hydrogen atoms and an alkyl; on the other hand, dimethylamine is a secondary amine, i.e. the nitrogen is bonded to one hydrogen and two alkyls; and trimethylamine is a tertiary amine, i.e. the nitrogen is bonded to three alkyls but no hydrogen. In general, hydrogen is polarized when it is bonded to the electronegative atoms, for instance, nitrogen and oxygen, and so it amplifies the electrostatic interaction. When alkyl is bonded to electronegative atoms, however, the polarization effect is weakened. Furthermore, alkyl group is bulkier and this limits the mobility of the molecule and the accessibility into confined spaces to improve interactions.

4.6 Summary

This section presented the MM/MD simulation of the adsorption of various small molecules, characterized by the functional groups they are carrying, onto a segment of a strand of collagen triple helix, which was regarded as a simplified but representative target for tissue adhesive study. Out of the two components, electrostatic interaction is more prominent than vdW interaction and it determines the adhesion performance of small molecules. It was shown that water has a strong adsorption onto collagen. All the functional groups in the study showed weaker adsorption than water. The only two exceptions were ammonia and dimethyl amide (or peptide). So, increasing amide (peptide) density in polymers could improve its adsorption and hence adhesion to biological tissues. This may be the origin of the adsorption of fibrin glue on tissues. The set of rules to small molecules may not be applicable to the big polymer molecules in application; the results nevertheless sketched the events in the initial stage in adhesive application, when monomer liquid or solution (small molecule) is applied. This initial stage is important for a good joint. Generally, addition polymerization adhesive systems should be more effective (as compared to solvent-evaporation systems) because they are applied in monomer (small molecule) form, which is more attractive to collagen, as shown in the study. The monomer should contain a higher density of functional groups that are made up of N atoms (in the forms of amine, urethane, and amide) and O atoms (in the forms of carbonate, urethane, and amide) because the study showed that these functional groups increase the electrostatic interaction. On the contrary, long and bulky alkyl chains should be reduced, especially to those that are blocking the functional groups.

Chapter 5
Computational Modeling and Simulation Part II: Study on Oligomer Adsorption on Model Collagen Surface

5.1 Introduction

In this chapter, Part II of the computational simulation works is presented. This part extends the studies of material-collagen interactions from that in the previous chapter to slightly more complex set-ups – interactions between oligomers and collagen surface. The conditions in this model are simplified and by no means comprehensive enough to represent the actual scenario. It is aimed primarily to provide insight to the adsorption events occurring at the interface at the molecular level. More importantly, from materials' point of view, it compares the effectiveness of different functional groups for adhesion. As would be shown, this is important for basic understanding and molecular design of TAs.

12 types of common oligomers are studied by placing their representative oligomers (in single-stranded form) directly on top of a structured collagen surface in dry and wet condition. Dry condition is approximated by vacuum; whereas wet environment is accomplished by building up a thick water layer. The assembly of oligomer, collagen surface and vacuum/water is then structurally optimized, agitated at high temperature,

and finally equilibrated to physiological temperature in order to generate the enthalpies of interaction for further analysis.

Simulation methods are detailed step-by-step in *Section 5.2*, which is followed by results in *Section 5.3* and discussions in *Section 5.4*. A conclusion is made in *Section 5.5*.

5.2 Simulation Methods

In this second part of the simulation studies, the non-specific interactions between a single strand of polymer and a collagen surface is the subject of interest. Hence, the studies started with the construction and preparation of the collagen surface and polymer molecules (to be more precise, oligomer molecules); followed by placing them together and letting equilibration take place at physiological temperature. Interaction energies were then computed based on the equilibrated systems. The simulation procedures are summarized in the flowchart in *Figure 5.1*; and the details of each procedure is presented step-by-step as followed.

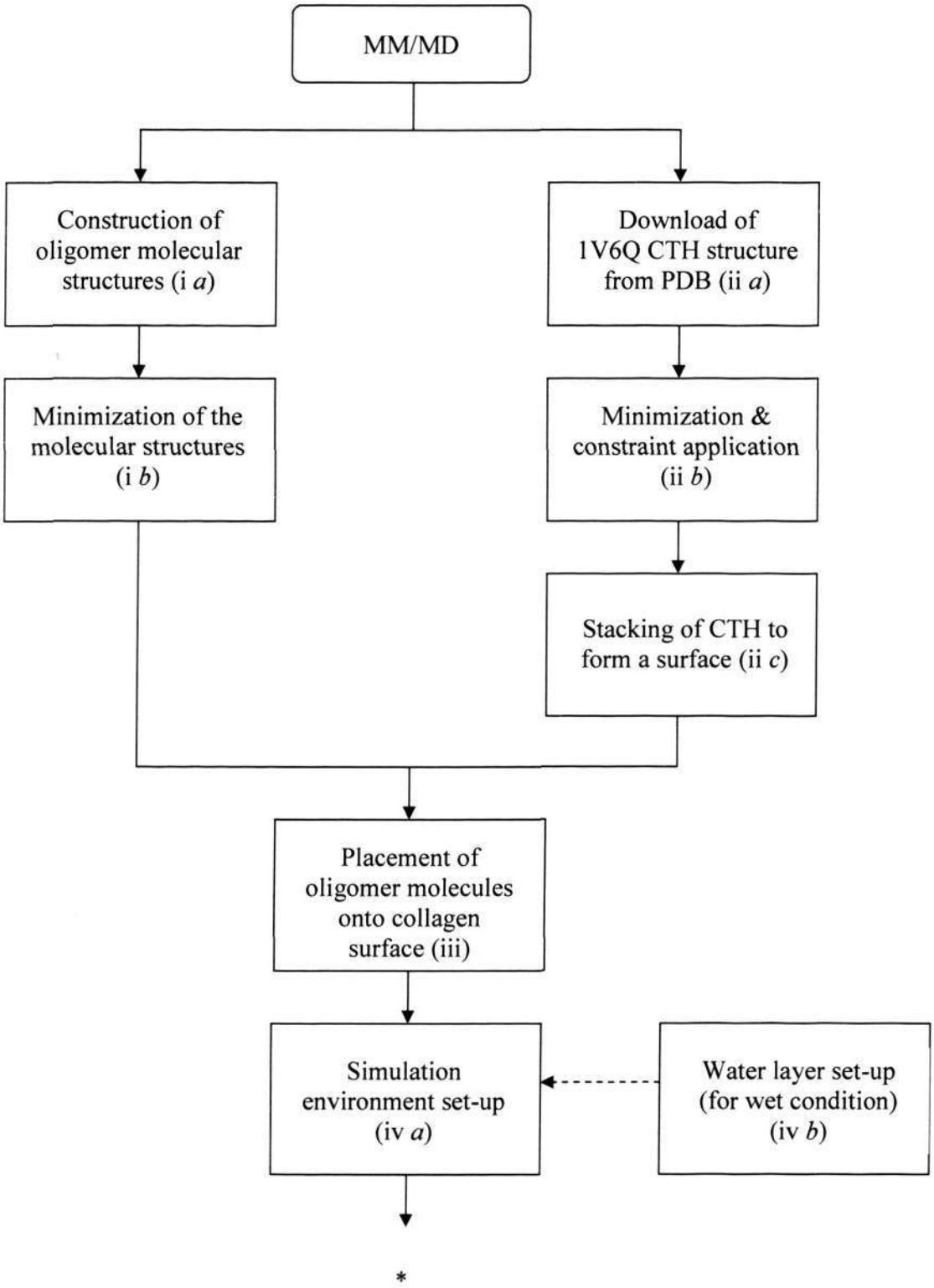

*

(Please Turn Over)

(Diagram continued from previous page)

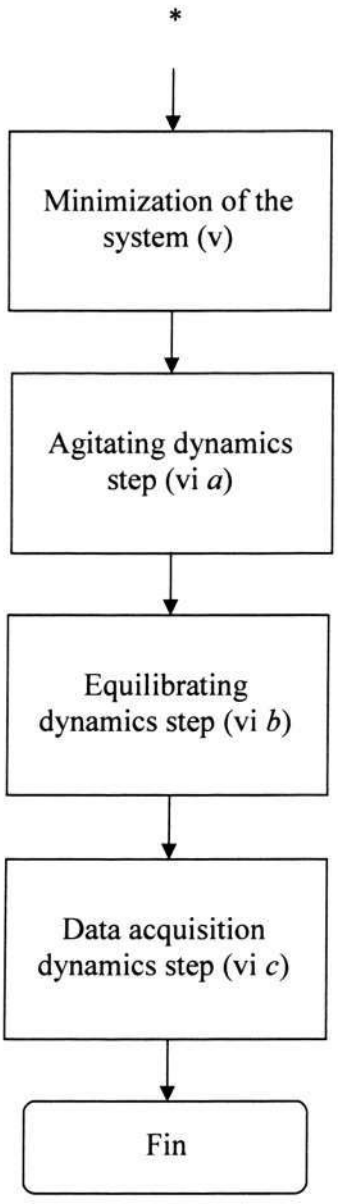

Figure 5.1 A flowchart showing the simulation procedures of the study in Part II. (The numbering in the parantheses are corresponded in the text where relevant.)

5.2.1 Construction of the Oligomer Molecules

All oligomer molecules were drawn by the *Sketch tools* in *Material Studio (i a)*. *Figure 5.2* shows all the oligomers. The similarities and differences among the structures of these oligomers can be seen in the figure. They were drawn by first placing the backbone carbon atoms (and oxygen atoms in PEO and PPO) in a linear configuration with joining covalent bonds; and then the side groups are added onto the structure by joining the atoms to the backbone through covalent bonds. The degree of polymerization was selected according to the length of the collagen triple-helix, i.e. ~ 24 Å. A polymer chain that has a comparable length with the collagen triple-helix is about 5 – 10 in the degree of polymerization depending on the length of the monomers. In this way, for all oligomers, the number of the atoms on the backbone is maintained at about 20.

After the construction, the type and the charge of the atoms were assigned automatically by COMPASS force field in Discover Modules and were manually checked for the correctness. The molecules were then structurally optimized to attain stable configurations *(i b)*.

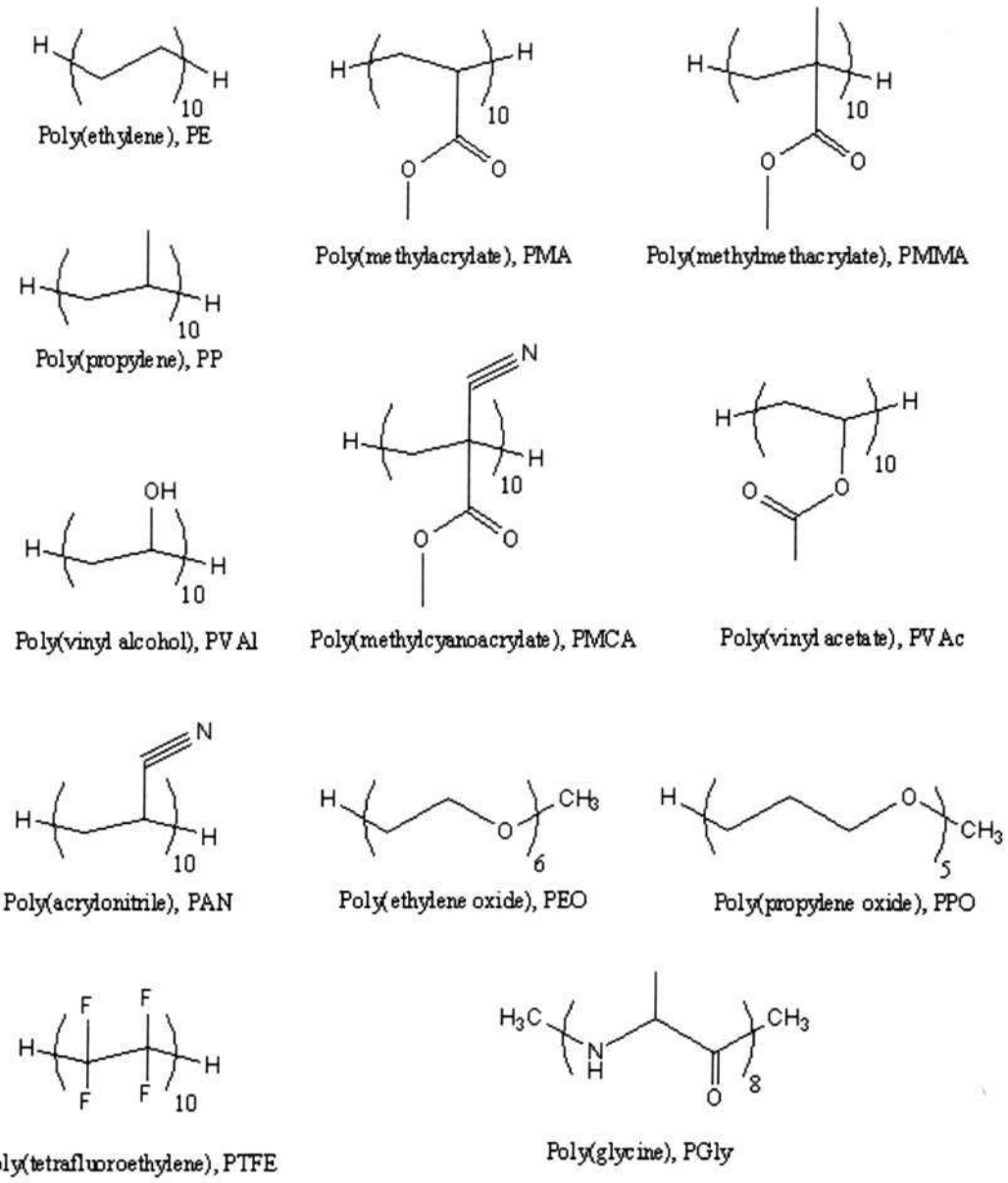

Figure 5.2 Twelve types of oligomers in Part II simulation study. (Note that the molecules in study are in fact oligomers, but for the sake of convenience, their names are the commonly used polymer names.)

5.2.2 Preparation of Collagen Surface

The CTH was obtained from the same source *(ii a)* and processed by the same methods *(ii b)* as described in *Part I.* To prepare the collagen surface, such as those in common collagenous tissues, e.g. tendon and cartilage, the CTHs are stacked in parallel with their long axes in a hexagonal lattice arrangement, in reference to the study of collagen suprafibrillar structure by D.J.S. Hulmes [72]. Collagenous tissue is made up of bundles of these micro-fibrils. In his study, it was found that a collagen fibril is a closed-packed collection of orderly arranged collagen triple-helices, as shown in *Figure 5.3*. The diameter of a CTH is ~ 15 Å; and the distance between any two triple-helices is ~ 15-16 Å. Therefore, the triple-helices are almost in touch with each other in an approximately hexagonal array.

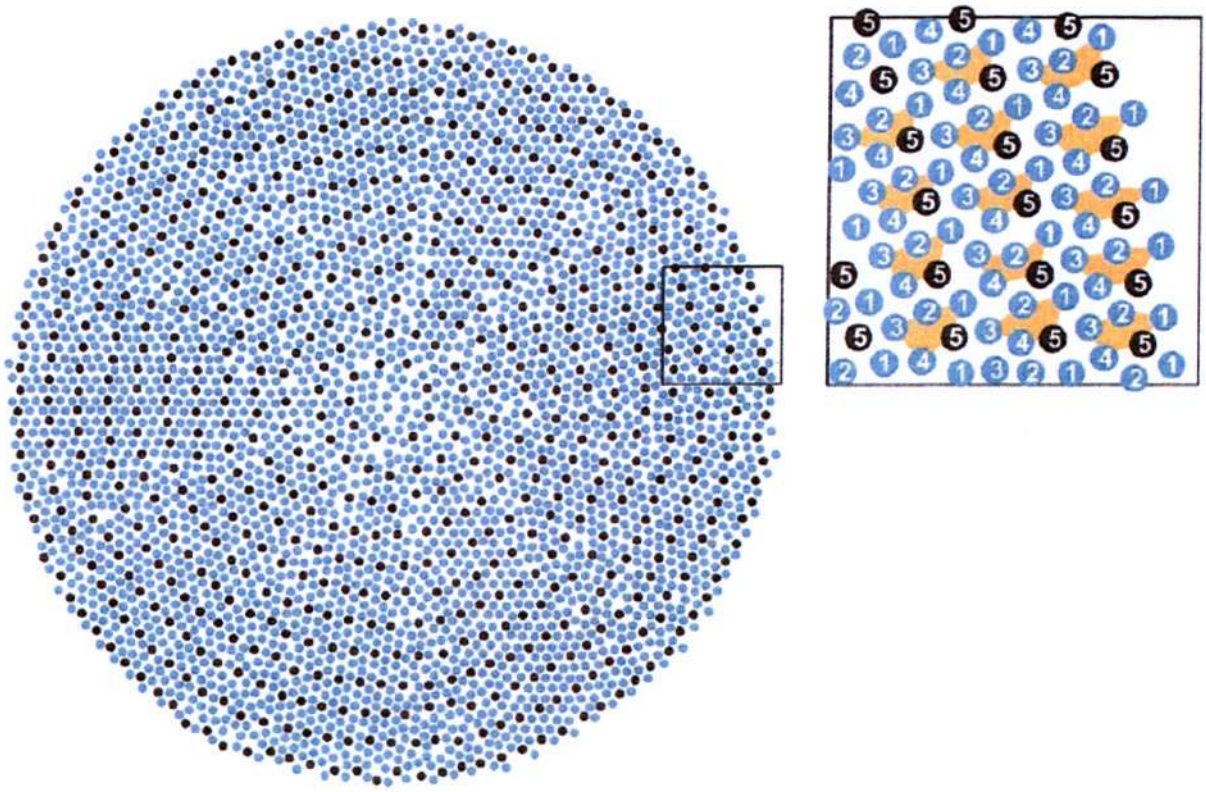

Figure 5.3 The representation of the structure of a strand of collagen that made up of thousands of micro-fibrils – triple-helices [72].

Apparently, it is not possible to include the whole collagen fibril in the study with the current-state atomistic and molecular simulation techniques due to heavy memory requirement. Hence, only a small portion on the surface of the fibril is focused. This is also at the dimension that is relevant to the interest of this thesis, which is the adsorption of functional groups with tissue surfaces. The surface of the fibril was constructed by placing 9 strands of minimized 1V6Q CTH obtained from Protein Databank in a hexagonal array in two rows (layers). The distance between the CTHs was set at ~ 15 – 16 Å *(ii c)*. Knowing the length of 1V6Q is ~ 24 Å, this procedure prepared an "exposed"

collagen surface of 1800 $Å^2$ for interactions to be modeled. The underlying layer of 4 CTHs provides the depth at which longer range physical interactions are operative.

Then, the constraints were imposed sparingly on only the α-carbons and the end-capping carbons in each helix to ensure that the overall collagen structure would not be disintegrated by the subsequent treatments. The structure was then minimized to a convergence level of 0.01 kcal/mol/Å and then equilibrated at 37 °C for 20 ps.

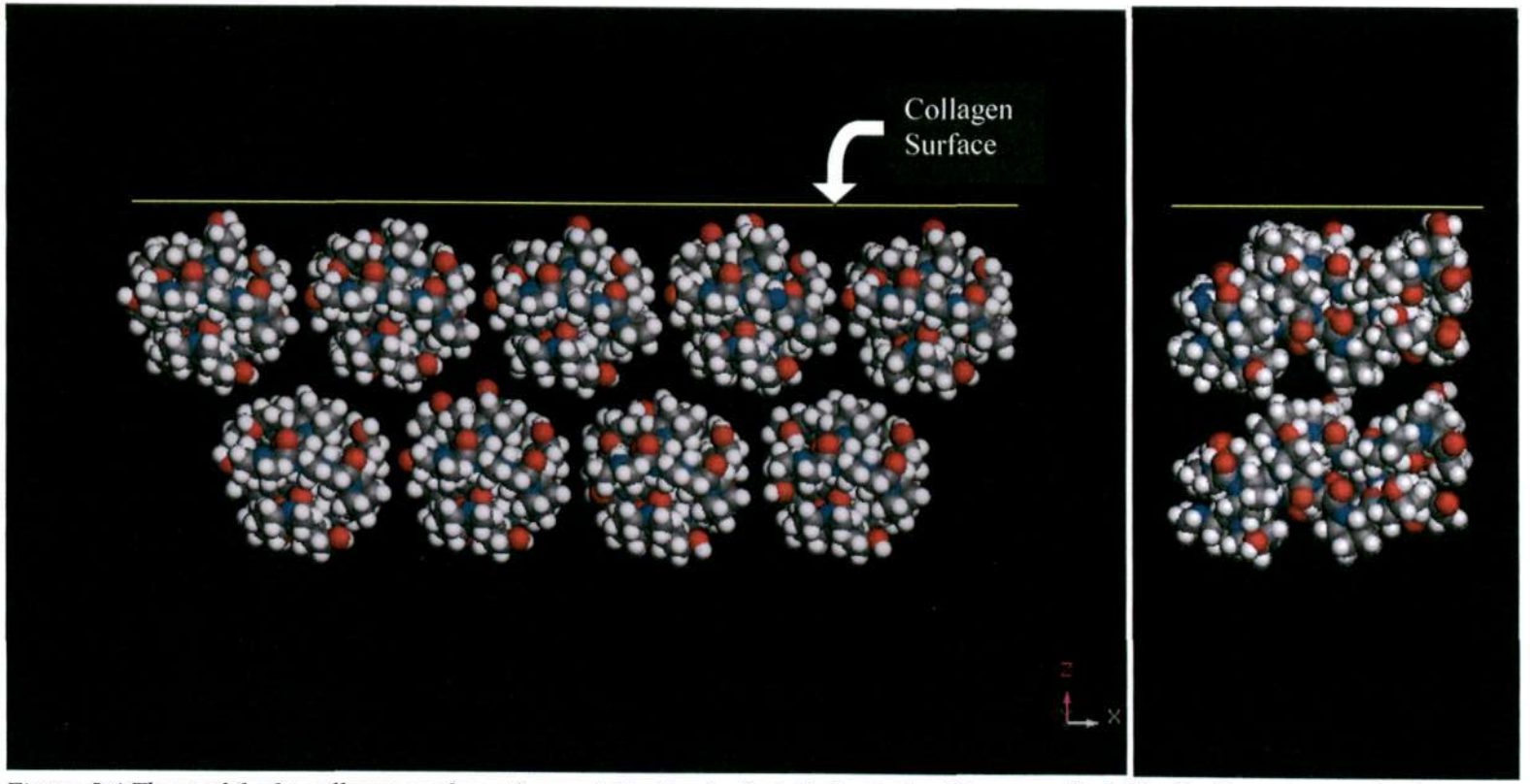

Figure 5.4 The model of a collagen surface after equilibration in Part II simulation.Figure on the left is the front view; and side view is shown on the right.

5.2.3 Placement of Molecules and Set-up of Simulation Environment

A strand of oligomer molecule was placed on top of the equilibrated collagen surface with the long axis of the molecules roughly parallel to that of the triple-helixes. It was placed directly on top of the triple-helix at the centre using *Positioning tools* in *Material Studio (iii)*. Overlapping was avoided. For the two different environmental set up – dry and wet conditions, the initial positions (coordinates) of the oligomer molecules were exactly the same.

After the placement of molecule atop collagen surface, the simulation environment is set up by setting parameters *(iv a)*, as described in the following paragraphs:

Periodic boundary condition

Dry condition is approximated by the vacuum condition in which the interference of gases on the molecular adsorption is considered negligible. Therefore there were only oligomer molecule and collagen surface in the system. They were contained in a "cell" with a dimension of 75 nm × 24 nm × 120 nm. Periodic boundary condition was imposed along the three Cartesian coordinates, i.e. the cell repeated itself in all three dimensions to form a lattice. This setting is particularly benefit for the study of interactions in wet condition. The dimensions of the cells are carefully chosen so that the interaction in one cell did not interfere with that from the adjacent cells. Therefore, each single cell can still be treated as an isolated system.

Fixed Atom Constraints

In the subsequent minimization and equilibration steps, the atoms of the lower collagen layer (which contains 4 triple-helices) were all constrained in space. The primary reason for these constraints was to reduce the computational time and memory. Nevertheless, these constrained atoms were still involved in the final calculations of the interaction energies. In addition, all the α-carbons and end-capping carbons in the upper collagen layer, as they had already been, were constrained in space to prevent the triple-helices to be denatured.

Water layer

For the study under wet condition, a thick water layer was built up and then placed on top of the assembly of oligomer molecule and collagen surfaces. This water layer must be thick enough to insulate the effective interaction region (i.e. the interface between the oligomer and collagen) from the vacuum above the layer, so that the region is fully immersed. The *Amorphous Cell* function in *Material Studio* was used to generate the water layer (*iv b)*. It is a function used to build a "cell" in which a number of input molecules are randomly placed at a predetermined density, i.e. amorphous. However, in *Material Studio 3.1* (an older version) where this work started with, the *Amorphous Cell* function can only handle at most 999 molecules and that would make a cell with an area of 75 nm × 24 nm (which is fixed by the collagen surface area) and a height of 16.6 nm. This height of such water layer is far too small to immerse the interaction region. Nonetheless, such a thin layer of 999 water molecules with a density of 1 g/cm^3 was constructed and equilibrated. Then, the *Layer* function was used to stack a number of

such layers to build up the needed water layer with an area of 75 nm × 24 nm and a height of 50 nm. The resulted water layer was topped with a 30 nm of vacuum so that these uppermost water molecules would not interact with the bottommost collagen structure whose presence is due to the repetitive boundary condition in z-direction. An example of the water shell is shown in Figure 5.5. The water molecules at the top of the cells were constrained in space so that they would not "evaporate" into the vacuum above during the dynamics run.

The resulted water layer has an orderly repeated structure of water molecules along z direction (the structure repeated every z nm) because the stacked cells are all identical. To remove this unrealistic situation which was resulted from the method of cell construction, an equilibration run was done on the resulted cell with dynamics at 37°C for 100 ps.

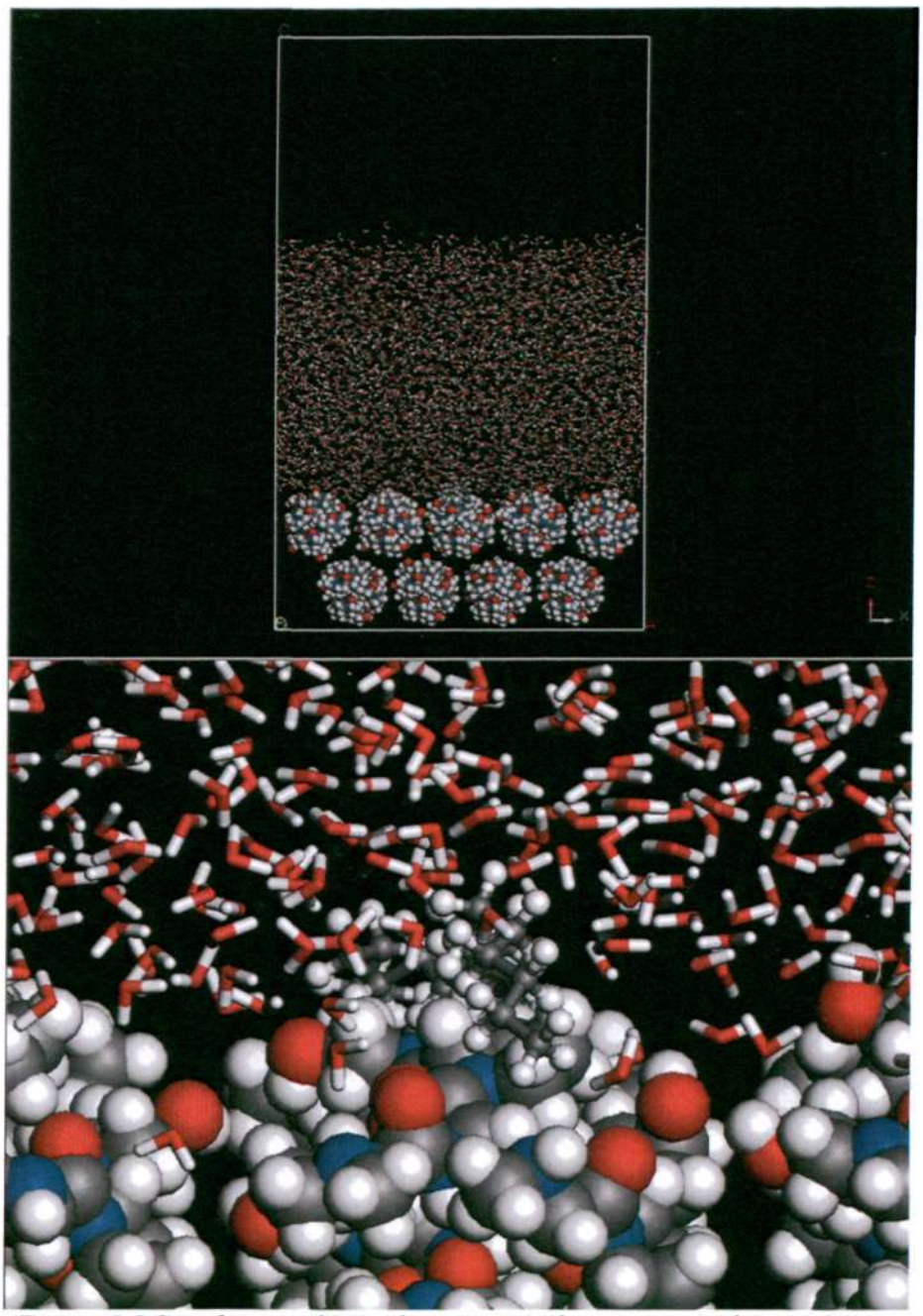

Figure 5.5 Simulation of PE adsorption in the presence of water layer.

Cut-off distance, spline width and buffer width

The values of the cut-off distance, spline width and buffer width were optimized in some preliminary studies. The optimized values that were used for the simulation steps as minimization and dynamics run are 20.50 Å, 3.00Å and 1.00 Å, respectively.

5.2.4 Minimization and Dynamics Set-up of the System

After putting together the components, i.e. collagen and oligomer, and (for wet condition) water, the system was then subjected to a minimization step. Steepest descent algorithm was used up to the energy convergence of 10 kcal/mol/Å and the following was done by conjugate gradient algorithm up to 0.01 kcal/mol/Å, which is sufficient to prepare the optimized structure for the ensuing dynamics run.

The dynamics run was divided into three steps: (a) agitating; (b) equilibrating step; and (c) data acquisition step. In the agitating step *(iv a)*, the simulation temperature was purposely set to a high value so that the molecules in study have sufficient energy and mobility to adjust their conformation to a more thermodynamically favorable one. This temperature was set to be 1000 K, at which the polymer molecule gain energy to adjust its conformation but does not dislodge from the collagen surface. The simulation time was 20 ps. A *simulated annealing* scheme was implemented when the temperature was raised. In this scheme, temperature was raised stepwise from low to high temperature, instead of ramping up to the target temperature (see *Figure 5.6*). After every stepwise increment, the system was held at that temperature for a certain elapsed time to equilibrate. In equilibration step *(iv b)*, temperature was set at the physiological temperature, the temperature at which TAs are functioning. Again, this temperature was

reached by the *simulated annealing* scheme and the system was equilibrated at this temperature for 20 ps. Data acquisition step *(iv c)* is simply an extension of the equilibrating step. It held the system at 37 °C for 10 ps and collected the trajectories of the system (i.e. positions, velocities and accelerations) every 500 fs. These trajectories were going to be extracted and analyzed. For all three steps, simulation parameters were set as followed: NVT statistical ensemble was used; dielectric constant = 1.00; cut off distance = 20.50 Å, spline width = 3.00 Å, buffer width = 1.00 Å; and time step = 1 fs.

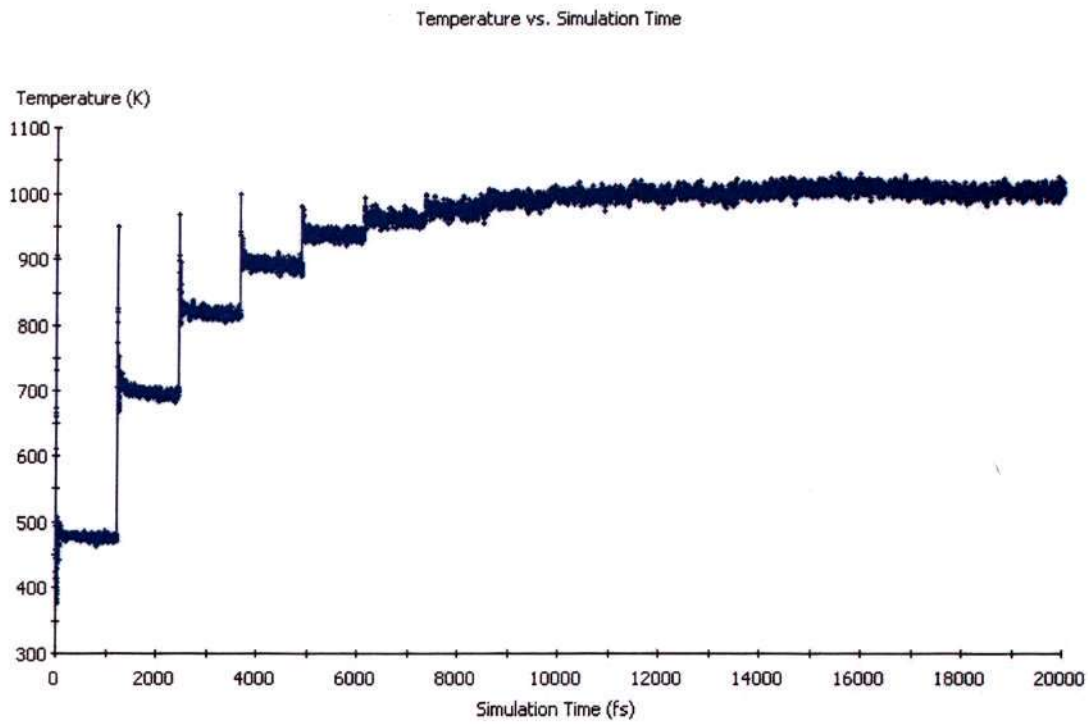

Figure 5.6 A simulated annealing process in which the temperature of the system is increased stepwise to the target temperature.

5.3 Results

5.3.1 Overview of Oligomer Molecule adsorption on Collagen in Dry Condition

Figure 5.7 shows the ranking of the interaction energies between the 12 types of oligomer molecules and collagen surface in vacuum, i.e. in dry condition. The total interaction energy, indicated by the relative contributions of vdW and electrostatic components, are presented. As mentioned in *Part I*, the energy in negative value means that there is attraction.

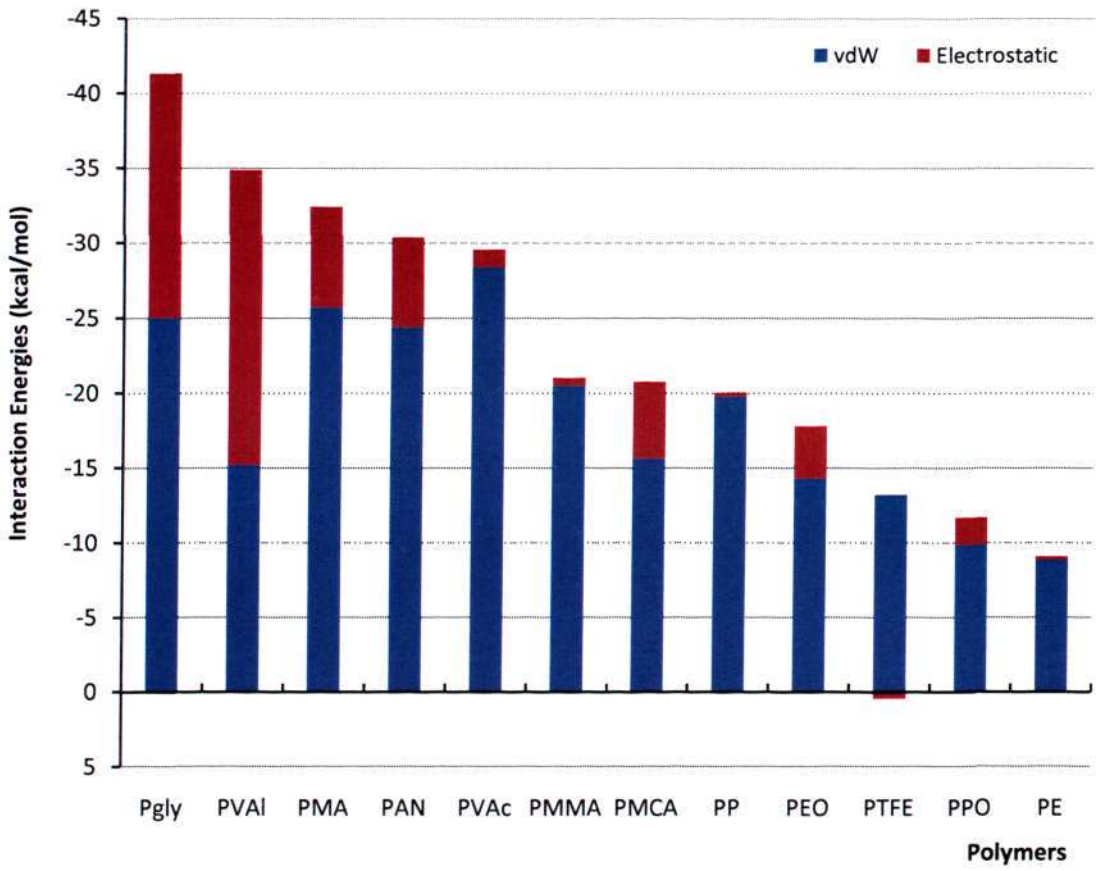

Figure 5.7 Adsorption energies of oligomers on collagen surface in dry environment. The oligomers are arranged in descending order according to their total interaction energies.

5.3.2 Overview of Oligomer Molecule adsorption on Collagen in Wet Condition

The interaction energies between oligomers and collagen under wet environment are presented in *Figure 5.8*. It is noted that the ranking of the oligomers is quite different than that in the dry condition.

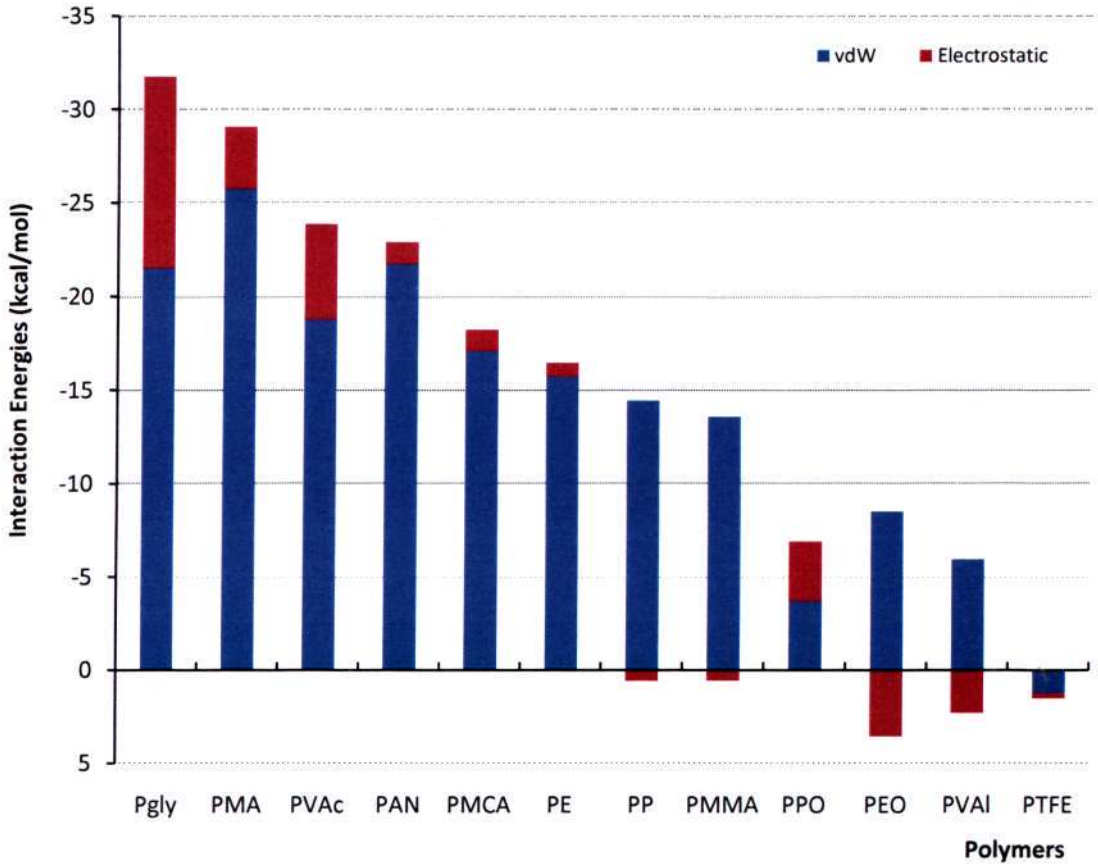

Figure 5.8 Adsorption energies of oligomers on collagen surface in wet environment.

5.4 Discussions

The Discrepancy in the Magnitude of Calculated Interaction Energies in Part I and II

Before any discussions, the difference in the calculated energy values in Part I and Part II shall be mentioned and commented. It is noted that the energy values calculated for *oligomer molecule-collagen surface* interactions are much smaller than those *small molecule-CTH* interactions. Given two different simulation set-ups for the studies in *Part I* and *Part II*, it is expected that the results will be different and some of the possible reasons for the discrepancies are:

(1) In *Part I*, around a CTH there are 30 small molecules which have good mobility due to their small size. Therefore, they could easily move to search for favorable "docking" positions *to each one of them*, thereby the total energy is minimized. Oligomer molecules in *Part II* is lacking of this mobility because all atoms is constrained by the adjacent bond-sharing neighbors.

(2) The contrast of the charge distributions on small molecules is greater than those on large molecules, e.g. carbon atoms on the terminals of the chains is more polar than those on the middle backbone (-0.159 vs. -0.106). The electrostatic interaction energy of small molecules with collagen is therefore stronger.

(3) In *Part I*, small molecules are placed around the triple-helix. Due to a different set-up in *Part II*, oligomers are confined only on top of the surface. So, the energetically favorable sites are lesser in number in the latter case, and hence smaller in adsorption energy.

The Dominance of VdW Component

It is observed in *Figure 5.7* that vdW component dominates over electrostatic interaction and is responsible for oligomers' affinities to collagen surface. This big contrast echoes the discussion made in *Section 4.5.4*, which says that the ratios of vdW to electrostatic components (V/E ratio) increases as the lengths of the alkyl chains in small molecules increase. This finding is not favorable for TAs because, despite its ubiquity among any molecules, vdW interaction is generally a weak interaction; and the adhesion it caused is temporary and tends to fluctuate. In the wet situation, as depicted in *Figure 5.8*, the dominance of vdW in most oligomers is getting more obvious. The electrostatic interaction energies, which are strong for small molecules (i.e. monomers before polymerization), further diminishes in the presence of water. This is one of the core reasons why wet environment does not support adhesion.

VdW interaction depends on two factors: (a) the number of atoms in the molecule; and (b) the spatial distance between molecule and collagen (see *Equation 3.1*). Even if the numbers of atoms of two oligomers are the same, they would not necessarily result in same vdW energies because the intermolecular distances differ. For example, PVAl and PAN both have 52 atoms in the molecules, their vdW interaction, however, differs by ~ 9 kcal/mol. The equilibrated distance is a result from the energy balancing at

the preset temperature, a process which involves not only vdW but also electrostatic interaction. In simpler terms, the vdW component of adsorption energy is a function of the equilibrated distance, which in turn is a function of the vdW and electrostatic energies during the equilibration process.

In the study, the magnitude of vdW interaction energy of all oligomers range between ~ -9 kcal/mol (PE) to ~ -28 kcal/mol (PVAc). Incidentally, the number of constituting atoms in the molecules ranges from 47 for PEO to 152 for PMMA. While the number of atoms per molecule varies greatly, the range of the vdW interaction energy is relatively narrow. In other words, modulation of vdW energy will not give rise to significant improvement in adhesion/attraction.

The Importance of Electrostatic Component in Dry Environment

Although the electrostatic component has been greatly reduced in the *Part II* compared to that in *Part I*, it still plays a role in determining whether the molecules adsorb to collagen surface or not.

Electrostatic interaction does not depend only on the numbers of atom, but, more importantly, depends on (1) the charge distributions and polarity of the molecules and (2) the dielectric constants of the medium (see *Equation 3.1*). From *Figure 5.7*, it is clear that the molecules that exhibit highest affinity to collagen in dry condition are those molecules that have prominently larger proportion of electrostatic component. These include poly(glycine) , PVAl, PMCA and PAN with the percentage of electrostatic

component of 39.4%, 56.3%, 20.7%, and 19.5%, respectively. On the other hand, molecules like PE, PP, and PMMA, which lie towards the lower end in the spectrum, have electrostatic percentages only ~ 2%. This finding can be extended to categorize the polymers into two groups: the "polar" oligomer group, whose electrostatic interaction is prominent, e.g. PGly, PVAl, PMA, PAN, PMCA, PEO and PPO; the "non-polar" oligomer group, whose electrostatic interaction is close to nil, e.g. PE, PP, PTFE, PMMA and PVAc. In general, the "polar" polymers outperform "non-polar" polymers in adhesion on collagen surface with their greater electrostatic components.

While all molecules show attractive electrostatic interaction, PTFE is one obvious exception. Inspecting the twenty frames of simulation trajectories from which data were compiled (*Figure 5.9*), it is seen that the electrostatic component is fluctuating around zero and in many cases they acquire positive values, a fact that hints electrostatic repulsion even in equilibrated condition. This can be linked to real situation where PTFE is one of the most difficult materials to "stick to". (PTFE is the non-stick coating on cooking wares and lab consumables.)

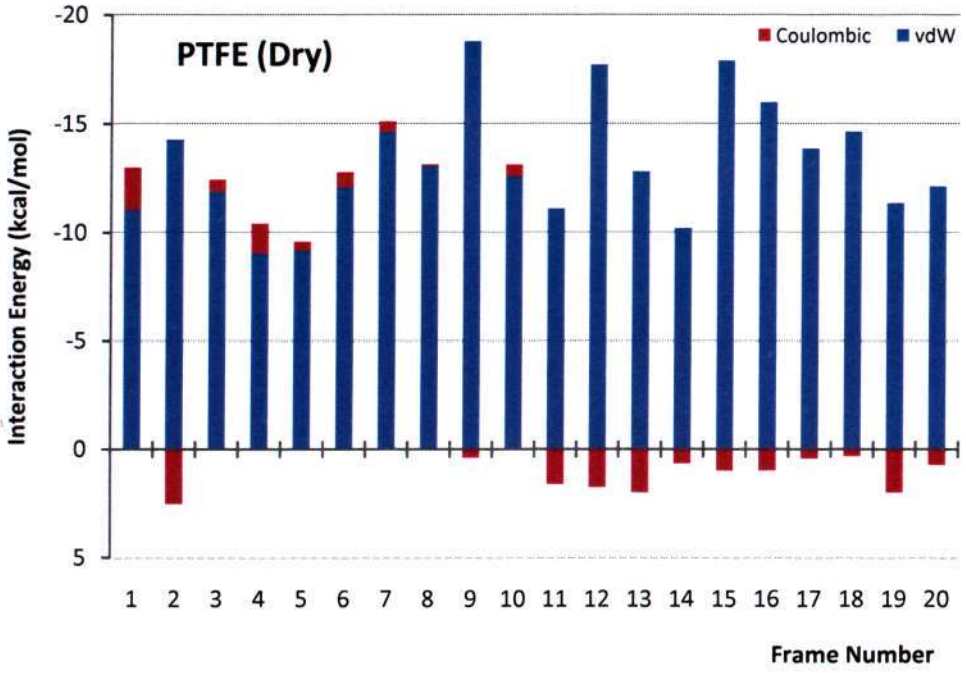

Figure 5.9 Interaction energies of all trajectory frames in data acquisition cycle for PTFE in dry.

The Adsorptions in Wet Environment

Comparing *Figures 5.6* and *5.7*, it is seen that the interaction energies in wet environment are overall reduced. It is followed that, in general, the adsorption interaction becomes more unfavorable in wet environment. Through some careful observations into the energy components, reductions in both vdW and electrostatic interaction energies are seen in most cases. While the reduction of the electrostatic component is due to the charge-screening effect, i.e. water's much greater permittivity reduces the electrostatic interaction energy; the drop in vdW component is purely due to the disruption of the water molecules and is inter-dependent on the accompanying electrostatic interaction (i.e. these together determine the equilibrium intermolecular distance). The differences in adsorption energies for the oligomers, from dry and wet environments, are tabulated in

Table 5.1. Both absolute drop and percentage drop (relative to the adsorption in dry environment) are presented.

The drop in electrostatic interaction, a phenomenon shared by a few oligomers, is a result of the disruption of the coulombic interaction by surrounding water molecules. This disruption is very apparent in the smaller (the diameter) "polar" polymers like PEO, PAN and PVAl, comparing both absolute drops and percentage drops in electrostatic components. For bulkier "polar" polymers, like PGly and PMCA, the drop is smaller. It is suggested that the orientations and conformations of the smaller molecules, due to their light weight, are more affected because of (1) the strong electrostatic interactions between water and polymer that reduce the desired interaction between polymer and collagen; (2) the disruption of the polymer-collagen adsorption sites by the agitated water molecules; (3) mechanical collisions of the aggressive water molecules on the local segments of the polymer that hinder the polymers from getting to the proximity of collagen surface.

Table 5.1 The differences between dry interaction energies and wet interaction energies, represented in absolute term and percentage term. (The values are obtained by subtracting energies in dry from energies in wet; hence, negative value means weaker interaction in wet, and vice versa.)

	Absolute (kcal/mol)			Percentage (%)		
	Total	VdW	Elec	Total	VdW	Elec
PE	7.44	6.89	0.55	82.1	77.6	309.0
PPO	-4.73	-6.18	1.45	-40.5	-62.6	81.7
PTFE	-14.29	-14.41	0.12	-111.7	-109.1	-29.0
PEO	-12.76	-5.76	-7.00	-71.8	-40.3	-201.2
PP	-6.08	-5.28	-0.80	-30.4	-26.8	-325.7
PMCA	-2.46	1.53	-3.98	-11.9	9.8	-78.0
PMMA	-7.89	-6.85	-1.04	-37.6	-33.5	-207.5
PVAc	-5.63	-9.56	3.93	-19.1	-33.7	335.3
PAN	-7.40	-2.59	-4.81	-24.4	-10.6	-80.6
PMA	-3.29	0.11	-3.40	-10.2	0.4	-50.6
PVAl	-31.14	-9.25	-21.89	-89.4	-60.8	-111.5
PGly	-9.56	-3.45	-6.10	-23.1	-13.8	-37.4

The effect of water disruption on the adsorption interaction in "non-polar" molecules is less predictable. PE is the only unique molecule that shows better adsorption behavior in wet environment. Both the vdW and electrostatic components show improved adsorption, i.e. improvement of PE's adsorption to collagen in wet condition. The hydrophobic PE molecule might be repelled by the water on top and pressed closer to collagen at bottom. This corresponds to the "hydrophobic interaction" in literature. The relatively flexible polymer chain makes it possible to conform to the hydrophobic regions on collagen that may result in the overall energy decrease.

For PTFE, vdW and electrostatic energies are both positive and that implies its complete repulsion from collagen in wet condition. The chemical nature of PTFE is exactly opposite to that of PE because of the different electronegativity values of C, H

and F atoms. In PE, backbone C is slightly negatively charged and H is slightly positively charged; In PTFE, backbone C is slightly positively charged and F is slightly negatively charged. The polarity in PTFE is greater due to the larger electronegativity difference between C and F. This unique chemical nature of PTFE results in the repulsion from collagen surface. The other "non-polar" polymers show reduction in overall energy in wet environment but no clear trend is observed in the two contributing components.

PVAl – From Best to Worst

PVAl experiences the greatest drop in total energy when exposed to water environment, two thirds of which is due to the drop in electrostatic energy. This is also the greatest drop in electrostatic energy among the other oligomers. *Figures 5.9a* and *b* compare the vdW and electrostatic components of PVAl in each of the 20 frames from which the averages in *Figures 5.6* and *5.7* are obtained for dry and wet environments, respectively. It can be seen that both vdW and electrostatic interactions are quite stable in the case of dry conditions but large fluctuation in the interaction energy is observed in the case of wet condition. Water and alcohol are known for their infinite miscibility; and therefore affinity of PVAl to water may be significantly higher than the affinity of PVAl to collagen. Due to this, the interaction of PVAl with collagen is greatly reduced. As a comparison, the twenty trajectory frames of PMCA, which is a typically less-perturbed system, in wet environment is shown in *Figure 5.11*. Although the electrostatic component is also fluctuating, the overall interaction is quite steady for all frames because of its bulkier size and sturdier structure.

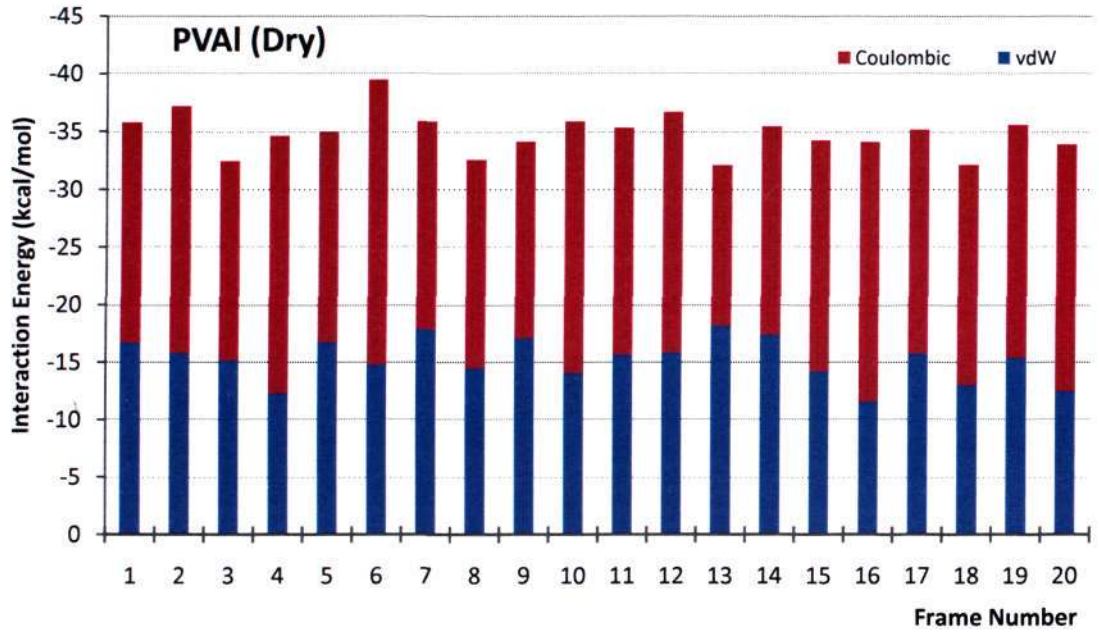

(a)

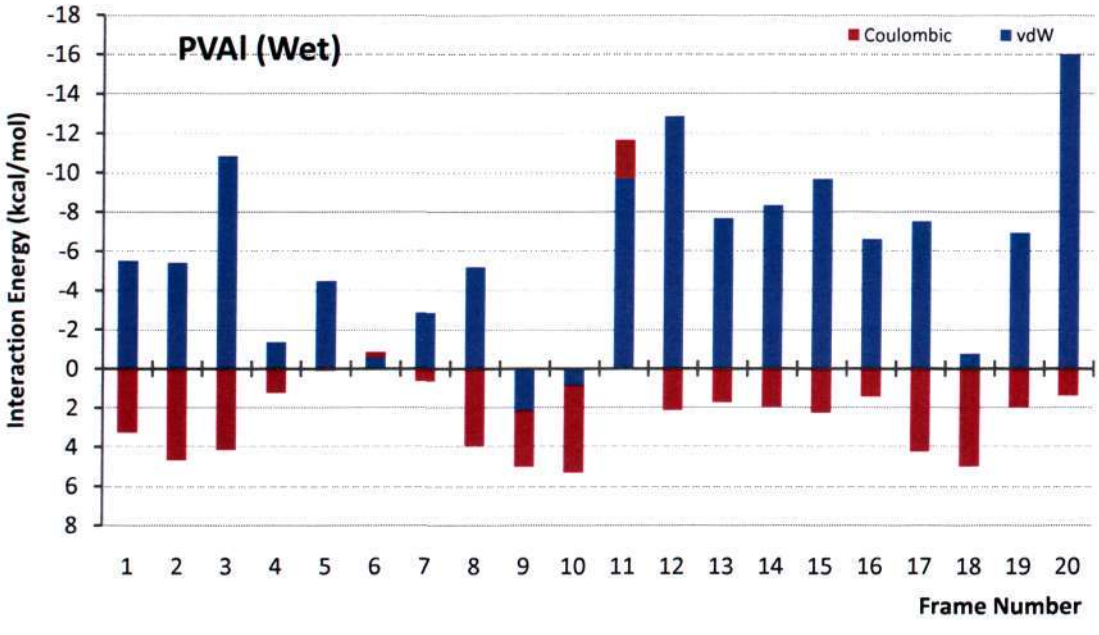

(b)

Figure 5.10 Interaction energies of all trajectory frames in data acquisition cycle for PVAl in (a) dry and (b) wet.

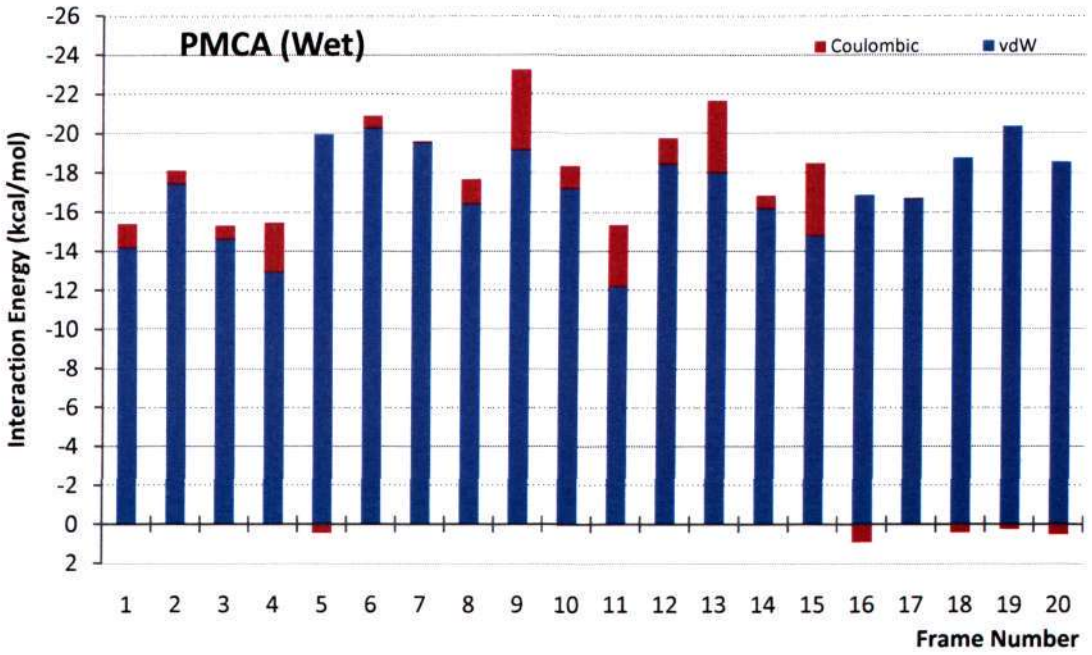

Figure 5.11 Interaction energies of all trajectory frames in data acquisition cycle for PMCA in wet.

Poly(glycine) – Proteins as Potential TA

PGly adsorbs most strongly onto collagen surface among the others in both dry and wet environments. This finding is in agreement with results in Part I simulation where small molecule with peptide functional group is found to be having a better affinity to collagen than that of water (see *Figure 4.3*). PGly is a "polar" oligomer and the outstanding adsorption of PGly is the consequence of its modest vdW interaction and strong electrostatic interaction. The strong electrostatic interaction is also seen in the small glycine molecules (with peptide group). So, it is believed that the peptide functional group (which is the only functional group in PGly) has good affinities with collagen, which also has peptide functional groups located in the inner part of the helical structure. In wet condition, the reduction in both vdW and electrostatic adsorption is rather small,

which means that, PGly still adsorbs well onto collagen surface even under the electrostatic screening effect and the mechanical disruption of water molecules. This may be due to the fact that PGly has a bulkier size and its conformation is then more difficult to be altered by the small water molecules.

PE, PP, PTFE, PAN, and PVAl

These oligomers (together with PVAl) share structural similarities. They are all relatively simple and carry simple functional groups (or, for some, no functional group at all). In dry condition, the plain PE has the lowest interaction energy and PP, its close relative, shows greater interaction, particularly due to greater vdW interaction. PTFE, a smaller molecule than PP, has an interaction energy lying between those of PE and PP (as discussed, the vdW is dominant and the electrostatic energy is unstable). PAN and PVAl are functional oligo-olefins; and both of them show greater adsorption in dry state due to the greater electrostatic component brought about by the polar functional groups. Here, alcohol group acts better than the cyano group.

In wet condition, it is a very different story. While PE shows stronger adsorption possibly due to hydrophobic interaction, all oligomers discussed in this section are less attracted to collagen surface due to diminished vdW and electrostatic adsorption. It is most obvious in PVAl which carries alcohol functional groups that has strong affinity to water; and in PTFE which is unique in its charge distribution. In the extreme, PTFE shows complete repulsion to collagen.

PMA, PMMA, PMCA and PVAc

Acrylates are often used as structural adhesives. In the simulation results, PMA, as the simplest acrylate oligomer, shows good adsorption on collagen substrate. It ranks the third out of all molecules studied. In dry, its vdW component is large and its electrostatic component helps to improve its interaction with collagen surface. Similar to PGly, in wet condition, PMA shows a small decrease in electrostatic component and nearly no difference in vdW component. Therefore, its adsorption is still rather good in wet condition.

PMMA, with an additional methyl group that is bonded to the same carbon on which acrylate group is bonded, changes the adhesiveness of the molecule substantially. The vdW interaction is weak, possibly due to the structural inflexibility and a low electrostatic interaction. In wet, the adsorption energy of PMMA lowers further with weakened vdW interaction and slightly repulsive electrostatic interaction.

As the well known cyanoacrylate quick glue, PMCA is however not showing especially good non-specific adsorption on collagen. In dry, it ranks lower than PMMA with an even smaller vdW interaction but larger electrostatic component (it has a lesser number of atoms but more abrupt charge distribution). In wet condition, its electrostatic component is reduced and vdW component remains roughly the same. It adsorbs better than PMMA in wet. This result implies that the adhesion of cyanoacrylate TA is not determined by non-specific interaction and some other mechanism(s) should be operative.

PVAc differs from PMA only in the different orientation of ester groups in its side groups. The adsorptions of PVAc on collagen in wet and dry conditions are more dependent on the vdW component and are weaker than that of PMA. However, the electrostatic energy of PVAc increases in wet condition.

PEO and PPO

These two simple molecules are close relative to each other but their properties are well known to be different. PEO is hydrophilic, due to its higher frequency of O atoms, and PPO is hydrophobic. In the study, both of them do not have strong adsorption to collagen but PEO is better than PPO due to greater vdW and electrostatic attraction. However, PEO's behavior is similar as PVAl's in the wet condition – its vdW interaction reduces and electrostatic interaction further reduces to the repulsion region. Similarly non-typical, PPO has a reduced vdW adsorption but an enhanced electrostatic attraction in wet condition. Again, an interaction between PEO and collagen is disrupted by the water because PEO favors water. PPO is hydrophobic and is therefore pressed against the collagen surface by the water layer, thereby increasing its electrostatic adsorption as well as vdW repulsion component. Again, these results strongly resonate with practical situations where PEO is known to be used in non-fouling coatings to prevent adhesion of proteins.

Polymerization

In Part I and Part II, interactions of small molecules (these small molecules can be regarded as adhesive monomers) and oligomers with collagen were studied, respectively. The polymerization process, i.e. from monomer to polymer is not covered in this study. Polymerization and cross-linking is a part of joint formation process. For it to contribute to good joint strength, prior diffusion of the monomers into the tissues is essential. Preceding diffusion in turn is good affinity of the monomers/oligomers to the tissues or substrate of interest and other factors such as rheological behavior which is usually not an issue for monomer solutions. While both diffusion and polymerization processes are important in contributing to a good joint as well, due to constraints in time and software, the scope of this thesis is around the affinity of functional groups to tissue. It is hoped that with future advancement in molecular simulation, concurrent diffusion and polymerization processes (which involve molecular chemistry) can be modeled to provide even more insight into the adhesion process in biological tissues.

5.5 Implications from Modeling and Simulation Works: A Conclusion

In this sub-chapter, conclusions and implications from the modeling and simulation work of previous 2 chapters will be summarized. Monomers have better affinity than oligomers (of similar functional group) towards collagen due to its mobility and stronger electrostatic interaction. This may imply that the affinity of the adhesive to the collagen decreases with polymerization time as the monomer converts to oligomers and then polymers over time. This then suggests that an ideal TA should use monomers that have high affinity to collagen to start with. This is also advantageous from diffusion point of view as monomers will probably have higher diffusion than oligomers and polymers.

Secondly, it was observed that generally functional groups that have high polarity resulted in greater physical adsorption in both dry state as well as when in the presence of water molecules. An exception is PVAl due to its strong affinity to water. However, in the presence of water the simulation results confirmed that the interaction of the functional groups to the substrate decreased drastically in general. This is due to a great part the reduction in the electrostatic interactions especially in the "polar polymers" caused by electrostatic screening and the great affinity of water to collagen (as seen in Part I) that destabilizes the desired adsorption events. The VdW energies can reduce too because the orientations of the molecules are disrupted. By far, polymers with amide/peptide bonds show exceptionally good adsorption in dry condition; and its adsorption in wet condition did not deteriorate as much as some other polymers. This can partly explain the effectiveness of fibrin adhesives.

Hydrophobic interaction, which is generally weaker was also observed and its origin is better understood through the simulations. It is caused by increased attraction in both vdW and electrostatic components that arise from the water-polymer repulsion. The origin of non-stickiness of PTFE also finds its root in the unique charge distributions on the polymers, a situation totally in the opposite to all other polymers. This conclusion however is still crude and has to be further investigated by more extensive studies.

This section marks the end of the simulation works of this PhD thesis. In the following chapters, experimental measurements at microscopic and macroscopic scales are carried out and the conclusions gained from *Chapters 4 & 5* would help to explain the experimental results.

Chapter 6
Adhesion Force Measurements on Microscopic Scale

6.1 Introduction

This chapter presents the work on experimental measurements of atomic force using Atomic Force Microscope (AFM). The measurements provide supporting results to the theoretical study of molecular adsorption in *Chapters 4 & 5*. Both molecular simulations and atomic force measurements are the tools introduced into the field of TAs for the first time by this thesis to improve understandings and designs.

The interactions of four functional groups, i.e. –COOH, –OH, $–NH_2$, and $–CH_3$, with a collagenous substrate were measured with the functionalized probe tips. Both dry and wet conditions were examined. While the exact correspondence to the functional groups studied in the molecular simulation is almost not viable, the results presented here aims to approximately relate the experimental results with the simulation results.

The following *Section 6.2* begins with underlining theory and instrumentation of AFM. A brief review on the works that have been done in measuring non-specific interactions using AFM is then introduced in *Section 6.3*. Next, *Section 6.4* details the procedures of the experiments and, finally, results and discussions are shown in *Section 6.5* and *Section 6.6*, respectively. A conclusion is made in *Section 6.7*.

6.2 Theory and Instrumentation

AFM, as one member in the scanning probe microscope family, "feels" the surface attraction or repulsion when the probe is approaching the substrate surface. The instrument can be divided into 4 parts based on their functions (see *Figure 6.1*):

(1) ***Probe***

The explanation of AFM working principle could be focused onto the most vital part of the instrument – the probe. The probe is a made up of a thin (in micron scale) and flexible cantilever beam and a very tiny pyramidal tip (in nano scale). The tip is located at near the front end of one side on the cantilever. Ideally, the tip has an extremely sharp peak that is, in theory, made up of only one atom. This ideal case however never exists and most of the tips have a tip radius of about 50-100 nm (see *Appendix 2*).

(2) ***Positioning system****, i.e. piezoelectric transducer and displacement motor*

The positioning system controls the vertical travelling of the probe towards the substrate surface. High-precision displacement motor is used for coarse adjustment when the probe is still far from the surface. When the probe (the tip, to be more precise) is in the proximity of the surface, piezoelectric transducer is used to fine-tune the z-distance. When the peak of the tip is pressed against the substrate surface, mechanical forces develop and cause the cantilever to deflect.

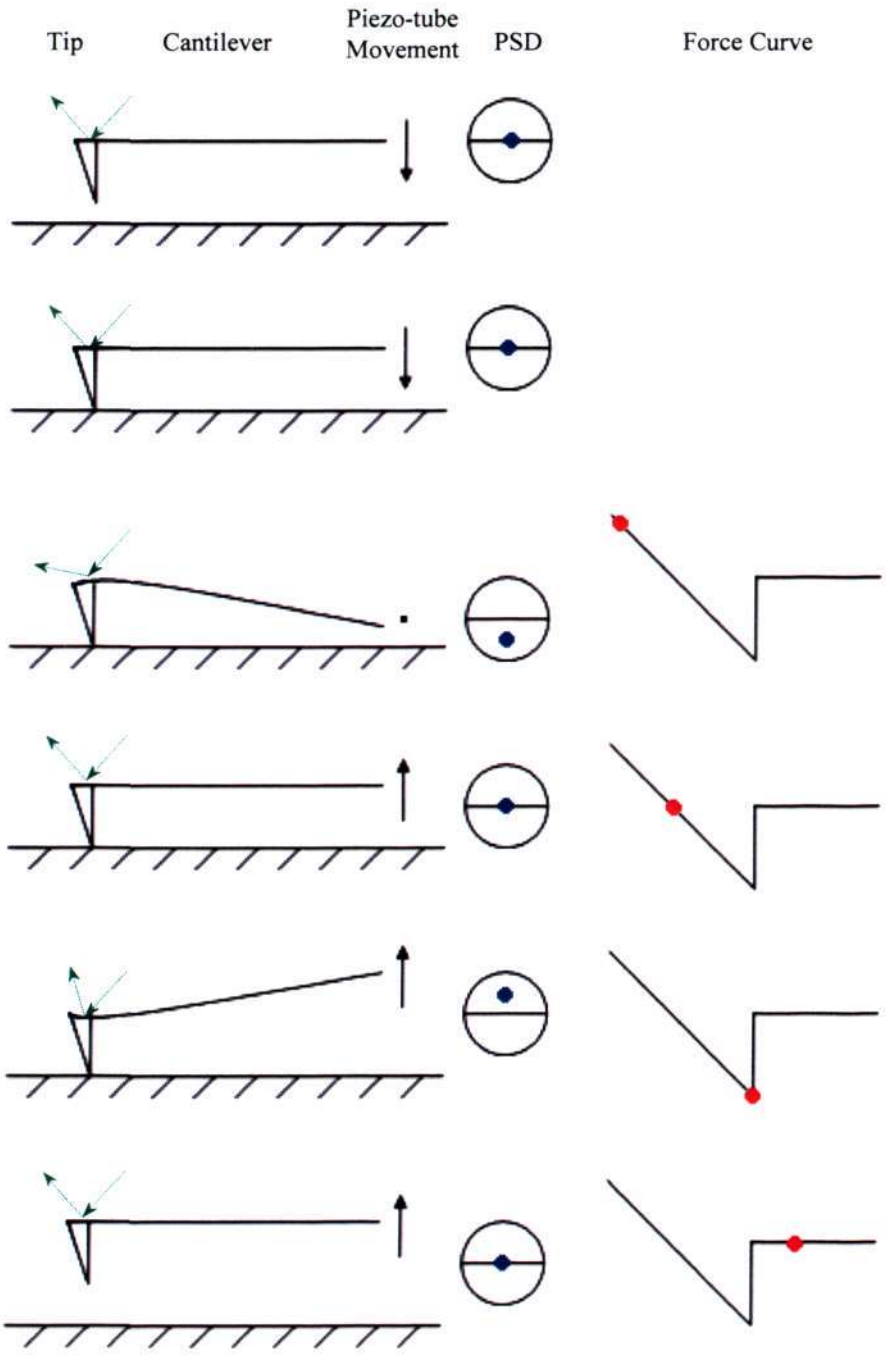

Figure 6.1 The tip-surface interactions and the corresponding retraction curve. The movement of the cantilever is controlled by the piezoelectric translator (measured by x-axis). The deflection of the tip, or more specifically, the inclination of the end of the cantilever, is measured by a reflected laser on photosensitive detector.

(3) ***Probe detecting system***, *i.e. laser light beam and photo-sensitive detector (PSD)*

The amount of the deflection, which is correlated to the magnitude of the force (which in turn is correlated to the z-displacement of the probe), is measured by the probe detecting system that pick the reflected laser beam focused onto the back of the cantilever.

(4) ***Feedback & control system***, *i.e. computer and software*

Feedback system then judge if the probe is pressing too hard or too weak onto the surface (based on user inputs) and command the controlling system to retract or extend the piezo transducer, respectively. This feedback loop is critical to imaging but not force measurements.

The deflection of the tip, the corresponding signal obtained on the PSD and the corresponding data point on the force curve are schematically represented in Figure 4.3. In the extension part (not shown), the tip is moving in a same pace as the piezoelectric translator until it meets the surface. Depending on the mechanical strength and hardness of the surface, the sharp tip can indent into it at some depth or can be stopped totally by the resisting force, causing cantilever deflection. Usually both of these processes happen at the same time. Therefore at the very left end of each of the curves, where the cantilever enters a retraction cycle, the tip has experienced the greatest resisting force and hence greatest deflection. It usually has indented into the sample at some depth (usually very small). As the cantilever continues retracting, the tip is less deflected, until it reaches a point, at which the tip has zero deflection while still touching the surface—"flat-tip

position". Beyond this position, although the piezoelectric translator moves away and tries pulling off the tip from the surfaces, due to the non-specific attractions between the surfaces with functional groups, the tip keeps adhering on the surface and the cantilever gets deflected in the opposite direction. Therefore, the time at which the tip leaves the surface is when the tip-surface attractive force is insufficient to hold them together—"free-tip position"—the vertical position at which the tip is freed, depends on the magnitude of the attractions. This interaction forces will be discussed in next section. After the tip is freed, the force acting on the cantilever is zero and therefore the deflection is zero.

6.3 Review on Non-Specific Interaction Measurement by AFM

Non-specific interactions of some fundamental chemical functional groups have been measured using AFM, though not as widely as specific interactions (for comparison, the strength of specific interactions ranges from 85 ± 10 pN for avidin-iminobiotin to 257 ± 25 pN for streptavidin-biotin, as studied by Florin et. al. [62]) In 1994, Frisbie et al. [73] first reported the force-extension curves of all combinations between hydrophilic COOH surface and hydrophobic CH_3 surface (Table 6.1). They then ranked the strengths of tip-surface interactions in ethanol in descending order: COOH/COOH > CH_3/CH_3 > COOH/CH_3. Applying Johnson-Kendall-Roberts (JKR) model, the authors were able to estimate the contact area between the tip and substrate surfaces at the snap-off point to be ~10nm^2. Knowing the density of the self-assembled monolayer, the authors estimated that the rupture force was contributed by 50 pairs of the functionalities.

Van der Vegte [74] et al. reported a more expanded work in 1997. They functionalized the probe and surface with CH_3, OH, NH_2, COOH, and $CONH_2$ using ω-functional n-alkanethiol and then measured the interaction in ethanol. Based on the JKR theory of adhesion mechanics, the single bond force is calculated. In Table 6.2, the shaded diagonal represents the interactions between similar functional groups. Each value lying out of this diagonal is of the same interaction with its mirror image and the only difference is the locations where the functionalities situated, i.e. tip and substrate. Except the COOH/COOH and OH/NH_2 interactions, all the other interactions give the same level of force regardless of their locations. The authors believed that the adhesion force arising

from these combinations (except CH_3) is actually due to the formation of hydrogen bond since the bond strength can be stronger or weaker depending on molecule polarity, bond length, environment, etc. Comparing the interactions with $CONH_2$, the hydrogen bond energy of each functional group in ethanol was ranked in descending order: COOH > $CONH_2$ > OH > NH_2. It is also interesting to compare the studies of Frisbie and van der Vegte. The former measured a larger interaction of COOH/COOH, a smaller interaction of CH_3/CH_3 and a smaller interaction of $COOH/CH_3$ than the latter. Nonetheless, COOH/COOH interaction was still the strongest in both studies.

Table 6.1 Non specific interactions measured by Frisbie et al [73].

Substrate	Tip	
	COOH	CH_3
COOH	174 ± 64	17 ± 9.8
CH_3	14.2 ± 7	54 ± 18.2

Table 6.2 Non specific interactions measured by van der Vegte et al [74].

Substrate	Tip				
	CH_3	OH	NH_2	COOH	$CONH_2$
CH_3	81	50	54	95	62
OH	57	101	88	109	110
NH_2	59	113	98	105	102
COOH	61	112	95	114	125
$CONH_2$	60	117	100	137	120

In van der Vegte's work, the dependency of the adhesion force of COOH/COOH, NH_2/NH_2 and OH/OH were also reported. NH_2 is ionized to be NH_3^+ at low pH and therefore the tip and substrate repel each other. Hence, NH_2/NH_2 interaction was only seen at high pH due to the formation of hydrogen bonds. The situation was reversed in the case of COOH/COOH as COOH is ionized to be COO^- at high pH. OH/OH interaction, on the other hand, is not affected by the pH value of the environment. Furthermore, the interactions of OH/COOH and OH/NH_2 were also studied by another group of researchers [75, 76]. In both situations, the adhesion forces are at their maximum when COOH or NH_2 is neutral. When they are ionized, the adhesion forces then reduce to near-zero. The negative indication of these relations is that in neutral physiological environment, the interaction forces of COOH/COOH and NH_2/NH_2 are not at their maximum and that of OH/OH is usually small. Therefore, the adhesion in physiological environment is even more difficult. Some detailed review papers on this development of this so-called "chemical force microscopy (CFM)" are published elsewhere [77, 78].

6.4 Experimental Methods

6.4.1 AFM, Probe & Liquid Measurement Set-up

DNP probes (for contact mode imaging) provided by *Veeco*, USA, was chosen for the measurements. DNP is a special probe with 4 cantilevers on a single chip, two on each side. All the cantilevers have triangular shapes but each of them has different length and width, and hence different force constant and spring frequency (See *Appendix 2*). Soft cantilever is needed to detect minute force as it deflects a greater distance at a given force level. However, if the cantilever is too soft, it will deflect too much and the reflected laser signal can be out of the detection range of PSD. Therefore, the cantilever used for each case was chosen carefully in the experiments. The probe consists of a thin V-shaped cantilever beam made of silicon nitride. A sharp pyramidal tip with a square base is located near the end of the cantilever (with a tip-setback of 4 μm). The size and shape of the tip is equivalent in all cantilevers. The detector side (top) of the cantilever is coated with a 15 nm-thick of chromium layer to aid its laser reflectivity while the tip side (bottom) of the cantilever is coated with a 60 nm-thick gold layer. The important parameters of the cantilevers and the tips are listed in *Appendix 2*. They are used in the calculation of the interaction force between a single-pair of functional groups in subsequent sections.

6.4.2 Functionalization of AFM Probe

The functionalization of the AFM probes was conducted by thiol-Au self assembly monolayer (SAM) methods, that is widely reported in various protocols. The functional groups of interest are those present abundantly in physiological environment, e.g. acid group (–COOH), amine group ($–NH_2$), hydroxyl group (–OH), and methyl group ($–CH_3$), etc.

First, the probes were cleaned by a regular 4-step cleaning procedure. Briefly, they were washed in chloroform for 10 min and then washed with piranha solution (3:1 v/v of sulfuric acid and 30% H_2O_2 in water) for 30 min. Piranha solution is a strong oxidizing agent and it can remove all the organic impurities reside on the surface. After this, they were washed with a copious amount of deionized water before they were put into a 180°C vacuum oven for complete drying.

Then, the SAM forming procedure was done with reference to the protocol provided by *Assemblon Inc*. The probes were immersed for 24 hrs in a solution of 11-amino-1-undecane thiol hydrochloride (99%), 11-mercapto-1-undecanoic acid (95%), 11-mercapto-1-undecanol (97%), 1-undecanethiol (98%) (all purchased from Sigma-Aldrich) in ethanol with a concentration level of 1 mM to generate $–NH_3$, –COOH, –OH, and $–CH_3$functionalized probe surfaces, respectively. The probes and surfaces were then kept in the solution prior to use.

6.4.3 Calibration of Probe Force Constants

The importance of the calibration of force constants of cantilevers is undoubted for micro-force measurements to give accurate results on the measured minute force. All the entailed calculations of interaction forces of a single-pair of functional groups between surfaces rely critically on these values. Although values of the force constants are given by supplier, the variations can be quite large from tip to tip (a range of these variations are given, too). Therefore for each of the tip, calibration of force constants is required.

Out of the reported methods, the study of the thermal noise method has been proved to be reliable and therefore it has become part of a force constant measurement protocol that is embedded into the software paired with *Asylum AFM*, US [79]. This method was employed for the force constant calibration in this work. AFM probe was first loaded and a hard silicon wafer was used as a substrate. After the careful alignment of the laser beam in the detecting system (see *section 6.2*), the cantilever was pressed against the substrate to obtain a force curve, which was represented as the signal voltage (as detected by the PSD) vs. z-displacement (the distance at which the piezo travelled towards the substrate). The sloped portion in the approaching force curve was set to be unity (i.e. the bending of the cantilever equals to the z-displacement, ideally) to achieve the sensitivity of the detecting system (a measure of the relationship between the bending of the cantilever and the resulting signal voltage recorded at the PSD). After this, 100 thermal vibration curves of the free cantilever were recorded and averaged; and then the first resonance peak was picked and modeled by Gaussian distribution function. The

force constant of the cantilever was then obtained. Force constants of the cantilevers used in the measurement were calibrated after the experiments, so that it would not be contaminated or damaged during calibration steps. These measured force constants and their corresponding cantilevers on the probe for the different functional groups are shown in *Table 6.3*.

Table 6.3 The calibrated force constants for the cantilevers used in the measurements.

Measuring Environment	Functional Groups	Corresponding Label on Probe	Calibrated Force Constants (N/m)
Dry	$-NH_2$	A	0.57
	–COOH	A	0.85
	–OH	B	0.15
	$-CH_3$	B	0.11
Wet	$-NH_2$	D	0.082
	–COOH	D	0.066
	–OH	D	0.040
	$-CH_3$	C	0.11

6.4.4 Microscopic Force Measurement

Nanoscope IIIa Scanning Probe Microscope (*Digital Instrument*, Santa Barbara, USA) was used for the measurements. It employs the optical lever technique, with which a beam of laser is directed onto the back of the probe cantilever and a PSD receives the reflected beam to give the readings of the cantilever deflection (see *Section 6.2* and *Figure 6.1*). The resolution of this technique in Nanoscope was claimed to be 0.1 Å with the time of measuring a pixel of the force curve is typically 0.1 ms [78]. The whole structure of the controller is situated on a soft *Sorbothane* mat on a sturdy table that absorbs the major part of external mechanical vibrations.

The probes immersed in solution were taken out and blown dry. They were then immediately loaded onto the probe holder and the sample seat. Vacuum was applied through a small nozzle under the sample to immobilize it. Freeze dried bovine tendon and fresh bovine tendon were use as collagenous substrates in dry and wet, respectively. The measurements started out by contact mode. To prevent the probe tip from wearing out, the deflection set-point was always set to be as low as possible so that the tip merely touched the surface when it started scanning. After, the set-point is monitored to optimum and the force curves were collected one by one at different locations on the surface using the X,Y-offset command on the Nanoscope software. The repeatable force curves are indirect evidence to the fact that the interactions are physical but not chemical. Each force curve contained an extension curve and retraction curve. Each of them was drawn by collecting 2048 points. The scan rate was set relatively slow, which was 0.5 Hz.

6.5 Results

6.5.1 Force Measurements in Dry and Wet Conditions

Figure 6.2 shows the typical examples of the retraction force curves collected between functionalized tips and dry bovine tendon. The forces experienced by the tip are plotted against the piezoelectric transducer distance in z-direction. Only retraction curves were analyzed and interpreted because they are the ones that contain information about tip-substrate adsorption. From top to bottom, they are arranged in terms of the magnitudes of the interaction forces.

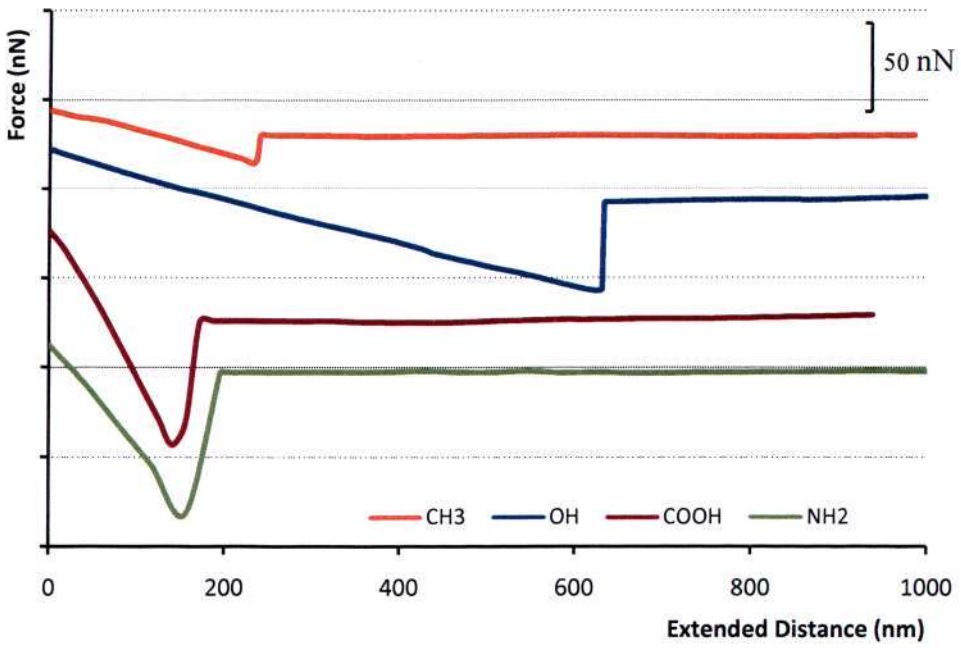

Figure 6.2 Examples of retraction force curves showing the non-specific interactions between each type of functionalized tip and bovine tendon in dry condition (50% RH).

Figure 6.3 shows the retraction force curves examples collected with immersed tip-substrate. Again, they are arranged from top down in ascending order in terms of interaction force.

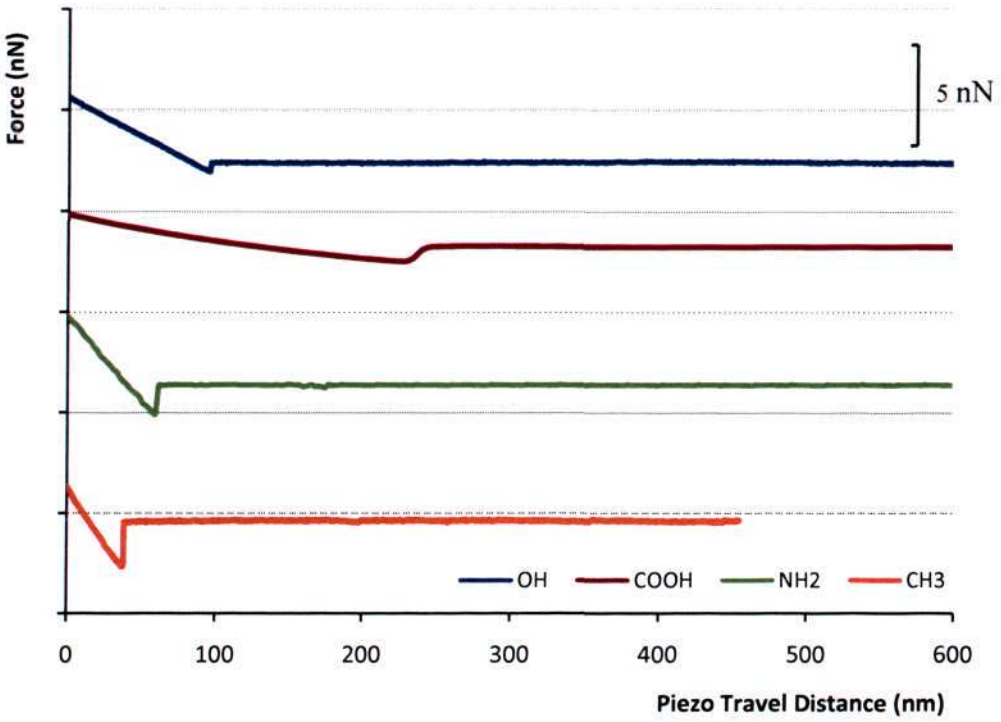

Figure 6.3 Examples of Retraction force curves showing the non-specific interactions between each type of functionalized tip and bovine tendon in wet condition (immersed in water).

6.5.2 Analysis of Force Curves

This analysis method has been established using functionalized surface as substrate and has been published [80]. A typical retraction force curve and the analysis method are demonstrated in *Figure 6.4*. Force curves typically have triangular shape as shown. Two parameters, which are important in the subsequent discussion, are derived from the force curves. They are rupture force (f) and distance span (d).

First, the mean value of all the data points in the horizontal portion of the curve, where the cantilever is not deformed by the substrate and is flat (see *Section 6.2*), was computed. This mean represents the force experienced by the cantilever when it is far from the surface; and hence, it always centers at about zero. Based on this computed value, a horizontal line is drawn and extended in leftward direction until it crosses the slanted portion, where the cantilever is being pulled away from the substrate. The point at which the horizontal line crosses the slanted line is the point where the cantilever returns to its flat configuration while it is still in touch with the substrate. At this point, called "flat-tip point", the force experienced by the tip is just balanced to zero.

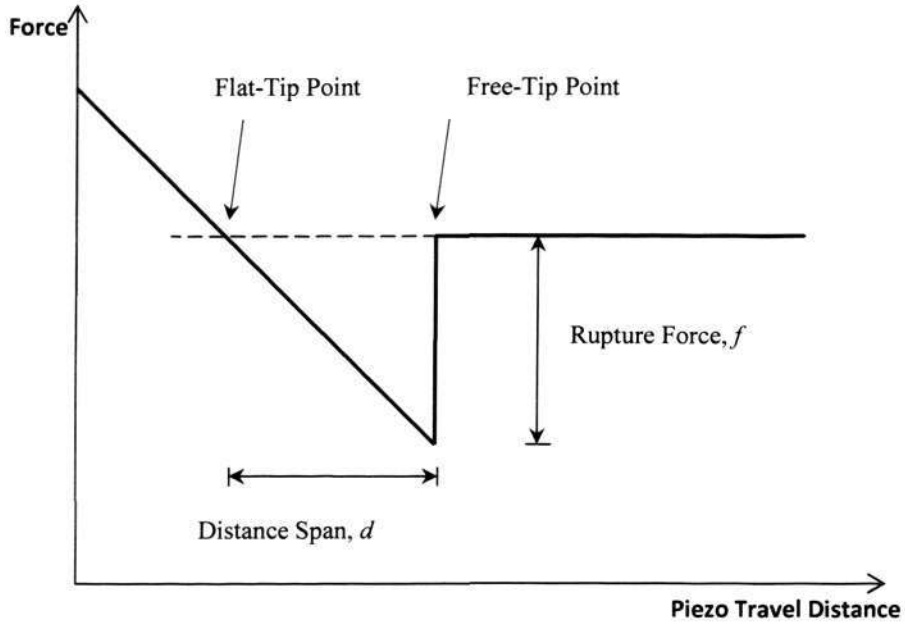

Figure 6.4 Demonstration of analysis of a retraction force curve.

As the piezoelectric transducer travels further away, the tip eventually snaps off the surface as the pulling force exceeds the adsorption. This is called "free-tip point". The distance span is the distance at which the transducer travels between flat-tip and free-tip points. Rupture force is the force difference between the lowest point and the horizontal line (zero-force line).

6.5.3 Rupture Forces

For each condition (i.e. dry and wet), 15 force curves from each type of functional group were analyzed to obtain the mean rupture force. This mean rupture force is the force corresponding to the lowest point in force curves, at which the adsorption between tip and substrate can no longer withstand the pulling force exerted by the piezoelectric transducer that is moving away. The results are consolidated in *Figure 6.5* and *Figure 6.6* for dry and wet conditions, respectively.

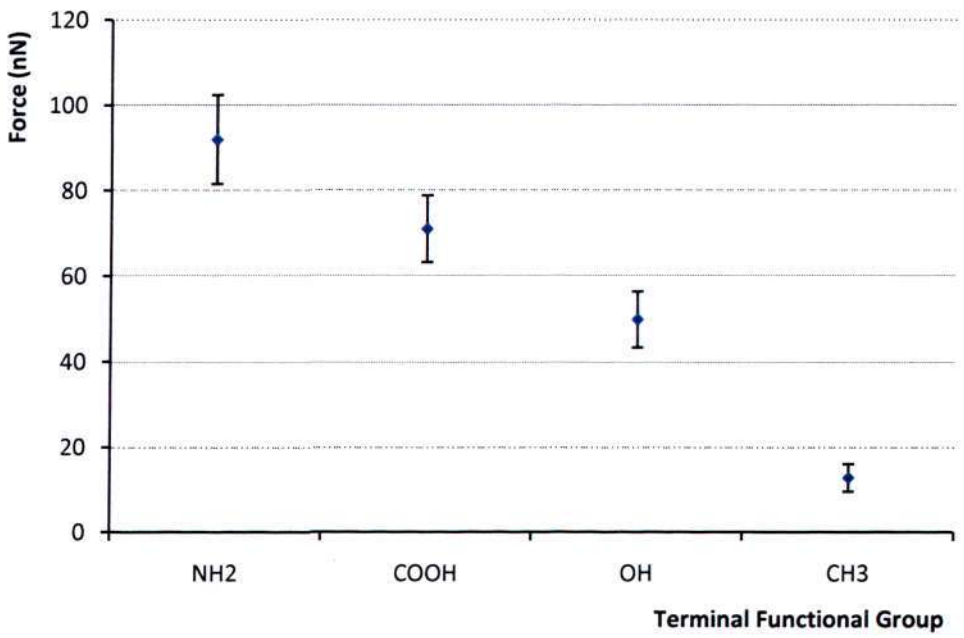

Figure 6.5 The mean forces of the interactions between tips modified with different functional groups and bovine tendon (dry condition).

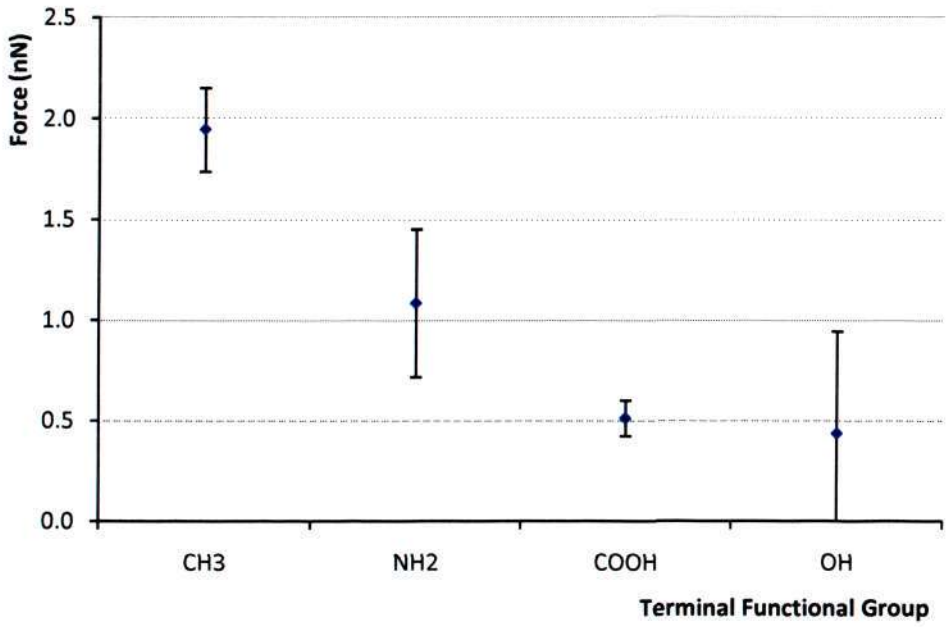

Figure 6.6 The mean forces of the interactions between tips modified with different functional groups and bovine tendon (wet condition).

6.5.4 Correlations between Rupture Force and Distance Span

From the curves of one type of functional group, in both dry and wet conditions, it is observed that distance span is linearly correlated with rupture force. One example is shown in *Figure 6.7*, where the 15 force curve samples from COOH-tendon interaction are plotted. The trend line is set to intercept with origin and the equation correlating the rupture force and distance span is obtained. The equations of each functional group under both conditions are summarized in *Table 6.4*.

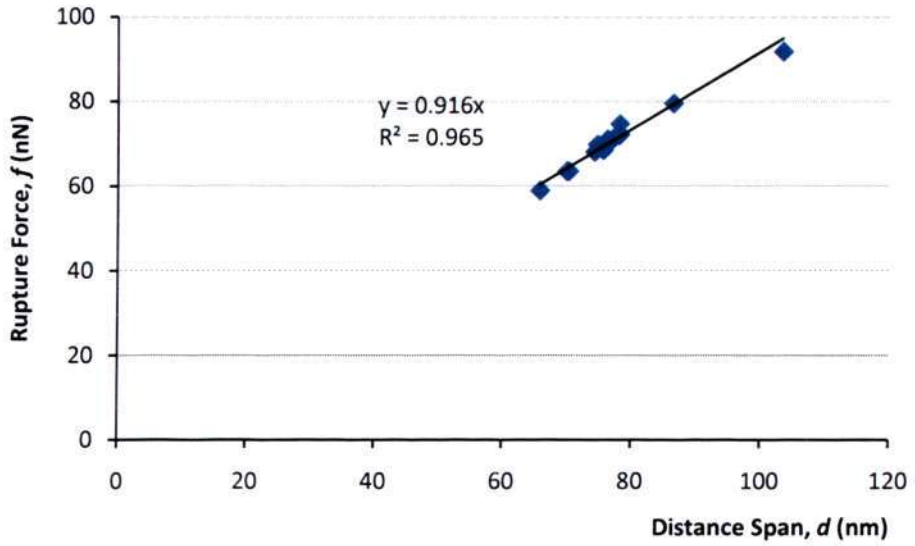

Figure 6.7 Linear Correlation between rupture force and distance span for COOH-tendon interactions in dry condition.

Table 6.4 The correlation equation between rupture force and distance span.

	Dry	Wet
	Trend Equation	Trend Equation
NH_2	$f = 0.4168d$	$f = 0.1055d$
COOH	$f = 0.9653d$	$f = 0.0164d$
OH	$f = 0.1097d$	$f = 0.0447d$
CH_3	$f = 0.1231d$	$f = 0.1074d$

The slope of the linear trend line reflects the number of interacting functional groups on the tip with the substrate. This correlation is used to estimate the average adhesion force per molecule (or per functional group) in the following section.

6.5.5 Calculations of the Average Adhesion Force per Molecule

In this section, the average one-to-one adhesion forces per molecule (or per functional group) are estimated by simple mathematical model. This estimation provides an interesting insight into the range and magnitude of the non-specific interaction forces that would contribute to overall adhesion. It provides a convenient way guiding the design of new TAs systems. Since the silicon nitrate tip is pressed against collagen, a softer biological tissue, it can be assumed that the deformation of the tip front is negligible.

The measured rupture force can be expressed as

$$f = nf^{(1)} = md \qquad \text{(Equation 6.1)}$$

where f is the measured rupture force;

$f^{(1)}$ is the average rupture force per molecule;

n is the number of interacting pairs of molecules;

m is the slope of the correlation equation (see *Section 6.5.4*); and

d is the distance span.

Next, assume that the density of the SAM, ρ, is known, and that the contact area between the tip and the surface is A, then

$$f = \rho A f^{(1)} = md \qquad \text{(Equation 6.2)}$$

Since the shape and dimensions of the tip are known, if it is very sharp, with merely a small blunted area, A_o, the contact is made on the four facets of the tip. The contact area can then be expressed as (see *Appendix 3*)

$$A = Jh'^2 + A_o \qquad \text{(Equation 6.3)}$$

where $J = \sqrt{\frac{xy}{H^2} + \left(\frac{a_o}{H}\right)^2}$,

h' is the effective interacting zone depth;

x and y are the lengths of the two diagonals on the tip's pyramidal base;

a_o is the length of the side of the pyramidal base; and

H is the height of the tip.

Some further elaboration is needed to explain the effective interaction zone depth. Since SAM is evenly populated on the tip surface, not only the molecules situated directly at the tip apex but also the molecules situated at some distance away from the apex are interacting with the substrate. As shown in *Figure 6.8,* this distance is equal to the extended length of the thiol molecule functionalizing the surface, which is about 1.5 nm. All molecules within this zone have high probability to interact with substrate.

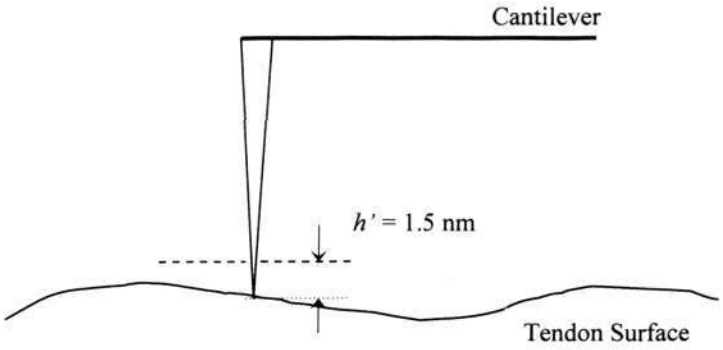

Figure 6.8 The contact between tip and tendon when tip is sharp and the effective interaction zone depth.

First Estimation

Knowing these values: $x = y \approx 4.20$ μm; $a_o \approx 5.94$ μm; and $H \approx 3$ μm, the value of J can then be computed: $J \approx 2.425$. Since $h' \approx 1.5$ nm, the first term on the right hand side of *Equation 6.3* can be computed $Jh'^2 = 2.425 \times 1.5^2 = 5.5\ nm^2$. ***First assuming that the tip is sufficiently sharp*** and therefore $A_o << 5.5$ nm^2, then $A = Jh' = 5.5$ nm^2. Also, the density of the SAM is given as 4.67 nm^{-2} [81, 82], the average interaction force per molecule, $f^{(1)}$, can be calculated using *Equation 6.2*.

Using COOH-tendon interactions as an example and assuming that the data point with the greatest interaction force corresponds to the situation at which all thiol molecules within h' are interacting, then $n \approx 26$, and

$$f^{(1)} = \frac{91.73}{4.67 \times 5.5} = 3.57\ nN.$$

This result from the first estimation is unrealistically large when compared to those reported in literature (see Section 6.3) and therefore is far from being accurate. In fact, the assumption that the tip is very sharp is incorrect.

Second Estimation

It is given in the specification that the tip has a radius of curvature of ~ 10 nm. While $h' \approx$ 1.5 nm, the better illustration of the contact point should be as the one shown in *Figure 6.9*. Hence, ***it should now assume that the substrate interacts with the spherical tip front instead of the pyramidal facets***; Jh' should be dropped out from the estimation and A_o has to be considered.

$$A_o = 2\pi h' R \qquad \text{(Equation 6.4)}$$

where R is the tip radius (see *Appendix 4*).

R is estimated as ~ 10 nm. Therefore, A_o can be computed: $A_o = 2\pi \times 1.5 \times 10 = 94.2\ nm^2$.

With second estimation using the same COOH-tendon interactions, then $n \approx 440$, and $f^{(1)} = \frac{91.73}{4.67 \times 94.2} \approx 208.5\ pN$.

This is much closer than what is expected and should be closer to the true value. So the second estimation method is used to compute the average interaction force per molecule for all the functional groups under dry and wet conditions. The estimation results are shown in *Table 6.5*.

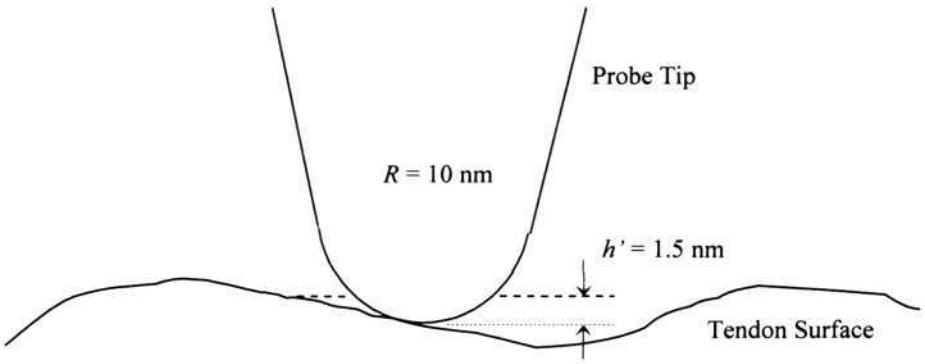

Figure 6.9 The contact between the tip and tendon for a spherical tip front.

Table 6.5 Interaction force per molecule between thiol molecule and tendon substrate.

	$f^{(1)}$ (pN)	
	Dry	Wet
NH_2	289.8	3.1
COOH	208.5	1.4
OH	140.1	1.1
CH_3	39.8	5.5

6.6 Discussions

6.6.1 Comparisons between Dry and Wet conditions

In the widely accepted theory, which also forms the basis of the molecular simulation study in *Chapters 4 & 5*, physical interaction energy (a.k.a. secondary interaction, non-specific interaction) is made up of two parts: van der Waals (vdW) interaction and electrostatic interaction. VdW interaction is ubiquitous and universal between any molecules/atoms because its origin lies in the time-dependent distribution of charge resulting from the vibrant quantum mechanical electron cloud. VdW is essentially the measure of the time-averaged interaction among electron clouds.

Electrostatic interaction is only applicable to permanently charged molecules/atoms. Under normal circumstances, the total charge of a molecule as a whole is zero (i.e. neutral). However, local polarities arise when atoms with dissimilar electronegativity values are bonded. The atoms with greater electronegativity draw the electron cloud towards itself and therefore are more negative. Likewise, the atoms with lower electronegativity loosen the grip on the electron cloud and therefore are more positive. These set up the local dipole (or multi-pole). When these non-symmetric electron clouds approach each other, these local charges attract or repel each other, as described by the Coulombic equation (*Equation 3.1*).

In fact, as what is shown in *Chapter 5*, even alkyl chain is multi-polar, although the partial charge distribution is usually considered to be rather flat and uniform because

the electronegativity values of C and H atoms are very close to each other. On the other hand, N and O atoms are more electronegative than C and H atoms. (Electronegativity values of C, H, O and N atoms are 2.55, 2.2, 3.44 and 3.04, respectively.) Therefore, molecules with N- and/or O- containing functional groups have multi-polar structures with greater charge difference. This concept is similar to that of "formal charge" in fundamental chemistry.

The interaction forces, for all functional groups, drop precipitously in wet/moist environment. In dry condition, where the relative permittivity is close to unity (in air), the electrostatic interaction is very much stronger than vdW interaction (*Section 4.5*). Furthermore, hydrogen bond, which is a strong form of electrostatic interaction, can form when H atoms are covalently bonded to strongly electronegative atoms, e.g. N and O.

The relative permittivity of water is about 80.1 at 20 °C. So the electrostatic interaction is screened off and weakened by about 80 times in water, as suggested by the Coulombic equation (*Equation 3.1*). As a result, the functional group whose adsorption to collagen in dry condition is due mainly to electrostatic interaction reduces on their interaction force in wet condition. This result is evident in the three N- and O-containing functional groups where the polarity is the greatest.

The drops in strength from dry to wet conditions are however greater than 80 folds, except for $-CH_3$ (*Table 6.5*). The water clearly does more harm to adsorption event besides screening off the electrostatic interaction. Water molecules cover the surface of

the substrate to prevent its interaction with functional groups on the tip. They also interact with the functional groups, especially for those polar groups, and thereby reducing their ability to interact with collagen. Furthermore, the high mobility (e.g. translations, rotations, vibrations) can further disrupt the interactions between substrate and tip functional groups.

6.6.2 Comparisons among Functional Groups

As expected, different functional groups show different levels of interaction with collagen substrate. In *Figure 6.2, 6.3, 6.5* and *6.6*, it is clear that functional group is an important determinant for the adsorption event. The types of functional groups determine how well the polymer adsorbs onto collagenous substrate, and therefore tissue surface (see *Section 4.1.2*). The correct choice of functional groups results in better adhesion, or, at least, helps in attracting the molecules closer to the substrate in the initial stage in application.

Interactions in Dry Condition

In dry condition, the average functional group with the greatest rupture force is $-NH_2$ (92.1 nN), which is followed by –COOH (71.2 nN), then –OH (49.9 nN), and finally $-CH_3$ (12.8 nN) (*Figure 6.2*). The estimated interaction forces per molecule are 289.9 pN, 208.5 pN, 140.1 pN and 39.8 pN (*Table 6.5*), respectively. The spreads of the data, as indicated by the standard deviation error bars, are moderate and acceptable.

The difference in the interaction forces of different functional groups could be explained by the difference in their charge distribution and local polarity. Of all the functional groups considered, $-CH_3$ is the least polar because of the small difference between electronegativity of C and H. The rest are all polar molecules due to the presence of N and O. The advantage of $-NH_2$ is that it carries two H atoms, increasing the chances of forming hydrogen bonds. This observation agrees with the simulation results in *Chapter 4* where the N-containing and O-containing functional groups generally perform better in adsorption (see *Figure 4.4*) and N-containing groups seem to adsorb better (except for –C≡N).

Interactions in Wet Condition

In wet condition, the rupture force of all functional groups reduces in a great amount and the trend is different from that in dry condition. The average rupture forces for $-CH_3$, $-NH_3$, –COOH and –OH are 1.94 nN, 1.08 nN, 0.52 nN and 0.44 nN, respectively. The estimated interaction forces per molecule are 5.5 pN, 3.1 pN, 1.4 pN and 1.1 pN, respectively. While the standard deviations of the rest are moderately acceptable (larger than those in dry), –OH shows great fluctuations in the data.

It is interesting to observe that the interaction that is coined "hydrophobic interaction" seems to be operative in the measurement results, although their magnitude is very small. Hydrophobic interaction is physical attraction occurring between two hydrophobic molecules/surfaces when they are immersed in water environment. Hydrophobic molecules tend then to aggregate in water environment to reduce their

contact area with water, thereby reducing the overall free energy of the system. $-CH_3$ is hydrophobic and it would intuitively search for the hydrophobic sites on the collagen surface when the functionalized tip is pressed against the tendon in wet environment (note that the entire thiol molecule is a hydrocarbon molecule in this case). This leads to the highest measured rupture force in the series of functional groups.

Even though the electrostatic interaction is greatly screened off and disrupted by water, $-NH_3$ still possesses slightly stronger interaction with collagen than other functional groups (except $-CH_3$) in wet condition. Possible reasons include the lesser extent in screening effect; or stronger electrostatic interaction even after screening.

–COOH and –OH are on par with each other in terms of their physical interactions with wet collagen. Their measured rupture forces are very small owing to, again, the screening effect. However, –OH shows a large standard deviation in the data. This could be due to the similarity of the functional group of –OH and the surrounding water. Alcohol and water like each other. So, besides screening off the electrostatic interaction, water also tries to attract the alcohol group and this leads to the instability of the alcohol adsorption to collagen.

6.7 Implications of Micro-adhesion Measurements & Simulation Results: A Conclusion

Force measurement using AFM is an unprecedented technique that was used to yield the experimental data on the interaction forces of selected functional groups with collagen. It involves just a tiny area of interaction (~hundreds of functional groups) and therefore shows the adsorption event at the molecular level without the complications (e.g. wettability, surface irregularities) that is present in macro-adhesion measurements.

Through the single-force derivation algorithm, the strength of adsorption of each functional group in dry state has a similar trend as predicted in the Parts I & II simulations, that is, N-containing amine group shows highest affinity, followed by O-containing groups, and then ethyl group. The rationale had been reckoned and discussed in previous chapters. Also, amine shows greatest adsorption in dry state and this result is in favor of adhesives with amide/peptide bonds, which has been emphasized.

It is no coincidence that the interactions of all functional groups in wet condition are greatly reduced as the adverse effects that water causes were already predicted in the simulation results. Even hydrophobic alkyl group, though usually not adhesive, can actually adhere better by hydrophobic interaction alone, as compared to the other functional groups, in wet conditon. This implies that for adhesion in wet condition, physical adsorption alone is too weak to form a strong joint. Having that said, it does not

mean that physical adsorption is not important as it determines all the other ensuing events that could happen, as it is always stressed on.

Chapter 7
Adhesion Force Measurements on Macroscopic Scale

7.1 Introduction

As in conventions, researchers assess the performance of an adhesive by conducting mechanical testing, which we term as macroscopic adhesion measurement (as opposed to the microscopic measurement presented in *Chapter 6*). These mechanical tests were heavily relied upon because of the simplicity of the basic idea underlining the tests and the direct correlation between the experimental observations and the final performance.

In this chapter, mechanical strengths of tissue adhesive joints were tested and reported. Two rectangular pieces of collagenous substrates were bonded together at the overlapping area of 1 cm × 1 cm with different tissue adhesives. Lap shear tests were done by applying a shear load to the joint. This testing method has advantages of simplicity, direct correlation to real situation, and minimal requirement on the adhesive amount (as TAs are very costly). The main disadvantage, however, is that it gives only the results on the joint breaking strength. Nonetheless, this information on breaking strength is sufficient as indications on whether the respective adhesives form good joints with collagenous tissues.

In this chapter, a brief review on mechanical joint tests is shown in *Section 7.2*. Next, *Section 7.3* states the procedures of the sample preparation and the test method; which is followed by the results in *Section 7.4* and discussions in *Section 7.5*. A conclusion is made in *Section 7.6*.

7.2 Reviews on Mechanical Tests on Adhesion Joint

7.2.1 The Types of Mechanical Joint Tests

There are at least four types of tests which are most common to the TAs: shear tests, peel tests, burst tests and butt joint tests (see *Figure 7.1*). All these tests have their pros and cons and the choice of test depends on the purposes, requirements, and limitations of the study.

Lap shear test is done by lapping two pieces of substrates over a pre-determined intersecting area, onto which pre-determined amount of adhesive is applied to form a joint, and then load is applied in the shear direction to the joint (i.e. in the longitudinal direction of the substrates, *Figure 7.1a*). Peel tests is done by lapping two pieces of substrates in parallel and the adhesive is applied along the interface for sufficiently long distance. The joint interface is then peeled open at a pre-determined angle (*Figure 7.1b*). Burst test is done by sealing the adhesive (usually in the form of film) over a punctured substrate and pressurized liquid or gas is purged through the nozzle connected to the puncture (*Figure 7.1c*). Butt joint test is done by joining the two substrate end-to-end with adhesive; and then the load is applied in the direction perpendicular to the joint (*Figure 7.1d*).

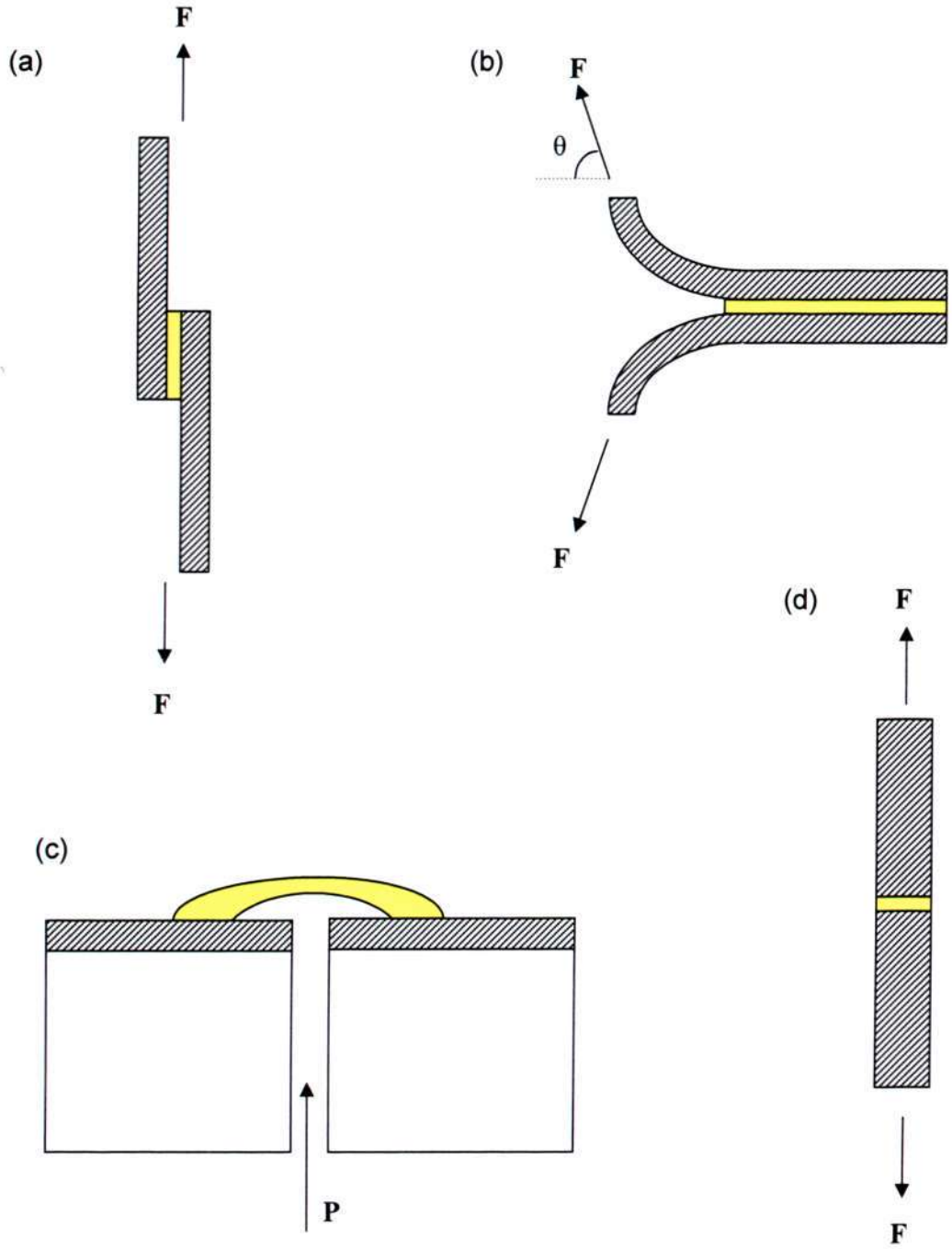

Figure 7.1 Schematic Representation of the four common mechanical tests for assessment of adhesive joint strength. (a) Lap shear test; (b) peel test; (c) burst test; and (d) butt joint test. (Shaded parts are the substrate and colored parts are the adhesives.)

7.2.2 Review on Joint Strength Measurements

So far, mechanical measurement was only employed to qualitatively compare the performance of different tissue adhesives on different substrates. The configuration of the test includes end-to-end butt joint tests [83-85], lap shear tests [14, 17, 41, 42], peel tests [86] and in-vivo and in-vitro blister/burst tests [16, 21, 83, 87]. It has been reviewed [27] and summarized in Table 2.1. It can be seen that generally cyanoacrylate adhesive gives an adhesion strength in the range from10^{-1} to 10^{0} MPa; while fibrin adhesive gives a adhesion strength in the range from 10^{-2} to 10^{-3} MPa. Nevertheless, the authors only used this measurement as a benchmark for comparison of other newly synthesized adhesives. None of them have been carefully analyzed in terms of the mechanics of the joint.

Table 7.1 joint strengths of cyanoacrylate adhesives and fibrin Adhesives measured on different tissue substrates and under different loading configurations.

No	Adherent	Adhesive	Bonding configuration	Pulling rate (mm/min)	Bond strength (MPa)	Remarks
1.	Bovine menisci [88]	Unspecified CN	Butt joint	30	0.6±0.2	
2.	Rabbit Achilles tendons [89]	Isobutyl-2-CN	Butt joint	600	0.5±0.3	Highest strength = 1.0 MPa
3.	Human foot flexor tendons [27]	n-butyl-2-CN	Butt joint	50	1.4	1 hr between application. and testing
4.	Tooth enamel/ dentin and plastic dental onlay [27]	Isobutyl-2-CN	Butt and lap joint	-	3 for butt; 2 for shear	Strength's reduced after 24h immersion
5.	Beef skin [27]	n-butyl-2-CN reinforced with Al plates	Lap joint	-	0.47±0.16	
6.	Rabbit skin [90]	Isobutyl-2-CN	Incision in vivo	-	0.1	Measured after 1h, based on approximate bond dimensions
7.	Rabbit eye [27]	Unspecified CN	Scleral incision in vivo	-	1.36	Just after surgery
8.	Aorta soft tissue [91]	Cyanoacrylate gel for domestic purposes	Butt joint	-	0.05	After 15 min
9.	Sheep aorta [91]	GRF	Butt joint	-	0.17±0.04 (dry); 0.048±0.018 (wet)	Lower pressure gave lower strength
10.	Beef muscle tissue [92]	GRF	Butt joint	-	0.016±0.005	Increase by 15% after 18h
11.	Lung parenchyma [93]	GRF	-	-	-	Superior strength on damp tissue but less in dry state
12.	Aorta [94]	Fibrin	Butt and lap joint	-	Max:	Varying time and

					0.036±0.003 (butt); 0.0029±0.0002 (lap)	concentration, max strength achieved for highest conc. and shortest time (5 min)
13.	Flat aorta [91]	Fibrin	Butt joint	-	0.008±0.003	
14.	Dura [95]	Fibrin, both commercial and autologous	Lap joint	-	Max: 0.028 (commercial); 0.038 (autologous)	Tested after 30 min; less than 10 min the bonds were rather weak
15.	Dura; Dermal face of porcine skin [96]	Fibrin (autologous)	Butt joint	-	0.005-0.006 (dura); 0.02-0.03 (skin)	
16.	Skin (dermal face) [97]	Fibrin	Lap joint	-	0.027±0.008	Tested after 90 min with highest fibrin conc.; *Tissucol* gave 0.017, probably showing low conc. of fibrin
17.	Skin graft in rats [98]	Fibrin	-	-	0.005±0.001 (1 min); 0.02 (120 min)	
18.	Corneoscleral [27]	Fibrin	In vivo	-	1.19	
19.	Rabbit skin [99]	Fibrin	In vivo	-	0.009±0.001	

7.3 Materials and Experimental Methods

7.3.1 Materials

Biological Substrate used in the Tests

Bovine tendon (cow Achilles tendon) was chosen as the substrate for the mechanical testing based on some reasons, as followed. First of all, a collagenous substrate should be used in this macro-mechanical testing so that the results obtained are comparable to the outcome of the computational modeling, in which collagen triple-helices are used as the target substrate. Secondly, tendon, as with ligament and cartilage, is a soft tissue that contains over 90% of collagen content. It is therefore a very representative collagenous biological. Besides, the bovine tendon is relatively bulky and easy to acquire and sample preparation is convenient.

Adhesives

Both commercial TAs and non-TAs were used to bond the sliced tendons into adhesion joints. These includes 3M's Vetbond cyanoacrylate adhesive, Baxter's Tisseel fibrin adhesive, Selleys' Epoxy Fix epoxy adhesive and Selleys' KWiK GRiP adhesive (unrevealed constituents).

(1) 3M Vetbond cyanoacrylate adhesive

Vetbond adhesive is a fast setting TA for veterinarian uses, e.g. declaw. It is a transparent monomeric liquid with low viscosity (close to that of water) and is

dyed in blue to enhance visibility. The set time of the glue is within ~5 – 20 seconds. The adhesives used in this study were courteously provided by 3M.

(2) Baxter Tisseel fibrin adhesive

Tisseel package contains four parts: fibrins concentrate (A), aprotinin solution (B), thrombin (C) and calcium chloride solution (D). A is the core component, which breaks down (i.e. fibrinolysis) into fibrinogen monomers when mix with C under the presence of Ca^{2+} in D. B is a fibrinolysis inhibitor that slow down the process to provide a sufficient handling time. The preparation procedure strictly abode to the instruction provided in the package insert.

(3) Selleys Epoxy Fix epoxy adhesive

This commercial glue is supplied in two parts: resin and hardener. The main constituent in the resin part is epoxy pre-polymer and that in hardener part is amine pre-polymer. The exact composition of the chemicals is not revealed. The set time for this adhesive is about 3 minute, the longest among the four, and it attains its maximum strength only after a few hours.

(4) Selleys KWiK GRiP adhesive

KWiK GRiP is a yellowish, moderately-viscous (close to that of honey), one-part adhesive that is designed for various materials such as shoes, porcelains, etc. It belongs to the solvent evaporation adhesive system (see *Section 1.1*) in which the

viscous polymer solution hardens into solid as the solvent evaporates. The exact composition of the chemicals is, again, not revealed by the manufacturers.

7.3.2 Sample Preparation

Slicing of bovine tendon

Tendons were frozen in the -60 °C freezer, where they were kept in a zip-lock bag to prevent tissue dehydration. To ensure a flat sliced surface, so that the contact surfaces between two slices of tendons in the samples had flat and good matching, the tendon were sliced immediately before it was thawed. The dimensions of the sample prepared were kept at 4 cm × 1 cm and the thickness, which require more skill to maintain and relatively less critical for the mechanical tests, was kept between 1 ~ 3 mm. The alignment of the collagen fibers in the tendon is in the axial direction along the lengthwise direction of the sample.

Preparation of dry tendon sample

Tendon dries up on lab bench in ambient conditions. However, this desiccating process is accompanying with shrinkage in dimensions. To prepare for dry sample, freeze-drying techniques was used for better control of the resulting dimensions. The problem of the warpage associated with the freeze-dried samples however needed to be overcome. Tendon samples were cut into slightly larger dimensions (~ 1.2 ×) and then the surfaces to be glued were pressed firmly against a flat glass slides. In this way, they were tied and fixed onto the glass slides with tapes. The samples were fully frozen at -60 °C before they were loaded onto the freeze-dryer, in which high vacuum at 0.060 mbar and temperature at -60 °C were applied overnight. The freeze-dried tendons were then unloaded from the machine and kept in desiccators before use.

7.3.3 Application of adhesives

The contact surface area between two collagen slices were fixed at 1 cm × 1 cm; in other words, the slices were overlapping each other for 1 cm in lengthwise direction. Glue was applied evenly onto this surface and the two pieces were pressed against each other for a short while before the joint was formed. To compare the effectiveness of the adhesives, the volume of adhesives was fixed at 5 μl. This is the sufficient amount of adhesives for the 1 cm^2 surface area; any amount greater than this would result in excess adhesives flowing out from the edges of the sample.

7.3.4 Equipment and Measurements

Tensile Tester

Instron 5848 Micro-Tensile Tester was used for the lap shear test. A 200 N-static load cell was used for adhesion joints on wet samples and a 1 kN-load cell was used for adhesion joints on dry samples (stronger joints, as predicted). The sensitivity (or force resolution) of the load cells is reported as 1/400 of their maximum load by the manufacturer. Mechanical grips were employed to ensure a stronger clamping force – strong clamping is especially needed for slippery samples like the wet ones. The tensile tester was computer-controlled with the use of *Instron Bluehill* software.

Procedure of the Lap-Shear Test

The upper and lower pieces of the glued sample were loaded clamped between the upper and lower grips, respectively. The clamped parts of the samples were wrapped by sand papers (with the coarse face facing the sample) also to prevent sample slippage out of the grips. The gauge length (distance between the upper and lower grips) was kept at ~ 5 cm and the length of the clamped part was ~ 1 cm. The joint surface was aligned parallel to the loading direction (*i.e.* joint surface normal was perpendicular to the loading direction) so that the stress to the joint was purely in shear nature. After aligning and gripping, the gauge length and load were reset. Extension was controlled at an increment rate of 1 mm/min in the shear direction (relative to the joint). The load developed due to the joint integrity at each level of extension was recorded and plotted against extension by the software.

7.4 Results

7.4.1 The Force-Extension Curves in Lap Shear Tests

The failure modes in the studies below are assumed to be adhesion failure. The assumption is based on firstly, direct visual inspection showing failure occurring directly at the interface. Second, from the fact that the adhesive is kept at an extremely thin layer at the interface, peeling off from the adhesive-substrate interface (rather than within the adhesive) is more likely to occur. The results of the experiments were represented by the plot where the ordinate is the force detected by the load cell and the abscissa is the distance travelled by the moving grip. Examples of force-extension curves of adhesive joints on dry bovine tendon are shown in *Figure 7.2*, whereas those on wet bovine tendon are shown in *Figure 7.3*. It could be seen that the shapes of the curves on dry and wet substrates are different, in addition to their difference in size.

KWiK GRiP shows almost a flat curve in *Figure 7.2* because its joint strength is far smaller than those of other adhesives. Furthermore, all samples prepared by KWiK GRiP on wet tendon failed before they were loaded onto the tensile tester. The joints were simply too weak to even withstand the cautious handling. So, there is no force-extension curve of KWiK GRiP on wet tendon shown in *Figure 7.3*.

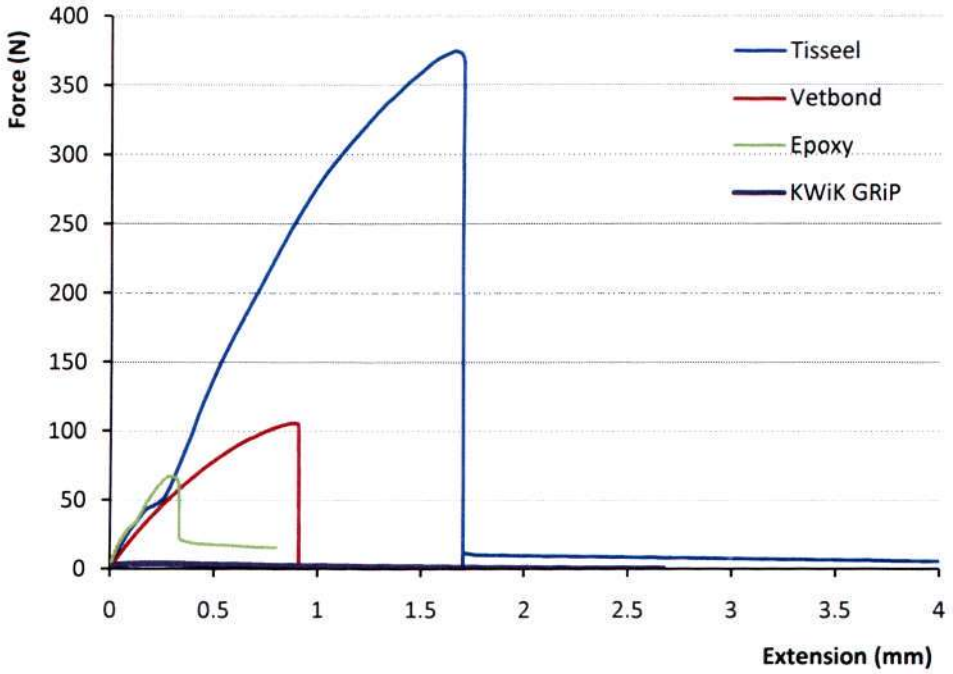

Figure 7.2 The force-extension curves of the adhesives on dry bovine tendon.

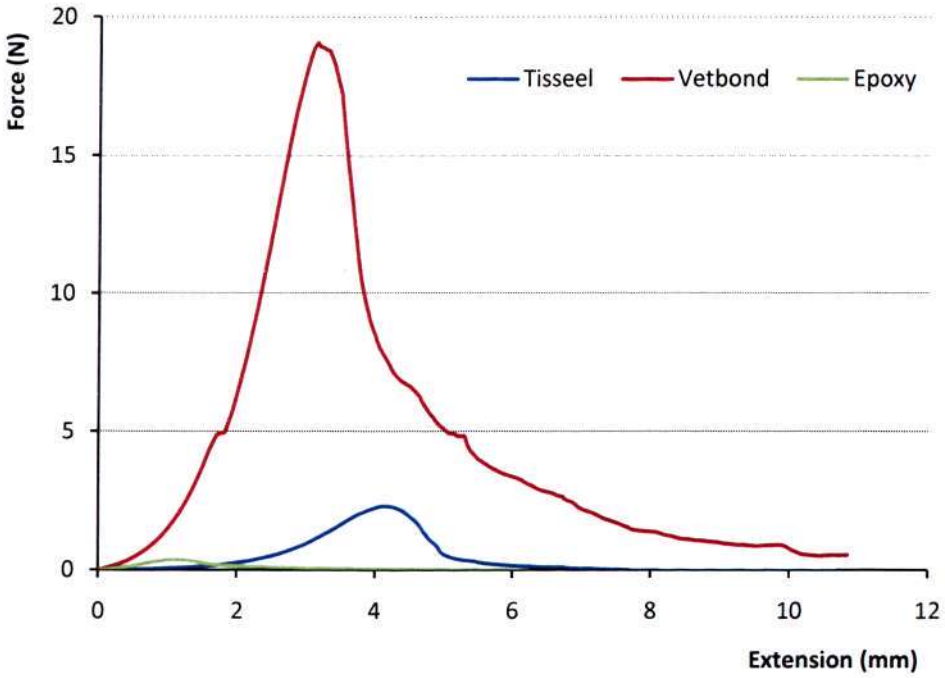

Figure 7.3 The force-extension curves of the adhesives on wet bovine tendon.

7.4.2 Ultimate Joint Strengths

The effectiveness of a joint is characterized by the joint strength. In this experiment, joint strength is defined as the maximum shear force that the joint can withstand. In other words, it is the highest point in the force-extension curve. The joint strengths of different adhesives on dry and wet tendons are shown in *Figure 7.4*. As what have been expected from *Figure 7.2* and *7.3*, the magnitudes of the strengths on dry and wet tendon are different by a great amount.

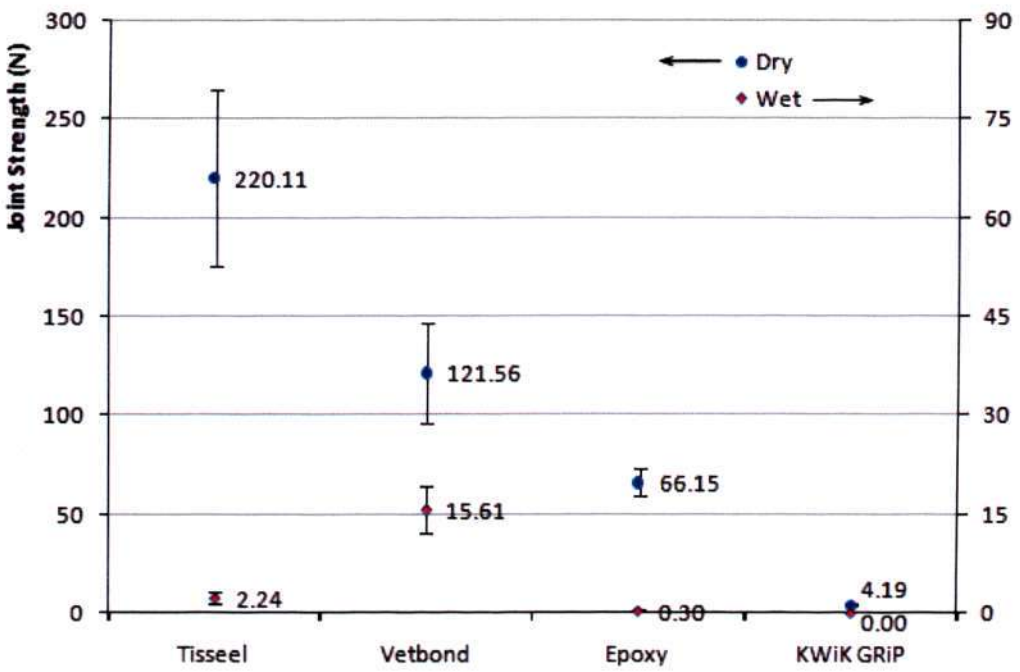

Figure 7.4 Joint strengths of adhesives on dry (blue) and wet (red) bovine tendons. (Note: All KWiK GRiP samples failed before the actual tests and the strength is conveniently taken as zero.)

As in many other mechanical tests, the results of the lap shear measurements for the samples in the same group usually spread over a wide range of values. These spreads are indicated by the error bar of standard deviation in the graphs. They are mainly due to the variations in the samples prepared, for example, chemical composition of substrates, roughness values of substrates (and hence the wetting behavior), the precision of the amount of adhesive applied and the effective amount of adhesive that stay at the joint, etc. Outliers calculated based on Huber's statistical method (devised by the Analytical Methods Committee in Royal Society of Chemistry) were eliminated [100]. In brief, the data points are assumed to have a Gaussian distribution; and the mean (μ) and standard deviations (σ) are calculated based on the raw data. Outliers are the points that fall outside $\mu \pm 1.5\sigma$. Those exceeding the upper limit are replaced by the upper limit; and likewise, those smaller than the lower limit are replaced by the lower limit. The calculation of mean and standard deviation iterates until the difference in the mean values obtained in two consecutive iterations is < 0.005 N. The results presented in *Figures 7.4* and *7.5* have already been processed by the Huber's Methods.

7.5 Discussions

7.5.1 The Adhesion Joints on Dry and Wet Bovine Tendons

The Shapes of the Load-Extension Curves

It can be seen in *Figure 7.2* and *Figure 7.3* that the shapes of the curves with dry substrate are different than that of the wet substrate. *Figure 7.5* and *Figure 7.6* show the general shapes of the force-extension curve with dry and wet substrates in simpler forms, respectively.

In *Figure 7.5*, the curve starts with an almost linear slope, before yielding and followed by rupture. Freeze-dried bovine tendon is very strong, hard and stiff, especially in the longitudinal direction of the collagen fibers (which was aligned to the load direction in the measurement). Therefore the maximum extension before which failure occurs is rather small (< 2 mm for all joints). At the initial linear part of the curve, the extension is a complex mix of the extension in the substrate and the extension in the joint. At low extension range, the load is completely transferred through the joint from one substrate to another. The load increases linearly with the extension as if the sample is a single piece of substrate (the adhesive is "perfect" in this extension range). The curve starts deviating from the linear line when the joint is weakened (Point A). The onset of the deviation depends on the rigidity (i.e. elastic modulus) of the joints. Finally, the joint failed suddenly in a "brittle" manner accompanied by a cracking sound.

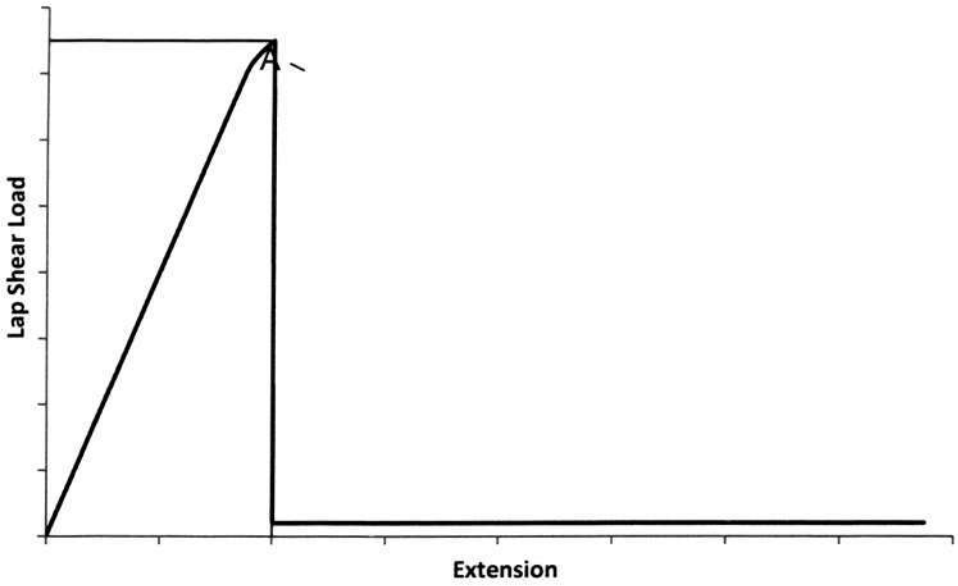

Figure 7.5 The general shape of a force-extension curve with dry substrate.

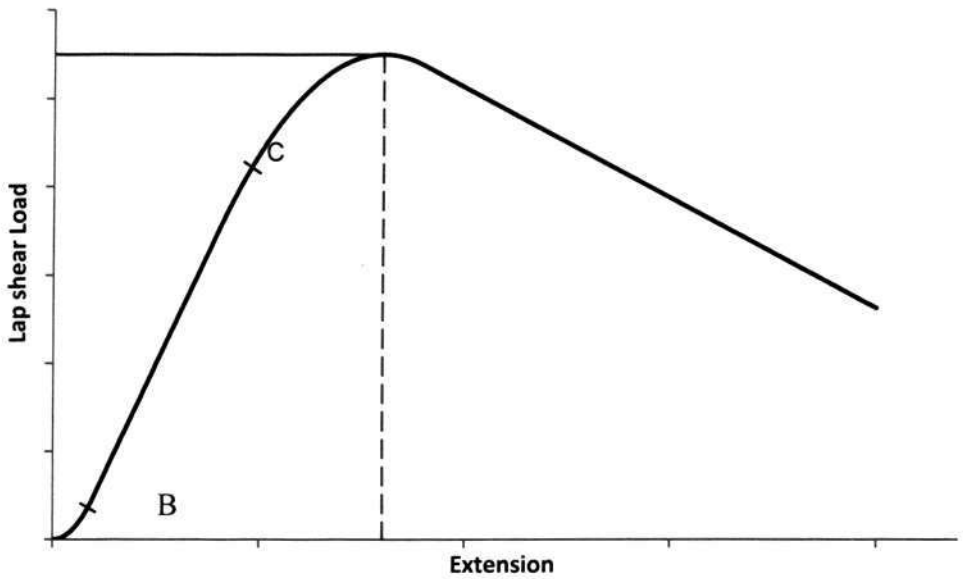

Figure 7.6 The general shape of a force-extension curve with wet substrate.

In *Figure 7.7* for the wet samples, the curve starts with a short concave part before entering the nearly-linear slope (Point B). It then showed yielding before failing in a gradual manner as opposed to abrupt failure in the samples of dry condition. The initial extension behavior reflects the typical mechanical behavior of biological tissue: the fresh tissue behaves as a very soft material that deforms easily at low extension range (from 0 up to Point B) but the modulus (i.e. the slope of the curve) increased continuously to reach its maximum and is holding at this value up to Point C. After Point C, when the substrate is almost fully stretched, the load at the joint builds up and the joint weakens. The curve then reaches the maximum in load level, and decreases gradually as the joint fails by sliding apart; i.e. the contact area is reducing. The failure mode is "ductile".

The Ultimate Joint Strengths

The difference of the ultimate joint strengths on wet and dry sample can be obviously seen in *Figure 7.4* and *Figure 7.5*. The difference between the strengths for each type of adhesive is shown in *Table 7.2*.

Table 7.2 Difference in ultimate joint strengths in wet and dry samples.

	Ultimate Strength (N)		
	Dry	Wet	Difference
Tisseel	220.11	2.24	-217.87
Vetbond	121.56	15.61	-105.96
EPOXY	66.15	0.30	-65.85
KWiK GRiP	4.19	-	-4.19

Tisseel adhesive has the greatest drop; while *Vetbond* adhesive's drop is also tremendous. *Epoxy Fix* and *KWiK GRiP* adhesives both show drops in smaller scale; however, they have actually lost > 99.5 % of their dry ultimate strengths; whereas *Tisseel* loses ~ 99 % and *Vetbond* loses ~ 87 %. It should be noted that although *Tisseel's* percentage drop in strength is great, the wet ultimate strength in absolute term is still larger than those of *Epoxy Fix* and *KWiK GRiP*.

There could be a few reasons that explain the tremendous drop in the ultimate joint strengths: (1) The strong dielectric constant of water has screened off the electrostatic attraction between adhesive and the substrate. This result agrees well with the molecular simulation works (see *Chapter 5*). The polar water molecules form a thin layer on top of the substrate and they align to the weak electric field imposed by the partial charge on the adhesive molecules and underlying collagen substrate. This effect hinders the potential electrostatic interactions, which is operative in dry samples, between the materials. (2) The active sites on collagen that could have attracted the adhesive molecules (and functional groups) are pre-occupied by the immense water molecules that are much more polar than the adhesives. Hence, the adhesive molecules cannot interact directly with these active sites as intended and the result is the reduction in the affinity of the molecules to the collagen. (3) Water, as small molecule, is a good diffuser that can penetrate into the network of the collagen bundles. They can soak the collagen by diffusing into the interstitial sites in among the collagen helices. The preoccupation of these sites by water molecules reduces the chance for the adhesive molecules to penetrate by diffusion, which is another important mechanism in adhesion. All of these prove that

the presence of water is really detrimental to an adhesion joint; which also shows up in the poorer adhesion in internal organs than external skin surfaces.

7.5.2 Comparison among the Types of Adhesives

From the results of the four glues, TAs (i.e. *Vetbond* and *Tisseel*) are performing better than non-TAs (*Epoxy Fix* and *KWiK GRiP*) when applied to biological tissues. This is seen in both dry and wet substrates (*Figure 7.4*), that *Vetbond* and *Tisseel* outperform *Epoxy Fix* and *KWiK GRiP*. The contrast is very obvious where water is not intervening in dry condition. Essentially, this tells that the choice of chemical functional groups is critical in forming good adsorption and adhesion. Furthermore, it depends on the substrate, too. Protein molecule and acrylate molecule are designed to target biological tissues because they are effective on these substrates.

In the theoretical simulation studies shown in *Chapters 4 & 5*, molecules with peptide bonds show strong affinity to collagenous substrate both in dry and wet conditions. This is partially in agreement with the experimental results here. In the dry substrate, Tisseel which carries peptide groups showed the highest ultimate strength but however, in the wet substrate, Vetbond cyanoacrylate adhesive is superior.

This discrepancy stems from the different situations in simulation set-up and experimental set-up. These can be discussed in a few different aspects:

(1) The limitation of Simulation

Chapters 4 & 5 simulate the collagen-affinity situations of the small molecules and of the polymerized oligomers, respectively. The transition between the two stages was not studied. The real wet situation is expected to be more dynamic and vibrant where water molecules will be constantly disrupting the adsorption as well as the polymerization/curing events. Because of this, the simulation in previous chapters may be more accurate for prediction of adhesion on dry substrate in the absence of water molecules.

(2) The difference in the sizes of adhesive monomers

In the simulations, the functional groups are connected to either –H or $–CH_3$, whichever is appropriate, to form simplest, small monomer molecules. In real TAs, the monomer or pre-polymer size however varies greatly. Fibrin molecule and cyanoacrylate molecules are apparently different in size; the former is a bulky protein molecule with a few amino acid residues and the latter is a small agile molecule with merely 21 constituting atoms. In a harsh environment where water molecules heavily interrupt the desired adhesion event, small molecules clearly have an advantage because they can adapt quickly to any changes in conformations of molecules in their vicinity. Therefore, fibrin molecules being bulkier may be kinetically disadvantaged than the glycine molecule modeled in theory.

(3) The effect of diffusion

Diffusion is another important determinant for good tissue adhesion and it has been put aside in all previous discussions (see *Section 2.1* for the reasoning). Diffusion is controlled by the size of the molecules; the smaller the molecules, the faster their diffusion rates are. Cyanoacrylate molecules are fast diffuser and fibrin monomers are less so due to the differences in sizes, as discussed earlier. In wet condition, where the adsorption mechanism is not as prevalent as in the case of dry substrate due to the presence of water, diffusion is much more important as a determining factor. The unique polarity of the cyanoacrylate monomer (the double bond is strongly polarized) should have made it more competitive to the water molecules. The overwhelming performance of cyanoacrylate in wet should be due to the greater penetration depth of the monomers, right before they are polymerized. The polymerized network is then interconnected with the network of collagen triple-helices to form adhesion inter-phase that bonds the two parts together.

KWiK GRiP – a different adhesive system

While Vetbond, Tisseel and *EPOXY FIX* all undergo polymerization/cross-linking to form a solid adhesive, *KWiK GRiP* is hardened by solvent evaporation. The adhesive is supplied with polymer dissolved in a sufficient amount of volatile solvent. Upon application, the solvent is evaporated and a hardened polymer is resulted. *KWiK GRiP* shows minimal adhesion strength to dry collagen and is completely unusable on moist collagen substrate. This is because: as bulky molecules, (1) they are not as active as

compared to small molecules (electrostatic interaction is greatly suppressed, see *Chapter 5*); and (2) they could not diffuse quickly to penetrate collagen to form interconnected network. This adhesive system can be concluded to be inappropriate for tissue adhesion, especially when water is present. In fact, evaporative adhesion system requires surface irregularities onto which the hardened polymer can hold after the solvent evaporates. Wet collagen surface is probably too soft for this mechanism to take effect.

Water as "adhesives"?

Water shows great affinity to collagen, in modeling results and also in daily observation. This trait would make water a good "adhesive". But it is not. One of the reasons why it is not is because water lacks integrity as solids do. It has no mechanical strength to hold the substrates. To test the idea of water as adhesive, ice were used. (As it is often observe in kitchens, fabrics and rags can adhere to ice and that requires some effort to be detached.) The water glue was applied onto the *dry* collagen in liquid form, and then "solidified" by freezing it. The lap shear test was then done immediately after the samples were taken out from the freezer. Water shows ultimate lap shear strength of 84.08 ± 32.76 N. The strength is better than that of *Epoxy Fix* but lower than those of TAs; but it forms a rather good adhesion joint with collagen.

7.5.3 The Failure Modes of the Adhesion Joints

The failure modes of the joints, i.e. adhesive or cohesive failure, could not be immediately identified because the layer of the adhesive between the substrate is extremely thin. If the adhesive does penetrate into the substrate, this thickness would be much thinner. However, there are sufficient evidences showing that the failure modes of most joints are adhesive failure (failure at the adhesion joint interface, as opposed to cohesive failure of substrate and cohesive failure of cured adhesive). First, from direct visual inspection, the failure occurs directly at the interface (but not inter-phase) as the two pieces of substrates were almost intact after failure. This denies the possibility of the cohesive failure of substrate. Second, from speculation, an extremely thin adhesive layer at the interface would be difficult to be split into two halves under shear load. Peeling off from the adhesive-substrate or adhesive-*inter-phase* interface is more likely to occur. So, adhesive failure is the most reasonable failure mode in the joints.

7.6 Implications of Macro-tests, Micro-tests & Simulation Results: A Conclusion

The lap shear test is one of the benchmarking methods used to judge the performances of adhesives by assessing the joint strengths. This chapter is important because (1) it testifies the predictions of the simulations; (2) it links the molecular interactions to lab mechanical measurements; and (3) it completes the explanation of adhesion mechanism, in particular, physical adsorption.

The three adhesives (all except *KWiK GRiP*) have known functional groups and therefore the comparison between the respective measured joint strengths and calculated interaction energies shall be discussed. Before that, it is worth to note that other factors, such as diffusion rate and surface irregularities, should have certain effect on the joint strengths, therefore the discussion here is not to consider in absolute but just to provide some thoughts into the effectiveness of each of the functional groups.

Fibrin, a protein adhesive system, has an abundant amount of peptide bonds in their structure. Furthermore, it is made up of peptide residues such as histidine and arginine whose side group is N-containing. All these functional groups, as the simulation results suggest (see *Chapters 4 & 5*), should be responsible for the physical adsorption in the initial stage. The strong initial adsorption could result in diffusion, despite the large monomer size, that makes up a joint. This could explain the strong joint formeed on dry

substrate, a situation where there is no hindrance of diffusion by preoccupied water molecules.

Vetbond, a medical-grade cyanoacrylate adhesive, possesses cyano and acrylate adhesive functional groups. While both of them are not exceptionally good in physical adsorption (see *Figure 4.3*), their combined advantages could render the adhesive a good one, as discussed in *Section 4.5*. This moderately strong adsorption enables the small cyanoacrylate monomers to diffuse deep into the substrate, which then results in the good joint. The competitiveness of cyanoacrylate with preoccupied water molecules is greater than that of fibrin because of much smaller monomer size. This could explain the stronger *Vetbond* joint strength on moist substrate.

EPOXY FIX is a two-part pre-polymer system; one part with epoxy groups and the other with amines. Although in theory they should form amide bond, which is strong in physical adsorption, the macro-testing results however show that weak joints are formed on collagen. First of all, as is discussed in *Chapter 5*, pre-polymer system is less favored than monomers for TAs because polymers have small adsorption energies and diffusion is slow. Secondly, as a pre-polymer system, the density of functional groups should be less than that of protein, as modeled in *Chapters 4 & 5*. These, in conjunction, resulted in the low-strength joint failure.

Chapter 8
Conclusions and Recommendations

8.1 Conclusions

From Chapter 2, it was understood that the major obstacle in the synthesis field is the lack of the understanding of adhesion at molecular level. The thesis then followed to provide a basic understanding on adhesion at the molecular level and on selection of the better functional groups (*Chapter 1, Objectives*). From Chapter 3, it was seen that the molecular mechanics and dynamics, though varies in set-up details, has been widely implemented and accepted in the study of physical interactions between biomaterials and biomolecules. The thesis is using a similar but yet different approach, in the sense that biomaterial (adhesive molecule) is the mobile entity and protein (collagen, biomolecules) is the static substrate, for the objectives set forth in Chapter 1.

In this thesis, unprecedented approaches have been implemented to tackle the fundamental problems, i.e. adhesion, currently encountered in TA development. These novel approaches include computer simulation (i.e. MM/MD) which focuses on the theoretical realm of physical adsorptions; and the AFM force measurement which measures the minute molecular forces at microscopic level. Alongside with the conventional macro-level joint strength measurements, these approaches together show a clearer picture on: (i) the physical adsorption mechanism of tissue adhesion; (ii) the

functional groups that may be favorable to promote adhesiveness; and (iii) the effect of the wet environment on molecular adsorption.

8.1.1 Summary of the Thesis

The results obtained in each section of the thesis are summarized as follow. Before monomers cure/polymerize, they interact strongly with collagen (see *Chapter 4*) because they are small in size; they have greater contrast in charge distribution; and they are mobile enough to search for preferential sites. All molecules show attraction to CTH at different magnitudes, which is strongly dependent on the electrostatic component. Therefore, polar molecules, i.e. molecules with functional groups that contain highly electronegative atoms, generally interact better with collagen than non-polar molecules with collagen. This initial affinity of monomer to collagen could promote the following events, e.g. diffusion and inter-phase formation, which improves the joint strength. Water adsorbs strongly to collagen and only a few functional groups show stronger affinity than water in that matter. This explains the adverse nature of moist/wet substrate in adhesion events. In general, N-containing groups have better affinity than O-containing groups, followed by halide and sulfur-containing groups, and finally hydrocarbons. The trend is proven experimentally by AFM micro-adhesion measurement and is also shown; though not as precisely; by lap shear joint tests.

As the adhesives cure/polymerize, their adsorption to collagen is greatly reduced as shown by the oligomers interaction with CTH in Chapter 5. Polymer molecules interaction with collagen is greatly dependent on vdW as the electrostatic interaction is

far limited when compared to that of small molecules due to (see *Chapter 5*) polymers low contrast in charge distribution and inflexibility in translational and rotational motions. Adsorption then relies heavily on weak vdW interaction. Nonetheless, polymers with stronger electrostatic interaction with collagen still have advantage as compared to those without. Polymers that can interact with collagen electrostatically place themselves among the better ones. However, the advantage could be turned into a disadvantage under the presence of water, for instance, OH group failed completely in water surrounding. This shows that the selection of functional group in synthesis is not really that straightforward and pre-studies, such as MM/MD and AFM explored in this thesis, can be carried out before synthesis to yield a better outcome.

As from the results in the thesis, amide/peptide functional group can result in strong physical adsorption, in both monomer and polymer forms, and under both dry and moist environments. From the macro-mechanical test, fibrin adhesive formed strong joint in dry substrate and this could be partially attributed to the good affinity of amide/peptide to collagen. Certain N- and O-containing functional groups give good adsorption too but, again, there is no strict correlation. For instance, N-containing cyano group is not performing any better than some other groups. The more N and O atoms that a functional group has; and the more functional groups that a molecule has, the greater physical adsorption. Functional groups that have great similarity and miscibility with water, e.g. OH, are not suggested because they are seriously perturbed by the water molecules in moist condition and the adsorption at molecular level is rendered unstable.

Water molecules have strong affinity to collagen. Besides, they screen off the electrostatic interaction and preoccupy the docking and interstitial sites on collagen. At body temperature, they move vibrantly around the joints, transferring impact to and weakening the formed adsorption. These characteristics make moist surface difficult to adhere onto. On one hand, they prevent contact and diffusion of hydrophobic molecules; on the other, they disturb the highly hydrophilic molecules. The implication is two-fold: for research scientists, they should design their molecules with intermediate hydrophilicity; and for surgeons, they should keep the substrate as dry as possible at the moment of application.

8.1.2 A Proposed Theory for Tissue Adhesion

It is impossible to explain the complete adhesion event with a single mechanism. Rather, interplay between a few different mechanisms contributes to a good joint. In this section, a partially complete theory of tissue adhesion, which is developed based on the results and implications in the thesis, is outlined.

Adsorption mechanism includes chemical adsorption and physical adsorption. The former involves primary bond formation between the adhesive and substrate. For instance, isocyanate and amine groups react to form urea linkage; ketone or aldehyde and amine groups react under acidic condition to form imine linkage; thiol group can react with thiol group on cysteine to form disulfide linkage. Most of these reaction target on the primary amine group on the tissue, a functional group that is abundant in protein. However, these reactions usually require elevated temperature and/or high pressure

and/or catalyst to work and therefore they are not practical and not applicable to biological tissues (TAs should be non-destructive and non-toxic to tissues). The thesis therefore focused on the study of physical adsorption because it precedes and in one way determines the effectiveness of all other events that follow.

As shown in the thesis (and as expected), physical adsorption alone is not sufficiently strong to result in a good adhesion joint. Nonetheless, its role is thought to be crucial as good affinity leads to good diffusion. Diffusion is thought to be another important requirement for a good joint. Besides the affinity of the material to substrate (which is the focus of this study), diffusion depends rheological properties of the adhesive and other parameters which cannot be engineered for biological environment, e.g. porosity of the substrate and diffusion time. These adhesive molecules diffuse into the interstitial sites of collagen and then polymerize to form a continuous inter-phase layer, which is a rigid inter-connected network between the adhesive and the substrate.

Mechanical interlocking, which was proposed in adhesion study on hard surfaces, e.g. metals and ceramics, is however considered to have little or minimal effect on ~~the~~ soft tissue. The reasons are: (1) the structure of soft tissue is loose, as compared to metals and ceramics, and the adhesive molecules diffuse into the interstitial sites to form inter-phase, rather than confined in the surface micro-environments to form local solidification/crystallization that interlocks with the surface (in a sense, diffusion and mechanical interlocking are mutually exclusive); (2) even if the local solidification/crystallization is formed, internal tissue is too weak to interlock with them

and they can be severely deformed under external loadings. More importantly, mechanical interlocking theory suggests that one can modify the surface roughness/irregularities to improve adhesion and this is definitely out of bounds for soft tissues

As a final note, a speculation on how cyanoacrylate and fibrin adhesives work based on the above is proposed. Cyanoacrylate, which is small in monomer size and weaker in affinity to collagen, is drawn close to substrate surface and diffuse deeper into it to form a rigid inter-phase. On the contrary, fibrin, which is bulkier and stronger in affinity, is drawn very close to substrate and diffuses shallower into it. As it is evidenced, both mechanisms results in acceptable joints for biomedical uses.

8.1.3 Limitations in the Studies

The thesis presented here is an introduction of novel study methods for TA development. As the first piece of work of its kind, the study definitely has limitations, as listed:

(1) Part I and Part II MM/MD studies the monomer and oligomer stages of polymer adsorption on collagen. Curing/polymerization is a dynamic process where monomers become oligomers then polymers with time; the information of this dynamic process and effects on adsorption is lacking in the model.

(2) The data collected from MM/MD are purely enthalpy-driven. Entropy information is lacking because entropic computation is complicated and time/space-

consuming and no algorithm is so far perfect enough to be popularized. Hence, it can only assume that the entropies of all small molecules are similar and that the entropies of all oligomer molecules are similar too due to the similarity in sizes.

(3) Collagen is representative for complex biological tissue but are still lacking in some other constituents like elastin and lipid. A careful blend of all these constituents to form biological tissue as substrate is a more realistic study but they are omitted for the sake of simplicity in this earliest study.

8.2 Recommendations

Here are some recommendations for the extension of the work in this thesis:

(1) Extension of simulation study

This thesis examines the non-specific adsorptions of the common and simple functional groups on collagen. The simulation method has been established and it could be refined and modified to extend the study from at least three aspects: (i) MM/MD simulations of molecules/oligomers with more complex functional groups, which are seen in some special polymers. Examples are imine, anhydride, and etc. (ii) MM/MD simulations of various amino acid residues in addition to glycine. In the thesis, peptide linkage is found to be adhesive to collagen and hence protein adhesive is a promising candidate. Real protein is made up of macromolecules of different amino acids, which are characterized by their side chain functional groups. Examples include arginine, lysine, glutamic acid, aspartic acid, DOPA (the alleged adhesive groups found in mussel feet), and etc. (iii) Tissues are far more complex than collagen alone (although some tissues, like tendon and cartilage, are mainly made up of collagen). MM/MD studies can be extended to include other common components of tissue, e.g. elastin, lipid, etc. This simulation will also benefit the study of biomaterials-tissue interaction.

(2) Synthesis of protein adhesives

One important finding in the thesis is that protein adhesives are a promising candidate as TA. The commercialized fibrin is one example. However, the strength of the adhesion joint is not strong on wet surface because adsorption is weakened by water and diffusion is inhibited by the bulky size of fibrinogen. New molecular designs can be further explored using this model as a start and followed by synthesis. In the literature, some syntheses of protein adhesives, in addition to fibrin, are underway and claimed to have good adhesiveness [14, 18, 22, 42, 101].

(3) Study on the diffusion of adhesive molecules into tissue substrate and the polymerization/cross-linking of adhesives

Diffusion, as discussed in previous sections, bears great importance to tissue adhesion. The study also indirectly shows that diffusion is influential on the resultant joint strength. While diffusing into the tissue, adhesive concurrently undergo polymerization or cross-linking process. This is also very crucial to the resultant joint because it determines the strength of the adhesive, as a material, and so the strength of the inter-phase. After successful adsorption of adhesive monomers, the ensuing interplay between diffusion and polymerization/cross-linking becomes the next important event for a good joint to form. The relative kinetics of these two events can be modeled and simulated.

(4) Estimation of entropy

Entropic effect should not be underestimated, on top of the enthalpic effect studied in the thesis. In the state-of-art MM/MD simulation theory, entropy is still an unsolvable realm. When the algorithm development is mature, entropy should be estimated to complete the consideration on interaction energy.

Reference

1. De Waard J, Trimbos B, and Peters L, Cosmetic results of lower midline abdominal incision: Donati stitches versus a continuous intracutaneous suture in a randomized clinical trial. Acta Obstetricia Et Gynecologica Scandinavica 2006; 85(8):955-959.

2. Niessen FB, Spauwen PHM, Kon M. The role of suture material in hyperthrophic scar formation: Monocryl versus Vicryl-rapide. Annual Plastic Surgery 1997; 39.

3. Trimbos JB, Mouw R, Ranke G, Trimbos KB, Zwinderman K. The Donati Stitch Revisited: Favorable Cosmetic Results in a Randomized Clinical Trial. J Surg Res 2002;107(1):131-134.

4. Capon A, Mordon S. Can thermal lasers promote skin wound healing? American Journal of Clinical Dermatology 2003;4(1):1-12.

5. Zeebregts CJ, Heijmen RH, van den Dungen JJ, van Schilfgaarde R. Non-suture methods of vascular anastomosis. British Journal of Surgery 2003;90(3):261-271.

6. Wolf -de Jonge ICD, Beek JF, Balm R. 25 years of laser assisted vascular anastomosis (LAVA): What have we learned? European Journal of Vascular and Endovascular Surgery 2004;27(5):466-476.

7. Spotnitz WD. Commercial fibrin sealants in surgical care. American Journal of Surgery 2001;182(2):8S-14S.

8. Doria C, Vaccino S. Topical hemostasis: a valuable adjunct to control bleeding in the operating room, with a special focus on thrombin and fibrin sealants. Expert Opinion on Biological Therapy 2009;9(2):243-247.

9. Mankad PS, Codispoti M. The role of fibrin sealants in hemostasis. American Journal of Surgery 2001;182(2):21S-28S.

10. Jackson MR. Fibrin sealants in surgical practice: An overview. American Journal of Surgery 2001;182(2):1S-7S.

11. Webster I, West PJ. Adhesives for Medical Applications. 2nd ed. New York: Marcel Dekker, 2002.

12. Conolly RB, Andersen ME. An Approach to Mechanism-Based Cancer Risk Assessment for Formaldehyde. Environ Health Perspect 1993;101:169-176.

13. Kobayashi H, Hyon SH, Ikada Y. Water-Curable and Biodegradable Prepolymers. J Biomed Mater Res 1991;25(12):1481-1494.

14. Otani Y, Tabata Y, Ikada Y. A new biological glue from gelatin and poly(L-glutamic acid). J Biomed Mater Res 1996;31(2):157-166.

15. Lando G, Cohn D. Introducing lactide-based biodegradable tissue adhesives. J Mater Sci-Mater Med 2003;14(2):181-186.

16. Ono K, Saito Y, Yura H, Ishikawa K, Kurita A, Akaike T, et al. Photocrosslinkable chitosan as a biological adhesive. J Biomed Mater Res 2000;49(2):289-295.

17. Zhao X, Kato K, Fukumoto Y, Nakamae K. Synthesis of bioadhesive hydrogels from chitin derivatives. Int J Adhes Adhes 2001;21(3):227-232.

18. Chen TH, Janjua R, McDermott MK, Bernstein SL, Steidl SM, Payne GF. Gelatin-based biomimetic tissue adhesive. Potential for retinal reattachment. Journal of Biomedical Materials Research Part B-Applied Biomaterials 2006;77B(2):416-422.

19. Hoffman BDRaAS. Physicochemical Surface Modification of Materials Used in Medicine. In: Buddy D. Ratner ASH, Frederick J. Schoen, Jack E. Lemons, editor. Biomaterials Science: An Introduction to Materials in Medicine. UK: Elsevier Academic Press, 2004.

20. Lauto A, Stoodley M, Marcel H, Avolio A, Sarris M, McKenzie G, et al. In vitro and in vivo tissue repair with laser-activated chitosan adhesive. Lasers in Surgery and Medicine 2007;39(1):19-27.

21. Ono K, Ishihara M, Ozeki Y, Deguchi H, Sato M, Saito Y, et al. Experimental evaluation of photocrosslinkable chitosan as a biologic adhesive with surgical applications. Surgery 2001;130(5):844-850.

22. Otani Y, Tabata Y, Ikada Y. Effect of additives on gelation and tissue adhesion of gelatin-poly(L-glutamic acid) mixture. Biomaterials 1998;19(23):2167-2173.

23. Messersmith PB. Mussel adhesive protein mimetics: Polymer-peptide bioconjugates for tissue adhesion and antifouling surfaces. 231st National Meeting of the American-Chemical-Society; 2006 Mar 26-30; Atlanta, GA; 2006: 85.

24. A.I. Everaerts LMC. Pressure sensitive adhesives. In: M. Chaudhury AVP, editor. Surfaces, Chemistry and Applications: Elsevier, 2002. p. 465-534.

25. Coover HN, Jaoyner FB, Sheere NH, Wicker TR. Chemistry and performance of cyanoacrylate adhesives. Journal of Social Plastic Surgery Engineering 1959;15:5-6.

26. Ayton JM. Polar hands: spontaneous skin fissures closed with cyanoacrylate (histoacryl blue) tissue adhesive in Antarctica. Antarctica Arctic Medical Research 1993;52:127-130.

27. Chivers RA, Wolowacz RG. The strength of adhesive-bonded tissue joints. Int J Adhes Adhes 1997;17(2):127-132.

28. Doraiswamy NV, Baig H, Hammett S, Hutton M. Which tissue adhesive for wound? International Journal of Care Injured 2003;34(564-567).

29. Donkerwolcke M, Burny F, Muster D. Tissue and bone adhesives-historical aspects. Biomaterials 1998;19(16):1461-1466.

30. Kjaergard HK. Suture support: Is it advantageous? American Journal of Surgery 2001;182(2):15S-20S.

31. Radosevich M, Goubran HA, Burnouf T. Fibrin sealant: Scientific rationale, production methods, properties, and current clinical use. Vox Sang 1997;72(3):133-143.

32. Martinowitz U, Spotnitz WD. Fibrin tissue adhesives. Thromb Haemost 1997;78(1):661-666.

33. Pipan CM, Glasheen WP, Matthew TL, Gonias SL, Hwang LJ, Jane JA, et al. Effects of Antifibrinolytic Agents on the Life-Span of Fibrin Sealant. J Surg Res 1992;53(4):402-407.

34. MacGillivray TE. Fibrin sealants and glues. J Card Surg 200;18(6):480-485.

35. Reece TB, Maxey TS, Kron IL. A prospectus on tissue adhesives. American Journal of Surgery 2001;182(2):40S-44S.

36. Guilmet D, Bachet J, Goudot B, Laurian C, Gigou F, Bical O, et al. Use of Biological Glue in Acute Aortic Dissection - Preliminary Clinical Results with a New Surgical Technique. J Thorac Cardiovasc Surg 1979;77(4):516-521.

37. Kucukaksu DS, Akgul A, Cagil K, Tasdemir O. Beneficial effect of BioGlue (R) surgical adhesive in repair of latrogenic aortic dissection. Tex Heart Inst J 2000;27(3):307-308.

38. Hewitt CW, Marra SW, Kann BR, Tran HS, Puc MM, Chrzanowski FA, et al. BioGlue surgical adhesive for thoracic aortic repair during coagulopathy: Efficacy and histopathology. Ann Thorac Surg 2001;71(5):1609-1612.

39. Ennker J, Ennker IC, Schoon D, Schoon HA, Dorge S, Meissler M, et al. The Impact of Gelatin-Resorcinol Glue on Aortic Tissue - a Histomorphologic Evaluation. J Vasc Surg 1994;20(1):34-43.

40. Nomori H, Horio H, Morinaga S, Suemasu K. Gelatin-resorcinol-formaldehyde-glutaraldehyde glue for sealing pulmonary air leaks during thoracoscopic operation. Ann Thorac Surg 1999;67(1):212-216.

41. Otani Y, Tabata Y, Ikada Y. Hemostatic capability of rapidly curable glues from gelatin, poly(L-glutamic acid), and carbodiimide. Biomaterials 1998;19(22):2091-2098.

42. Otani Y, Tabata Y, Ikada Y. Sealing effect of rapidly curable gelatin-poly (L-glutamic acid) hydrogel glue on lung air leak. Ann Thorac Surg 1999;67(4):922-926.

43. Waite JH. Natures Underwater Adhesive Specialist. Int J Adhes Adhes 1987;7(1):9-14.

44. Strausberg RL, Link RP. Protein-Based Medical Adhesives. Trends Biotechnol 1990;8(2):53-57.

45. Waite JH, inventor. Polypeptide monomers, linear extended and/or crosslinked formed thereof, and applications thereof. US Patent No. 5574134, 1996.

46. Yu ME, Deming TJ. Synthetic polypeptide mimics of marine adhesives. Macromolecules 1998;31(15):4739-4745.

47. Yu ME, Hwang JY, Deming TJ. Role of L-3,4-dihydroxyphenylalanine in mussel adhesive proteins. J Am Chem Soc 1999;121(24):5825-5826.

48. Strausberg RL, Strausberg SL, inventors. Composite yeast vectors. US Patent No. 5013652, 1991.

49. Pangburn SH, Trescony PV, Heller J. Lysozyme Degradation of Partially Deacetylated Chitin, Its Films and Hydrogels. Biomaterials 1982;3(2):105-108.

50. Prudden JF, Migel P, Hanson P, Friedric.L, Balassa L. Discovery of a Potent Pure Chemical Wound-Healing Accelerator. American Journal of Surgery 1970;119(5):560-568.

51. Radhakrishan VV, S. VM, M. S, M. J, Rao SB. Haemostatic potential of chitosan. Biomedicine 1991;2:3-6.

52. Fukasawa M, Abe H, Masaoka T, Orita H, Horikawa H, Campeau JD, et al. The Hemostatic Effect of Deacetylated Chitin Membrane on Peritoneal Injury in Rabbit Model. Surg Today-Jpn J Surg 1992;22(4):333-338.

53. Wang PY. Adhesion mechanism for polyurethane prepolymers bonding biological tissue. In: Gregor HP, editor. Biomedical application of polymers (Polymer science and technology). New York: Plenum Press, 1975, p. 111.

54. Salvatore JE, Mandarino MP. Polyurethane Polymer, Its Use in Osseous Lesions - an Experimental Sudy. Ann Surg 1959;149(1):107-109.

55. Sawhney AS, Pathak CP, Hubbell JA. Bioerodible Hydrogels Based on Photopolymerized Poly(Ethylene Glycol)-Co-Poly(Alpha-Hydroxy Acid) Diacrylate Macromers. Macromolecules 1993;26(4):581-587.

56. Sawhney AS, Poff B, Powell M, Messier K, Doherty E, Yao F, et al. Bioabsorbable synthetic hydrogel as a surgical lung sealant. Abstr Pap Am Chem Soc 1998;216:U851-U851.

57. Sun H. COMPASS: An ab Initio Forcefield Optimized for Condensed-Phase Applications - Overview with Detail on Alkane and Benzene Coumpounds. Journal of Physical Chemistry B 1998;102:27.

58. Sun H, Ren P, Fried JR. The COMPASS Forcefield: Parameterization and Validation for Polyphosphazenes. Computational and theoretical Polymer Science 1998;8((1/2)):28.

59. Rigby D, Sun H, Eichinger BE. Computer simulation of poly(ethylene oxides): Forcefield, PVT diagram and cyclization bahavior. Polymer International 1998;44:20.

60. Pitt WG, Weaver DR. Calculation of Protein-Polymer Force Fields Using Molecular Dynamics. Journal of Colloid and Interface Science 1997;185(1):258-264.

61. Bujnowski AM, Pitt WG. Water structure around enkephalin near a PE surface: A molecular dynamics study. Journal of Colloid and Interface Science 1998;203(1):47-58.

62. Nicholls A, Sharp KA, Honig B.Protein folding and association – Insights from the interfacial and thermodynamic properties of hydrocarbons. Proteins 1991;11(4):281-296.

63. Natarajan U, Misra S, Mattice WL. Atomistic simulation of a polymer-polymer interface: interfacial energy and work of adhesion. Computational and Theoretical Polymer Science 1998;8(3-4):323-329.

64. Latour RA. Molecular modeling of biomaterial surfaces. Curr Opin Solid State Mat Sci 1999;4(4):413-417.

65. Latour RA, Rini CJ. Theoretical analysis of adsorption thermodynamics for hydrophobic peptide residues on SAM surfaces of varying functionality. Journal of Biomedical Materials Research 2002;60(4):564-577.

66. Basalyga DM, Latour RA. Theoretical analysis of adsorption thermodynamics for charged peptide residues on SAM surfaces of varying functionality. Journal of Biomedical Materials Research Part A 2003;64A(1):120-130.

67. Wilson K, Stuart SJ, Garcia A, Latour RA. A molecular modeling study of the effect of surface chemistry on the adsorption of a fibronectin fragment spanning the 7-10th type-III repeats. Journal of Biomedical Materials Research Part A 2004;69A(4):686-698.

68. Yannas IV. Natural Materials. In: Buddy D. Ratner ASH, Frederick J. Schoen, Jack E. Lemons, editor. Biomaterials Science: An Introduction to Materials in Medicine. 2nd ed. London: Elsevier Academic Press, 2004. P. 127-136.

69. Okuyama K, Hongo C, Fukushima R, Wu GG, Narita H, Noguchi K, et al. Crystal structures of collagen model peptides with Pro-Hyp-Gly repeating sequence at 1.26 angstrom resolution: Implications for proline ring puckering. Biopolymers 2004;76(5):367-377.

70. Comyn, J., Theories of Adhesion. In: Cognard P, editor. Adhesives and Sealants. Vol 2, 1st ed. Great Britian: Elsevier, 2006. p. 1-50.

71. Sheikh N, Katbab AA, Mirzadeh H. Isocyanate-terminated urethane prepolymer as bioadhesive base material: synthesis and characterization. Int J Adhes Adhes 2000;20(4):299-304.

72. Hulmes DJS. Building collagen molecules, fibrils, and suprafibrillar structures. Workshop on Coiled-Coils, Collagen, and Co-Proteins; 200; Alpbach, Austria; 2001. p. 2-10.

73. Frisbie CD, Rozsnyai LF, Noy A, Wrighton MS, Lieber CM. Functional-Group Imaging by Chemical Force Microscopy. Science 1994;265(5181):2071-2074.

74. vanderVegte EW, Hadziioannou G. Scanning force microscopy with chemical specificity: An extensive study of chemically specific tip-surface interactions and the chemical imaging of surface functional groups. Langmuir 1997;13(16):4357-4368.

75. He HX, Huang W, Zhang H, Li QG, Li SFY, Liu ZF. Demonstration of high-resolution capability of chemical force titration via study of acid/base properties of a patterned self-assembled monolayer. Langmuir 2000;16(2):517-521.

76. Zhang H, He HX, Wang J, Mu T, Liu ZF. Force titration of amino group-terminated self-assembled monolayers using chemical force microscopy. Applied Physics a-Materials Science & Processing 1998;66:S269-S271.

77. Vezenov DV, Noy A, Ashby P. Chemical force microscopy: probing chemical origin of interfacial forces and adhesion. Journal of Adhesion Science and Technology 2005;19(3-5):313-364.

78. Butt HJ, Cappella B, Kappl M. Force measurements with the atomic force microscope: Technique, interpretation and applications. Surface Science Reports 2005;59(1-6):1-152.

79. Hutter JL, Bechhoefer J. Calibration of Atomic-Force Microscope Tips. Review of Scientific Instruments 1993;64(7):1868-1873.

80. Lim KP, Tan LP. Interaction force measurements for the design of tissue adhesives. Acta Biomaterialia 2009;5(1):84-92.

81. Patrick DL, Flanagan JF, Kohl P, Lynden-Bell RM. Atomistic molecular dynamics Simulations of chemical force microscopy. Journal of the American Chemical Society 2003;125(22):6762-6773.

82. Ulman A. Formation and structure of self-assembled monolayers. Chemical Reviews 1996;96(4):1533-1554.

83. Sierra DH, Eberhardt AW, Lemons JE. Failure characteristics of multiple-component fibrin-based adhesives. J Biomed Mater Res 2002;59(1):1-11.

84. Dickneite G, Metzner H, Pfeifer T, Kroez M, Witzke G. A comparison of fibrin sealants in relation to their in vitro and in vivo properties. Thromb Res 2003;112(1-2):73-82.

85. Ninan L, Monahan J, Stroshine RL, Wilker JJ, Shi RY. Adhesive strength of marine mussel extracts on porcine skin. Biomaterials 2003;24(22):4091-4099.

86. Bundy K, Schlegel U, Rahn B, Geret V, Perren S. An improved peel test method for measurement of adhesion to biomaterials. J Mater Sci-Mater Med 2000;11(8):517-521.

87. Singer AJ, Zimmerman T, Rooney J, Cameau P, Rudomen G, McClain SA. Comparison of wound-bursting strengths and surface characteristics of FDA-approved tissue adhesives for skin closure. J Adhes Sci Technol 2004;18(1):19-27.

88. Koukoubis TD, Glisson RR, Feagin JA, Seaber AV, Vail TP. Augmentation of Meniscal Repairs with Cyanoacrylate Glue. Journal of Biomedical Materials Research 1995;29(6):715-720.

89. Bonutti PM, Weiker GG, Andrish JT. Isobutyl Cyanoacrylate as a Soft-Tissue Adhesive - an Invitro Study in the Rabbit Achilles-Tendon. Clinical Orthopaedics and Related Research 1988 (229):241-248.

90. Tseng YC, Hyon SH, Ikada Y, Shimizu Y, Tamura K, Hitomi S. Invivo Evaluation of 2-Cyanoacrylates as Surgical Adhesives. Journal of Applied Biomaterials 1990;1(2):111-119.

91. Albes JM, Krettek C, Hausen B, Rohde R, Haverich A, Borst HG, et al. Biophysical Properties of the Gelatin-Resorcinol-Formaldehyde Glutaraldehyde Adhesive. Annals of Thoracic Surgery 1993;56(4):910-915.

92. Braunwal NS, Gay W, Tatooles CJ. Evaluation of Crosslinked Gelatin as a Tissue Adhesive and Hemostatic Agent - an Experimental Study. Surgery 1966;59(6):1024-1032.

93. Ennker IC, Ennker J, Schoon D, Schoon HA, Rimpler M, Hetzer R. Formaldehyde-Free Collagen Glue in Experimental Lung Gluing. Annals of Thoracic Surgery 1994;57(6):1622-1627.

94. Flahiff C, Feldman D, Saltz R, Huang S. Mechanical-Properties of Fibrin Adhesives for Blood-Vessel Anastomosis. Journal of Biomedical Materials Research 1992;26(4):481-491.

95. Siedentop KH, Harris DM, Sanchez B. Autologous Fibrin Tissue Adhesive - Factors Influencing Bonding Power. Laryngoscope 1988;98(7):731-733.

96. Siedentop KH, Park JJ, Sanchez B. An Autologous Fibrin Tissue Adhesive with Greater Bonding Power. Archives of Otolaryngology-Head & Neck Surgery 1995;121(7):769-772.

97. Sierra DH, Feldman DS, Saltz R, Huang S. A Method to Determine Shear Adhesive Strength of Fibrin Sealants. Journal of Applied Biomaterials 1992;3(2):147-151.

98. Burnoufradosevich M, Burnouf T, Huart JJ. Biochemical and Physical-Properties of a Solvent-Detergent-Treated Fibrin Glue. Vox Sanguinis 1990;58(2):77-84.

99. Jorgensen PH, Jensen KH, Andreassen TT. Mechanical Strength in Rat Skin Incisional Wounds Treated with Fibrin Sealant. Journal of Surgical Research 1987;42(3):237-241.

100. Analytical Methods Committee. Robust statistics: A method of coping with outliers. In: AMC technical brief. London: Royal Society of Chemistry. Online. 2001. Available from URL: http://www.rsc.org/images/brief6_tcm18-25948.pdf.

101. McDermott MK, Chen TH, Williams CM, Markley KM, Payne GF. Mechanical properties of biomimetic tissue adhesive based on the microbial transglutaminase-catalyzed crosslinking of gelatin. Biomacromolecules 2004;5(4):1270-1279.

Appendix 1. Atom types and selected COMPASS parameters

Equivalence Table

atom	formal type	actual type					description
		nonb	bond	angl	tors	oop	
carbon	c2t	c2t	c2t	c2t	c2t	c2t	carbon, sp, triple bond
	c3	c3	c3	c3	c3	c3	carbon, sp2, generic
	c4	c4	c4	c4	c4	c4	carbon, sp3, generic
	c4o	c4o	c4	c4	c4	c4	carbon, sp3, bond to oxygen
hydrogen	h1	h1	h1	h1	h1	h1	hydrogen, nonpolar
	h1n	h1n	h1	h1	h1	h1	hydrogen, bond to N, Cl
	h1o	h1o	h1	h1	h1	h1	hydrogen, bond to O, F
oxygen	o1-	o1-	o1-	o1-	o1-	o1-	oxygen, sp2, in carboxylate
	o1=	o1=	o1=	o1=	o1=	o1=	oxygen, sp2, in carbonyl
	o2c	o2c	o2c	o2	o2	o2	oxygen, sp3, in acid
	o2e	o2e	o2e	o2	o2	o2	oxygen, sp3, in ethers
	o2h	o2h	o2h	o2	o2	o2	oxygen, sp3 in alcohol
	o2s	o2s	o2e	o2	o2	o2	oxygen, sp3, in esters
nitrogen	n1t	n1t	n1t	n1t	n1t	n1t	nitrogen, sp, one triple bond
	n2t	n1t	n1t	n1t	n1t	n1t	nitrogen, sp, one triple bond, non-aromatic
	n3h1	n3h1	n3	n3	n3	n3	nitrogen, sp3, in amines with one H
	n3h2	n3h2	n3	n3	n3	n3	nitrogen, sp3, in amines with two H
sulfur	s2	s2	s2	s2	s2	s2	sulfur, 2 single bonds (-S-)
fluorine	f1	f1	f1	f1	f1	f1	fluorine, one bond

COMPASS parameters for selected atoms

Bond Increments

c4	c4	0.0000
c4	h1	-0.0530
c4	o2e	0.1600
c4	o2h	0.1600
h1	o2	0.4200
h1	o2h	0.4200

Quartic Bond

I	J	b_o	K_2	K_3	K_4
c4	c4	1.5300	299.6700	-501.7700	679.8100
c4	h1	1.1010	345.0000	-691.8900	844.6000
c4	o2e	1.4200	400.3954	-835.1951	1313.0142
c4	o2h	1.4200	400.3954	-835.1951	1313.0142
h1	o2h	0.9494	540.3633	-1311.8663	2132.4446

Quartic Angle

I	J	K	θ_o	H_2	H_3	H_4
c4	c4	c4	112.6700	39.5160	-7.4430	-9.5583
c4	c4	h1	110.7700	41.4530	-10.6040	5.1290
h1	c4	h1	107.6600	39.6410	-12.9210	-2.4318
c4	c4	o2	111.2700	54.5381	-8.3642	-13.0838
h1	c4	o2	108.7280	58.5446	-10.8088	-12.4006
c4	o2	c4	104.5000	35.7454	-10.0067	-6.2729
c4	o2	h1	105.8000	52.7061	-12.1090	-9.8681

Torsion

I	J	K	L	V_1	V_2	V_3
c4	c4	c4	c4	0.0000	0.0514	-0.1430
c4	c4	c4	c4	0.0000	0.0316	-0.1681
h1	c4	c4	h1	-0.1432	0.0617	-0.1530
*	c4	c4	*	0.0000	0.0000	-0.1530
c4	c4	c4	o2	0.7137	0.2660	-0.2545
h1	c4	c4	o2	-0.1435	0.2530	0.0905
o2	c4	c4	o2	1.1000	-0.0500	-0.1441
c4	c4	o2	c4	-0.4000	-0.4028	-0.2450
c4	c4	o2	h1	-0.6732	-0.4778	-0.1670
h1	c4	o2	c4	0.5302	0.0000	-0.3966
h1	c4	o2	h1	0.1863	-0.4338	-0.2121

Bond-bond

I	J	K	$F_{bb'}$ (IJ/JK)
c4	c4	h1	3.3872
h1	c4	h1	5.3316
c4	c4	o2	11.4318
h1	c4	o2	8.2983
c4	o2	c4	-7.1131
c4	o2	h1	-9.6879

Bond-angle

I	J	K	$F_{b\theta}$(IJ/IJK)	$F_{b\theta}$(JK/IJK)
c4	c4	c4	8.0160	8.0160
c4	c4	h1	20.7540	11.4210
h1	c4	h1	18.1030	18.1030
c4	c4	o2	2.6868	20.4033
h1	c4	o2	4.6189	55.3270
c4	o2	c4	-2.8112	-2.8112
c4	o2	h1	28.5800	18.9277

Angle-angle

I	J	K	L	$F_{\theta\theta'}$ (ijk/jkl)
c4	c4	c4	o2	-0.8330
h1	c4	c4	o2	2.5926
c4	c4	h1	o2	3.9177
h1	c4	h1	o2	2.4259
c4	c4	o2	c4	-3.5744
c4	c4	o2	h1	0.1689
h1	c4	o2	h1	2.1283

End bond-torsion

I	J	K	L	I-J/I-J-K-L			K-L/I-J-K-L		
				V_1	V_2	V_3	V_1	V_2	V_3
c4	c4	c4	c4	-0.0732	0.0000	0.0000	0.0000	0.0000	0.0000
c4	c4	c4	h1	0.2486	0.2422	-0.0925	0.0814	0.0591	0.2219
h1	c4	c4	h1	0.2130	0.3120	0.0777	0.2130	0.3120	0.0777
c4	c4	c4	o2	-0.3190	0.4411	-0.7174	1.1538	0.8409	-0.9138
h1	c4	c4	o2	0.9681	0.9551	0.0436	0.5903	0.6669	0.8584
o2	c4	c4	o2	1.0165	0.7553	-0.4609			
c4	c4	o2	c4	-0.2456	1.0517	-0.7795	0.4741	1.2635	0.5576
c4	c4	o2	h1	-0.5800	0.9004	0.0000	0.0000	0.5343	0.9025
h1	c4	o2	c4	-0.6054	1.3339	0.9648	-0.1620	0.1564	-1.1408
h1	c4	o2	h1	-1.7554	1.3145	0.2263	0.2493	0.6803	0.0000

Middle bond-torsion

I	J	K	L	V_1	V_2	V_3
c4	c4	c4	c4	-17.7870	-1.1877	0.0000
c4	c4	c4	h1	-14.8790	-3.6581	-0.3138
h1	c4	c4	h1	-14.2610	-0.5322	-0.4864
c4	c4	c4	o2	-21.8842	-7.6764	-0.6868
h1	c4	c4	o2	-16.7975	-1.2296	-0.2750
o2	c4	c4	o2	-17.2585	-3.6157	-0.8364
c4	c4	o2	c4	-5.9288	-2.7007	-0.3175
c4	c4	o2	h1	1.2472	0.0000	0.7485
h1	c4	o2	c4	-6.8007	-4.6546	-1.4104
h1	c4	o2	h1	0.0000	0.9224	-0.5889

Angle-torsion

I	J	K	L	I-J-K/I-J-K-L			J-K-L/I-J-K-L		
				V_1	V_2	V_3	V_1	V_2	V_3
c4	c4	c4	c4	0.3886	-0.3139	0.1389	0.3886	-0.3139	0.1389
c4	c4	c4	h1	-0.2454	0.0000	-0.1136	0.3113	0.4516	-0.1988
h1	c4	c4	h1	-0.8085	0.5569	-0.2466	-0.8085	0.5569	-0.2466
c4	c4	c4	o2	0.5623	-0.3041	-0.4015	0.9672	-0.7566	-1.2331
h1	c4	c4	o2	2.3668	2.4920	-1.0122	-0.1892	0.4918	0.7273
o2	c4	c4	o2	0.5511	0.9737	-0.6673			
c4	c4	o2	c4	-2.7466	1.4877	-0.8955	0.5675	0.9450	0.0703
c4	c4	o2	h1	-3.5903	2.5225	0.4888	0.8726	-0.3577	0.3888
h1	c4	o2	c4	-1.8234	1.6393	0.5144	-0.7777	0.4340	-0.6653
h1	c4	o2	h1	-3.4060	1.6396	0.0737	0.0000	-0.2810	-0.5944

Angle-angle-torsion

I	J	K	L	K (IJ/IJKL/JKL)
c4	c4	c4	c4	-22.0450
c4	c4	c4	h1	-16.1640
h1	c4	c4	h1	-12.5640
c4	c4	c4	o2	-29.0420
h1	c4	c4	o2	20.2006
o2	c4	c4	o2	-14.0484
c4	c4	o2	c4	-19.0059
c4	c4	o2	h1	-12.1038
h1	c4	o2	c4	-16.4438
h1	c4	o2	h1	-10.5093

Non-bond (LJ 9-6)

I	ro	εo
c4	3.8540	0.0620
c4o	3.8150	0.0680
h1	2.8780	0.0230
h1o	1.0870	0.0080
o2	3.3000	0.0800
o2e	3.3000	0.1200
o2h	3.5800	0.0960

Appendix 2. Geometry and Specifications of the DNP Probe

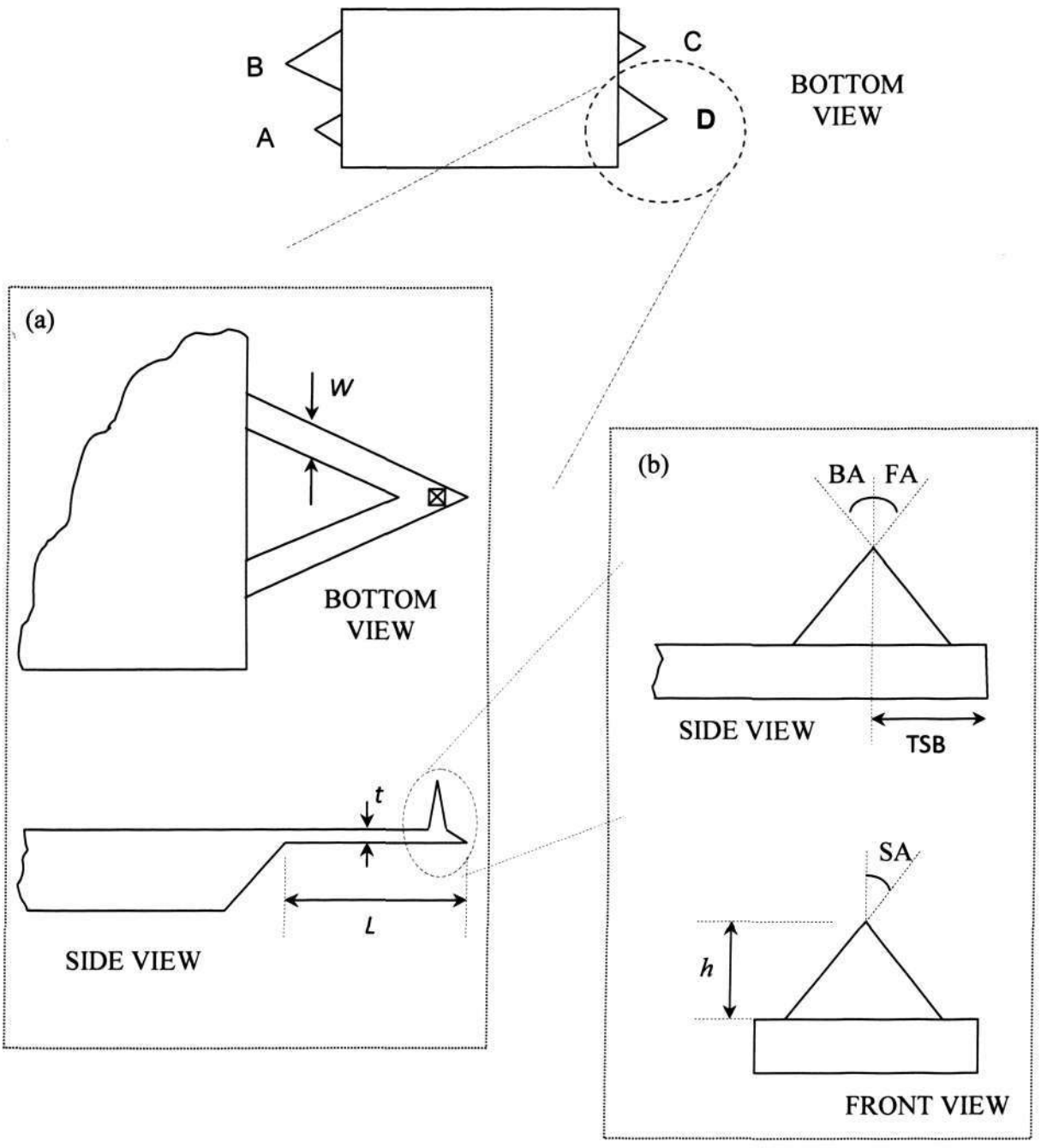

Figure A1 Schematic representation of (a) D Triangular in DNP probe; and (b) the pyramidal tip. (W: width of cantilever; L: length of cantilever; t: thickness of cantilever; FA: front angle of tip; BA: back angle of tip; SA: side angle of tip; TSB: tip-setback; h: height of tip.)

Table A1 The specifications of the four cantilevers on one DNP probe.

Cantilever Specifications		
Cantilever A		
	Nominal Value	Range
Width (*W*)	25 μm	20 – 30 μm
Length (*L*)	115 μm	100 – 130 μm
Thickness (*t*)	0.6 μm	0.4-0.7 μm
Force Constant (*k*)	0.58 N/m	0.29 – 1.2 N/m
Resonance Frequency (*f*)	57 kHz	40 – 75 kHz
Cantilever B		
	Nominal Value	Range
Width (*W*)	41 μm	33 – 49 μm
Length (*L*)	196 μm	180 – 212 μm
Thickness (*t*)	0.6 μm	0.4 – 0.7 μm
Force Constant (*k*)	0.12 N/m	0.06 – 0.24 N/m
Resonance Frequency (*f*)	20 kHz	14 – 26 kHz
Cantilever C		
	Nominal Value	Range
Width (*W*)	17 μm	13 – 21 μm
Length (*L*)	115 μm	100 – 130 μm
Thickness (*t*)	0.6 μm	0.4 – 0.7 μm
Force Constant (*k*)	0.32 N/m	0.16 – 0.74 N/m
Resonance Frequency (*f*)	56 kHz	40 – 75 kHz
Cantilever D		
	Nominal Value	Range
Width (*W*)	23 μm	18 – 28 μm
Length (*L*)	196 μm	180 – 212 μm
Thickness (*t*)	0.6 μm	0.4-0.7 μm
Force Constant (*k*)	0.06 N/m	0.03 – 0.12 N/m
Resonance Frequency (*f*)	18 kHz	12 – 24 kHz
Tip Specifications (same for all)		
Tip Radius (*r*)	10 nm	(40 nm at max)
Front Angle (FA)	35°	33°-37°
Back Angle (BA)	35°	33°-37°
Side Angle (SA)	35°	33°-37°
Tip Height (*h*)	3 μm	2.5-3.5 μm
Tip-Setback (TSB)	4 μm	3-5.5 μm

Appendix 3. Derivation of Equation 4.3

By the theorem of equipartition (see geometry on the next page),

$$\frac{a}{a_o} = \frac{l}{L} = \frac{h}{H}$$

Therefore,

$$\begin{aligned} A &= 4A' + A_o \\ &= 4 \times \frac{1}{2} al + A_o \\ &= 2al + A_o \\ &= \frac{2a_o L}{H^2} h^2 + A_o \end{aligned}$$

Now we are going to eliminate L and replace with measurable dimension,

In ΔADE,

$$AE = \sqrt{H^2 + x^2}$$
$$DE = \sqrt{H^2 + y^2}$$

By cosine theorem,

$$\cos\theta = \frac{AE^2 + DE^2 - a_o^2}{2AE \cdot DE}$$

$$\cos\theta = \frac{x^2 + y^2 + 2H^2 - a_o^2}{2AE \cdot DE}$$

$\because x^2 + y^2 = a_o^2$, $\quad \cos\theta = \dfrac{H^2}{AE \cdot DE}$

$$\sin\theta = \frac{\sqrt{x^2 y^2 + H^2 a_o^2}}{AE \cdot DE}$$

Calculate the area of the surface of ΔADE

$$A = \frac{1}{2} AE \cdot DE \sin\theta = \frac{1}{2} a_o L$$

$$\therefore L = \frac{1}{a_o}\sqrt{x^2y^2 + H^2a_o^2}$$

So, the contact area

$$= \frac{2a_o}{H^2} \cdot \frac{1}{a_o}\sqrt{x^2y^2 + H^2a_o^2} \cdot h^2 + A_o$$

$$= 2\sqrt{\left(\frac{xy}{H}\right)^2 + \left(\frac{a_o}{H}\right)^2} \cdot h^2 + A_o$$

Let $J = 2\sqrt{\left(\frac{xy}{H}\right)^2 + \left(\frac{a_o}{H}\right)^2}$

Then $\underline{A = Jh^2 + A_o}$.

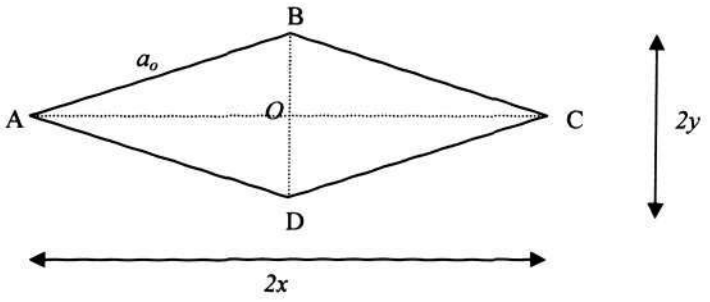

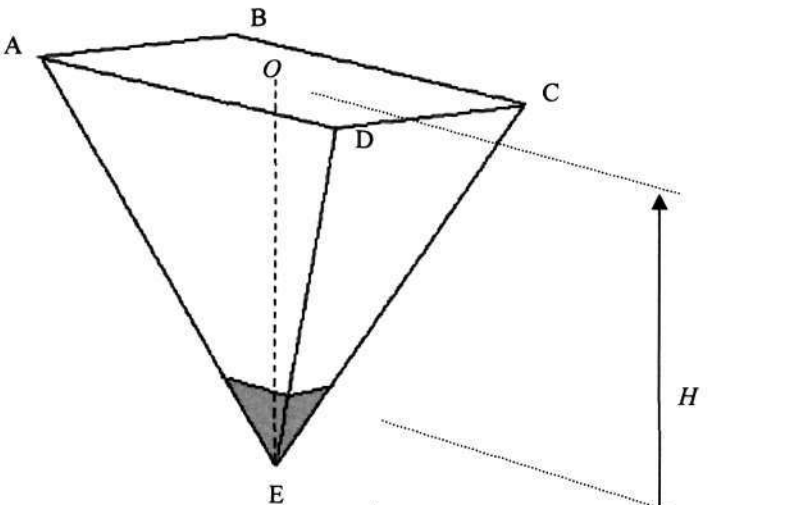

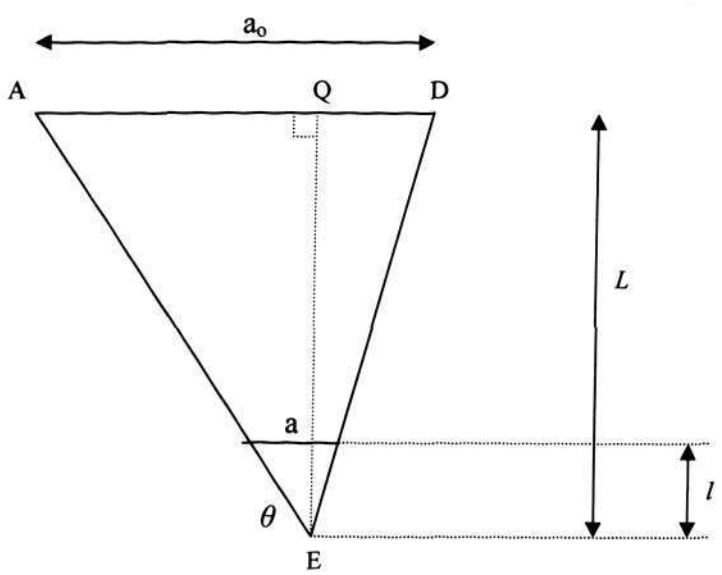

Appendix 4. Derivative of Equation 4.10

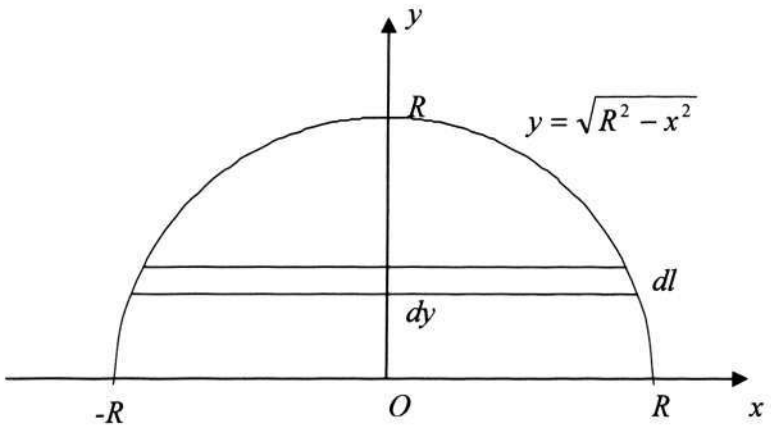

The infinitesimally small circumference *dl* is given as

$$dl = \sqrt{1 + \left(\frac{dx}{dy}\right)^2}\, dy$$

Therefore the surface area of which dl rotates for 360° with respect to *y*-axis is

$$dA = 2\pi x \sqrt{1 + \left(\frac{dx}{dy}\right)^2}\, dy$$

$$= 2\pi x \sqrt{1 + \frac{y^2}{x^2}} dy$$

$$= \frac{2\pi R}{x} dy$$

$$= \frac{2\pi R}{\sqrt{R^2 - y^2}} dy$$

Integrating, from $y=a$ to $y=R$, we obtain

$$A = \int_a^R \frac{2\pi R}{\sqrt{R^2 - y^2}} dy$$

$$= 2\pi R\left[\sin^{-1}\frac{y}{R}\right]_a^R$$

$$= 2\pi R\left(\frac{\pi}{2} - \sin^{-1}\frac{a}{R}\right)$$

$\because h' = R - a$

$$\therefore A = \pi^2 R\left[1 - \frac{2}{\pi}\sin^{-1}\left(1 - \frac{h'}{R}\right)\right]$$